DESIGN AND DEVELOPMENT OF MIMO ANTENNA FOR 5G APPLICATIONS

Thesis Submitted for the Award of the Degree of

DOCTOR OF PHILOSOPHY

in

Electronics & Communication Engineering

By

Sanket Ashok Nirmal

Registration Number: 41900725

Supervised By

Dr. Sumit Kumar (24786)

School of Electronics & Electrical Engineering (Associate Professor)

Lovely Professional University, Punjab

Co-Supervised by

Dr. Richa Chandel

Department of Electronics & Communication Engineering (Assistant Professor)

UIT, Himachal Pradesh University, Shimla.



LOVELY PROFESSIONAL UNIVERSITY, PUNJAB

2026

DECLARATION

I, hereby declared that the presented work in the thesis entitled "**Design and Development of MIMO Antenna for 5G Applications**" in fulfilment of degree of **Doctor of Philosophy (Ph. D.)** is outcome of research work carried out by me under the supervision **Dr. Sumit Kumar,** working as Associate Professor, in the School of Electronics and Electrical Engineering of Lovely Professional University, Punjab, India and **Dr. Richa Chandel,** Assistant Professor, University Institute of Technology, Himachal Pradesh University, Shimla. In keeping with general practice of reporting scientific observations, due acknowledgements have been made whenever work described here has been based on findings of other investigator. This work has not been submitted in part or full to any other University or Institute for the award of any degree.



Name of the scholar: Sanket Ashok Nirmal

Registration No.: 41900725

Department/school: School of Electronics and Electrical Engineering

Lovely Professional University, Punjab, India

CERTIFICATE

This is to certify that the work reported in the Ph. D. thesis entitled **"Design and Development of MIMO Antenna for 5G Applications"** submitted in fulfillment of the requirement for the reward of degree of **Doctor of Philosophy (Ph.D.)** in the School of Electronics and Electrical Engineering, is a research work carried out by **Sanket Ashok Nirmal, 41900725**, is bonafide record of his original work carried out under my supervision and that no part of thesis has been submitted for any other degree, diploma or equivalent course.



Signature of Supervisor

Dr. Sumit Kumar (24786)
Associate Professor
School of Electronics & Electrical Engineering
Lovely Professional University, Punjab



Signature of Co-Supervisor

Dr. Richa Chandel
Assistant Professor
Department of ECE,
University Institute of Technology,
Himachal Pradesh University, Shimla.

Signature of Head of Department

Dr. Shelej Khera

Signature of Head of School

Dr. Gaurav Sethi

ABSTRACT

A 5G technique which is used in developing a popular IoT will require MIMO antenna and it is also challengeable as well as interesting to know 5G mobile communication devices uses MIMO/Massive MIMO. The MIMO antennas can significantly enhance communication capacity in the sub-6 GHz band and widely increases the channel capacity by employing multiple antennas at the transmitter and receiver with spatial multiplexing to overcome multipath fading. The MIMO antenna will improve range of communication and can increase channel capacity widely by increasing more numbers of antennas at transmitter and receiver by using spatial multiplexing and to encounter multipath fading. Due to its unique standards, such as improved data speed and channel capability and to reduce absorption from the close proximity of EM (electromagnetic) waves, MIMO technology has emerged as the most challenging communication system. Additionally, the demand for 5G is the antenna size reduction and improved MIMO performance parameter such as correlation among antenna element isolation (ECC<0.5), adequate bandwidth, maximum efficiency and reduction in mutual coupling which makes it an incomparable antenna which within acceptable range.

In the beginning, the partial ground structure with square-shaped patch and parallel stub line is implemented for single element MIMO configuration and after the optimization, the implementation of 2-element MIMO array with dimension of 34×20 mm^2 is formed. To improve mutual coupling among neighbouring antenna, an an inverted T-shaped ground is developed. Also, the two symmetrical antenna elements with asymmetric feed line are used in this structure with frequency vary from 2.92 to 5.72 GHz. The minimum efficiency and gain were obtained around 86 % and upto 3.1 dB across the band of interest respectively.

Secondly, in order to improve necessary mutual coupling, the quad patch elements are arranged in face-to-face method with adequate spacing between antenna elements. The enhanced structure consists of inverted T-shape partial ground and square type patch with stub elements on both sides to enhance impedance matching. Also, the role of twin stub and rectangular notch on top right corner of patch is deliberated. The operation of Quad port antenna with a structure of dimension (W × L) 31 × 40 mm^2. With this compact size, the impedance bandwidth (-10 dB) of 2.27 to 5.34 GHz is attained. The analysis of antenna performance parameters like ECC, DG

and isolation have been measured. Furthermore, it exhibits a remarkable ECC ≤ 0.3 in the working band.

Finally, the four-element microstrip fed modified rectangular U-shape radiating elements are placed in same orientation with mirror image so as to achieve antenna diversity, resulting in good isolation. The overall dimensions of protype antenna are 52 mm × 31mm × 1.6mm. This quad-port MIMO operates in sub-6 5G-NR band which includes n77/ n78/ n79 and WLAN band with Wi-Fi-5 (5.15-5.85 GHz) & Wi-Fi-6 (5.925-7.125 GHz) band. The antenna structure using a single-element antenna, and subsequently design a four-port enhanced MIMO antenna with an uneven but parallel strip-line on the ground side to enhance mutual coupling. The antenna covers the band from 3.06 GHz to 7.56 GHz with a maximum gain from 2 to 7 dBi and efficiency of more than 82%. Further, the proposed 5G LTCC/diversity antenna is designed with low temperature co-fired ceramic (LTCC) and effect of device housing on antenna parameter is studied.

ACKNOWLEDGEMENT

Firstly, I would like to thank my supervisors, Dr. Sumit Kumar and Dr. Richa Chandel, for providing me with exceptional experiences during the research and for their supervision, guidance, and advice from the very beginning. I consider myself really fortunate to be able to work with them. I found this guidance to be extremely valuable.

I express my gratitude to the entire family of Lovely Professional University for providing me a suitable research environment to carry out my work in proper time. I would like to thank the Division of Research & Development, and School of Electronics & Electrical Engineering for all the support and encouragement throughout the research work. I am grateful to Dr. Ashok Mittal, Honourable Chancellor, Lovely Professional University, for providing the facilities and support necessary to complete the present study. I express my heartfelt gratitude to the head and staff of the School of Electronics and Electrical Engineering for all time co-operation and support.

I appreciate the helpful advice that my friends and fellow scholars have given me. In particular, I am grateful to Dr. N. A. Patil for enlightening me the first glance of research and the department of Electronics & Communication Engineering for providing necessary facilities, co-operation and moral support during the entire research period.

I heartily thank Mr. Ashok Nirmal and Mrs. Manda Nirmal, my parents, for their constant encouragement and blessings and for teaching me the values of dedication and perseverance. I would also like to express my cordial thanks to my wife Sayali, dear brother Shritej for their constant encouragement and support during the long and strenuous period of my work that made the compilation of the thesis possible. Finally, I thank God for sailing me through all the rough and tough times.

Date: 28/01/2026 Sanket Ashok Nirmal

TABLE OF CONTENTS

Declaration ii

Certificate iii

Abstract iv

Acknowledgment vi

Table of Contents vii

List of Figures x

List of Tables xiv

List of Abbreviations xv

1. Introduction **1**

1.1 Introduction 1

1.2 5G Technology and its main capabilities 3

1.2.1 eMBB 5

1.2.2 uRLLC 5

1.2.3 mMTC 5

1.3 Planar Monopole Antenna 5

1.4 Multiple Antenna Features and Types of MIMO 7

1.5 Necessities for sub-6-5G MIMO antenna 8

1.5.1 Reflection Coefficient and VSWR 8

1.5.2 Spatial Multiplexing 9

1.5.3 Multipath Diversity 9

1.5.4 MIMO Performance Parameters 10

1.6 Motivation for the Present Research 11

1.7 Research gaps/ Challenges in Antenna Design 12

1.8 Research Problem Statement 12

1.9 Design methodology 12

1.10 Thesis Organisation 16

1.11 Summary 17

2. Literature Review **18**

2.1 Introduction 18

2.2 Review on Performance enhancement technique of MIMO Antenna 19

2.3 Literature based on performance parameters of **MIMO antennas for 5G and WLAN** 22
2.4 Inferences drawn from the literature survey 29
2.5 Summary 30
3. High Isolation 2-element MIMO for WLAN/Sub-6 GHz (n77, n78 and n79) 5G applications **32**
3.1 Introduction 32
3.2 Antenna Design configurations and simulated Results 34
3.2.1 Antenna Design 34
3.2.2 Simulation Results (Scattering Parameters) 35
3.2.3 Current Distribution 38
3.3 Experimental Results and Discussion 39
3.3.1. S-Parameters 39
3.3.2. Radiation Performance 42
3.4 MIMO Performance Parameters 44
3.4.1 Envelope correlation coefficient (ECC) 44
3.4.2 Diversity Gain (DG) 45
3.4.3 Total Active Reflection Coefficient (TARC) 45
3.4.4 Mean Effective Gain (MEG) 47
3.4.5 Channel Capacity Loss (CCL) 47
3.5 Summary 49
4. Quad-Radiator MIMO with asymmetric feed line for (n77/n78/n79/WLAN) 5G-Wireless Applications **50**
4.1 Introduction 50
4.2 Antenna Design and Configurations 52
4.3 Results and Discussion 55
4.4 Diversity Performance 58
4.5 Summary 61
5. Quad-port Staircase U-Shaped Wideband MIMO Antenna for 5G New Radio Applications **62**
5.1 Introduction 62
5.2 Antenna Design and Analysis 64
5.2.1 Single Element MIMO Antenna 65

5.2.2 Mathematical Modelling of Single element Rectangular Patch 66
5.2.3 Quad Port MIMO Antenna 67
5.2.4 Effect of Ground Plane on Four-Element MIMO Antenna 67
5.3 Experimental Analysis of MIMO Antenna 69
5.4 Diversity Performance 73
5.5 Device Enclosure and Packaging 76
5.6 Implementation of 4-element MIMO using Low-temperature cofired ceramic (LTCC) Technology 77
5.6.1 Introduction of LTCC Technology 77
5.6.2 Geometry and analysis of 5G-LTCC MIMO antenna 77
5.6.3 Radiation Performance of 5G-LTCC MIMO 81
5.7 Summary 83
6. Conclusion and Future Scope **84**
6.1 Conclusion 84
6.2 Future Scope 85
Appendix-A Supplementary Information 87
References 102
List of Publications 119

LIST OF FIGURES

Sr. No.	Description	Page No.
1.1	Evolution of various generation of cellular communications	2
1.2	Cellular generations along with its parametric changes	2
1.3	Key applications of the 5G	4
1.4	Key features of 5G	4
1.5	Monopole antenna	6
1.6	Different planar monopole radiator shapes	6
1.7	Different MIMO configuration	7
1.8	Data stream transmitted through spatial multiplexing	9
1.9	Multipath diversity	10
1.10	Various performance parameter of the MIMO antenna	11
1.11	Process design flow for obtaining desired result	15
2.1	Pictorial representation of 5G MIMO antenna with substrate materials, 5G antenna types and application	19
3.1	Configuration of 2-element MIMO with optimized parameter	35
3.2	Simulated S_{11} against frequency for various design stages.	36
3.3	Simulated S_{11} against frequency for different values of W_f	36
3.4	Simulated S_{11} against frequency for different values of L_g	37
3.5	Simulated S_{11} against frequency for different values of W_3	37
3.6	Current distributions of the designed antenna, with and without an I-shaped stub, with port 2 excited at 4.5 GHz	38
3.7	Measurement of two element MIMO using Rohde and Schwarz vector network analyser	39
3.8	Simulated and measured s-parameter of developed 5G MIMO antenna	40
3.9	Measured and simulated radiation characteristics of 2-element MIMO antenna.	43
3.10	Realized gain and radiation efficiency of the 2-Element MIMO antenna	44
3.11	Simulated and measured results of ECC and DG versus frequency for a two-element MIMO antenna.	45

3.12	Simulated and measured result of the TARC for the two-element MIMO antenna.	46
3.13	Simulated and measured MEG versus frequency for the 2-Element MIMO antenna.	48
3.14	Simulated and measured CCL versus frequency for the 2-Element MIMO antenna.	48
4.1	(a) Antenna geometry (b) With U-shape cut on ground (c) Current distribution of a single element MIMO at 5 GHz	52
4.2	Reflection coefficient (S11) of 4- element MIMO (a) Without U-Slot (b) With U-slot on ground	53
4.3	Configuration of 4-element asymmetric feed antenna (a) Geometry of patch (b) Parallel strip line for mutual coupling reduction (c) Combined geometry of 4-element antenna (d) Antenna with U-shape slot on the ground	54
4.4	Current distribution of quad radiator MIMO at 4.5 GHz	55
4.5	S-parameter results for quad-radiator MIMO with asymmetric feed line (a) Plot of S11 (b) Plot of S11/S12/S13/S14 (c) Plot of S11/S22/S33/S44 (d) Plot of varying width of feed line from 1.5 mm to 3 mm (e) Plot of S11for varying substrate thickness	56
4.6	(a), (b) 3-D radiation pattern and (c), (d) 2-D radiation pattern of quad-radiator MIMO with asymmetric feed line at centre frequency	57
4.7	Four element MIMO antenna fabricated for measurements (a) front view (b) back view	58
4.8	S-parameter of fabricated four element MIMO antenna	58
4.9	(a) Diversity gain (DG) and (b) ECC of quad-radiator MIMO of asymmetric feed line	59
5.1	Figure 5.1 (a) front view, (b) back view, (c) Layout of the suggested MIMO antenna (d) modified I-shaped structure dimension	65
5.2	Effect of S_{11} due to development steps of single-element antenna	66
5.3	Evolution of Isolation structure (a) without I-shaped (b) with I-shaped and corner slit (c) Modified I-shaped.	67
5.4	S-parameters against frequency for different isolation structures.	68

5.5	Surface current distribution of 4-element MIMO at (a) 3.4 GHz (b) 5.2 GHz	69
5.6	Measured and simulated S-Parameter against frequency of 4-element MIMO Antenna.	70
5.7	Fabricated MIMO antenna (a) Top view (b) Bottom view and (c) Measurement environment.	70
5.8	Measured and simulated Efficiency and Gain of the suggested MIMO Antenna	71
5.9	Simulated and measured radiation pattern in XZ-plane and YZ-plane at (a) 3.4 GHz and (b) 5.2 GHz	71
5.10	Measured and simulated ECC and Diversity Gain versus frequency of the MIMO antenna.	74
5.11	Measured and simulated TARC and CCL versus frequency for the proposed MIMO antenna.	75
5.12	Measured and simulated mean effective gain (MEG)	76
5.13	Housing of the designed MIMO antenna	76
5.14	S-parameters for various materials with the designed MIMO antenna (a) Return loss and (b) Isolation parameters.	77
5.15	(a) Side perspective view (b) Front perspective view of prototype LTCC MIMO antenna	78
5.16	S-parameter of four-element MIMO with LTCC technique	79
5.17	S-Parameter of four-element MIMO-LTCC Antenna for varying ground width (gw)	80
5.18	S-Parameter of four-element MIMO-LTCC Antenna for varying feed line width (wf)	80
5.19	2-D simulated radiation pattern of four port LTCC-MIMO along XZ and YZ Plane	81
S.1	Geometry of the Single element antenna	88
S.2	Reflection coefficient (S_{11}) of Single element antenna	89
S.3	Vector current density of reference antenna	89
S.4	Geometry of the proposed two-element antenna	90
S.5	S-parameter of proposed 2-element MIMO	91
S.6	Vector current density of 2-element antenna	91

S.7	2-D Radiation Pattern	92
S.8	(A) Correlation coefficient versus frequency, (B) TARC and DG versus frequency, (C) (MEG_1/MEG_2) versus frequency, (D) channel capacity loss (CCL) versus frequency	93
S.9	Simulated S-parameters (S11) against frequency and single element Geometry	96
S.10	(A) 4-element patch placement of proposed antenna, (B) Perspective view of proposed antenna	97
S.11	(A) Simulated S-parameters (S_{11} and S_{12}) versus frequency, (B) Simulated S-parameters ($S_{11}/S_{21}/S_{31}/S_{41}$) versus frequency, (C) Plot of simulated S-parameters versus frequency for different value of Wf	98
S.12	(A) Plot of simulated S-parameters versus frequency for different values Lg1, (B) Plot of simulated S-parameters versus frequency for different values (Lg3)	99
S.13	(A) Simulated ECC of the proposed MIMO, (B) Simulated Diversity gain	100
S.14	Two-dimensional radiation pattern of corporate-fed microstrip array antenna: (a) at 4 GHz, (b) at 5.5 GHz, (c) at 8 GHz, and (d) at 9.5 GHz.	100

LIST OF TABLES

Sr. No.	Description	Page No.
2.1	Performance comparisons of the multiple-input multiple-output antennas of 5G	28
3.1	Design parameter of the two-element antenna.	35
3.2	Comparison of developed MIMO antenna with recently reported design.	40
3.3	MEG at various frequencies of the 2-Element MIMO antenna.	47
4.1	Comparative study of various diversity antennas	59
5.1	Comparison of the proposed work with other previously reported MIMO Antenna	72
5.2	Optimized parameters with dimensions	79
5.3	Comparative study with previously published Sub-6 LTCC planar patch	81
S.1	Single element antenna parameters (in mm).	88
S.2	Two element antenna geometry (in mm)	90
S.3	Comparative investigation of MIMO antennas	93
S.4	Proposed parameters of the four-element antenna	97

LIST OF ABBREVIATIONS

Acronym	Definition
1G – 5G	First to fifth generation
3GPP	3rd Generation Partnership Project
5G-PPP	5G Public Private Partnership
BW	Bandwidth
CCL	Channel capacity loss
DG	Diversity Gain
EBG	Energy band gap
ECC	Envelop correlation coefficient
FCC	Federal Communications Commission
FEM	Finite Element Method
GSM	Global System for Mobile Communications
HFSS	High Frequency Structure Simulator
IEEE	Institute of Electrical and Electronics Engineering
IMT-A	International Mobile Telecommunications-Advanced
IoT	Internet of Things
ITU	International Telecommunication Union
ITU-R	International Telecommunications Union – Radio
LTCC	Low temperature co-fired ceramic
LTE	Long Term Evolution
LTE-A	Long Term Evolution-Advanced
MEG	Mean Effective Gain
MIMO	Multiple Input Multiple Output
mmwave	Millimetre wave
NOMA	Non-orthogonal Multiple Access
NR	New Radio
PCB	Printed Circuit Board
RF	Radio Frequency
SNR	Signal to Noise Ratio
TARC	Total active reflection coefficient

UMTS	Universal Mobile Telecommunication System
VNA	Vector Network Analyzer
VSWR	Voltage Standing Wave Ratio
Wi-Bro	Wireless Broadband
Wi-Fi	Wireless-fidelity
WiMAX	Worldwide Interoperability Microwave Access
W-LAN	Wireless-local area network

1 Introduction

"Antennas are the eyes and ears of wireless communication."

-- John D. Kraus

1.1 Introduction

The journey of wireless communication began in the pre-cellular era (1921 to 1980), marked by the initiation of mobile communication through electromagnetic waves. Earlier telephone network faced challenges such as handoff and limited coverage [1]. The World War II in 1940, encouraged advancements in radio communication, leads to the extensive development of integrated network handheld devices. This revolutionized mobile communication marked as the cellular era. In the last two decades, there has been a significant transformation in communication technologies [2].

These systems owe much to the development of MIMO antenna technologies, acting as an essential pillar that has propelled the technology to remarkable heights and emerged as a pivotal game-changer, enhancing the capabilities and efficiency of wireless networks. The world has witnessed this transformation through advanced communication technology like 5G, that reshaped the deployment of various MIMO structures and enables a wide range of communication possibilities. At present, the demands for robust internet connectivity with high data rates has become crucial for global economic growth and the digitalization of cities. The evolution from 1G to 5G, with each generation offering improved data rates and service quality as shown in figure 1.1. The 1G supported only voice, while 2G introduced GSM, the first global standard. 3G adopted IMTS, enabling faster downloads and separate voice/data channels [3]. Enhancements like 3.5G, 3.75G, 4G, and LTE-Advanced (LTE-A) further improved speed, latency, and capacity [4]. Growing internet demand led to 4G, which uses VoIP for efficient data management [5]. The 5G, aims to address the increasing necessity for faster data rates. This wireless communication technology enables seamless wireless communication between individuals and machines, emphasizing high data rates and expected to integrate various technological advancements such as sub-6 GHz, millimetre wave and MIMO communication [6].



Figure 1.1 Evolution of various generation of cellular communications

In near future, more than 100 billion devices are expected to be connected to a global network, requiring high bandwidth and low latency to meet the growing demand for faster data transmission on mobile networks. Moreover, by offering scalability, 5G enhances data transfer rates on wireless networks and is anticipated to meet these demands [7].

Scenario of Mobile Network	Cellular Generation				
Generations	First	Second	Third	Fourth	Fifth
Multiple Access Schemes	FDMA	TDMA	CDMA	OFDMA	OFDMA / NOMA
Duplexing Method used	FDD	FDD	FDD/ TDD	FDD/ TDD	FDD/ TDD
Physical Resources Used	Frequenc y	Time	Time slot /PN code	Time/ Frequency	Time/ Frequency
Key Applications	Voice	Voice/low speed data	Voice/Mid speed data	High speed Data/ Broadband	eMBB, mMTC, uRLLC

Figure 1.2 Cellular Generations

The figure 1.2 displays the different access techniques employed in each generation along with the allocation of physical resources to users and the key applications. The

TDMA and FDMA scheme allocate time and frequency among users whereas in CDMA, multiple users utilize the available spectrum. while, OFDMA employs orthogonality, by employing suitable network to users so as to avoid interference among each other [8]. The OFDMA approach achieves significant spectral efficiency, which leads to better data transfer. Currently, the 5G uses the NOMA technique, which consists of a power domain and a code domain with flexible and scalable time intervals. In addition, the full duplex communication methods such as Time Division Duplex (TDD) and Frequency Division Duplex (FDD) are used. [9].

The primary need in today's cellular communication framework to achieve high data rates (in Gbps) and a widespread spectrum of 5G, in conjunction with MIMO (Figure 1.3). The 5G-IoT in integration with MIMO has applications, like Augmented Reality, video streaming, smart cities, e-health monitoring, (AI) artificial intelligence, machine and deep learning, distant monitoring and several value-added services etc. All these applications require huge amount of data and higher bandwidth [10]. A 5G technique which is used in developing a popular IoT will require MIMO array antenna and it is both challenging and interesting to note 5G mobile communication devices use a single element MIMO as well as multi-element MIMO array antenna [11]. This unique combination of MIMO array antenna for IoT and 5G communication which will make the system more efficient. The MIMO antennas can significantly enhance communication capacity in sub-6 GHz bands by employing multiple antennas at transmitter and receiver which improves the communication range up to Terahertz (THz) and results in wider channel capacity [12].

1.2 5G Technology and its key capabilities by ITU-R

Due to the widespread use of wireless technology around the world, there is a need for 5G wireless communication equipment’s to accommodate increased traffic [13]. To address the issue, wireless local area networks (LANs) are spaced only a few hundred meters apart are installed at various locations as these devices offer rapid data speed in gigabits per second (Gbps) range, minimal delay, efficient radiation, quality of service (QoS), broader bandwidth, polarization, and reduced power consumption. Figure 1.4 outlines some prominent characteristics of 5G [14].



Figure 1.3 Key applications of the 5G [4]

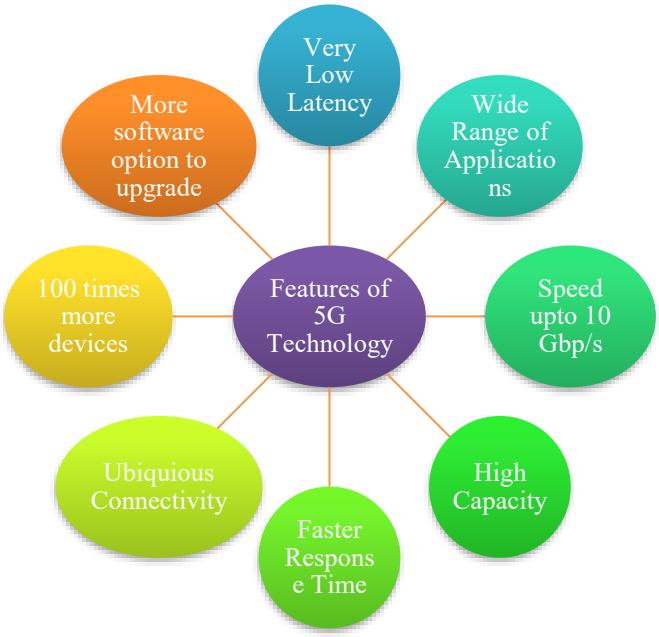


Figure 1.4 Key features of 5G

Additionally, ITU-R stated two primary spectrums used by the 5G system: mm-wave (> 6 GHz) and sub-6 GHz (< 6 GHz). The 3rd generation partnership project (3 GPP) has released a new standard for 5G communication [15]. They have introduced NR bands, namely n77, n78 & n79 operates within the frequency ranges of 3300–4200 MHz, 3300–3800 MHz, and 4400–5000 MHz respectively. Moreover, several nations

employ the frequency bands FR-1 (3.4–3.8 GHz) and FR-2 (24.25–27.5 GHz) for 5G communication [16].

The 5G-enables real-time machine control using mobile devices through device-to-device (D-D) and appliance-to-appliance (A-A) approach. The key capabilities investigated by ITU-R by considering IMT 2020 and 3-GPP standard are, massive machine-type communications (m-MTC), ultra-reliable low-latency communications (u-RLLC), and enhanced mobile broadband (e-MBB) [17-18].

1.2.1 eMBB: The primary goal of eMBB is to offer rapid data transmission with the ability to dynamically and adaptively distribute information in real-time. Additionally, it facilitates the services such as augmented and virtual reality.

1.2.2 uRLLC: It improves the latency to minimum of one millisecond and has applications in smart transportation, industrial automation, public safety, e-health etc.

1.2.3 mMTC: It provides a wide range of internet enabled devices and provides various applications like IoT based smart farms, smart cities, advanced power grids and many more.

1.3 Planar Monopole Antenna

The wireless communications technology would not have advanced to this point without antennas. As per the IEEE, Antenna term is explained as a device used for radiating and receiving radio waves. Therefore, the growing popularity of wireless devices requires high performing antennas owing to properties like compact, lightweight, and low-profile without compromising characteristics [19].

In communication systems, the primary concern is to develop a compact, and versatile antenna that seamlessly integrates with portable devices [20]. This section elucidates the fundamentals of planar monopole antenna. The monopole antenna comes into existence when one arm of a dipole is halved which replaces infinite ground plane. The setup primarily consists of a short wire, 'l' in length, positioned above an infinitely large ground plane. The monopole is placed over a metallic ground plane, which transforms into a dipole antenna. The EM field of the monopole antenna, positioned above the ground plane can match with the dipole. The long monopole radiator is notable for its lack of radiation below the ground plane and ability to effectively match a 50 Ω impedance. As a result, it effectively connects to a feed point and ground plane.

The requirements of forthcoming communication system necessitate antennas capable of operating across multiple bands with wide bandwidth while ensuring cost-effectiveness and optimal performance. Planar monopole antennas have emerged through the replacement of the wire component in traditional monopole antennas with a planar element. These antennas offer considerable advantages owing to their planar structure, cost-effectiveness in fabrication, compact size, lightweight design, and seamless integration, making them highly suitable for a variety of wireless applications [21].

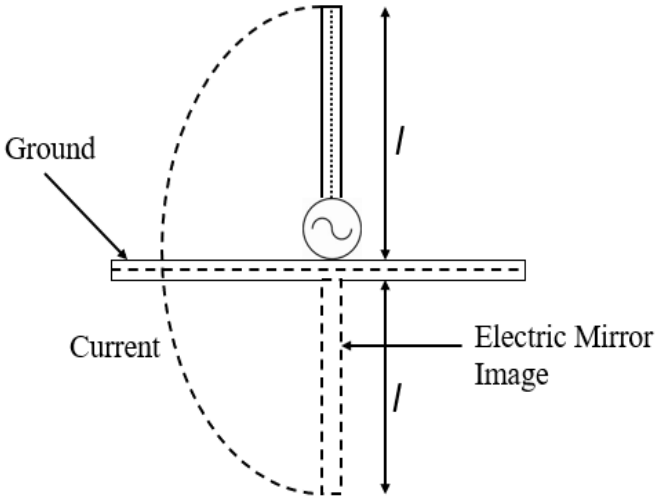


Figure 1.5 Monopole Antenna

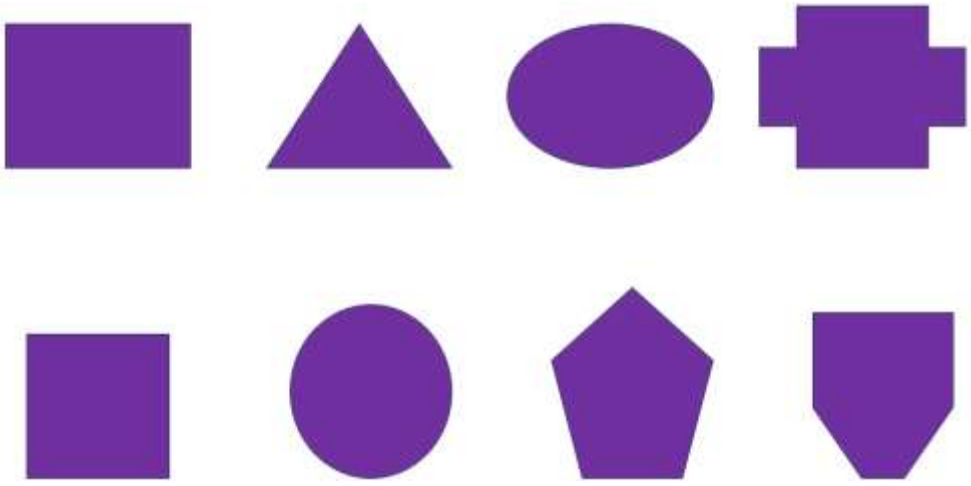


Figure 1.6 Different planar monopole radiator shapes

Unlike conventional monopole designs, planar configuration offer variations such as rectangular, triangular, elliptical, square, cross, circular, pentagon and corner

etched shapes, contributing to increased surface area. This increased surface area directly influences the bandwidth capacity and reliable radiation properties. Hence, in this design approach a planar monopole is considered as the primary radiating component for the sub-6 GHz 5G system [22]- [24].

1.4 Multiple Antenna Features and Types of MIMO

Across the world, cellular communication technology uses MIMO systems on an extensive scale. Hence to improve performance and reliability, MIMO system requires a plenty of antennas on the transceiver link. Figure 1.7 (a-d) illustrates various configurations used in transmitter and receiver antennas. Previously, 5-G predominantly utilizes MIMO technology to meet the demands of high data rates within constrained bandwidth and power limitations. MIMO technology utilizes numerous antennas for trans-reception, resulting in improved performance and reliability. The objective is to enhance the data rate by utilizing numerous antennas while operating within the constraints of restricted bandwidth and power levels.

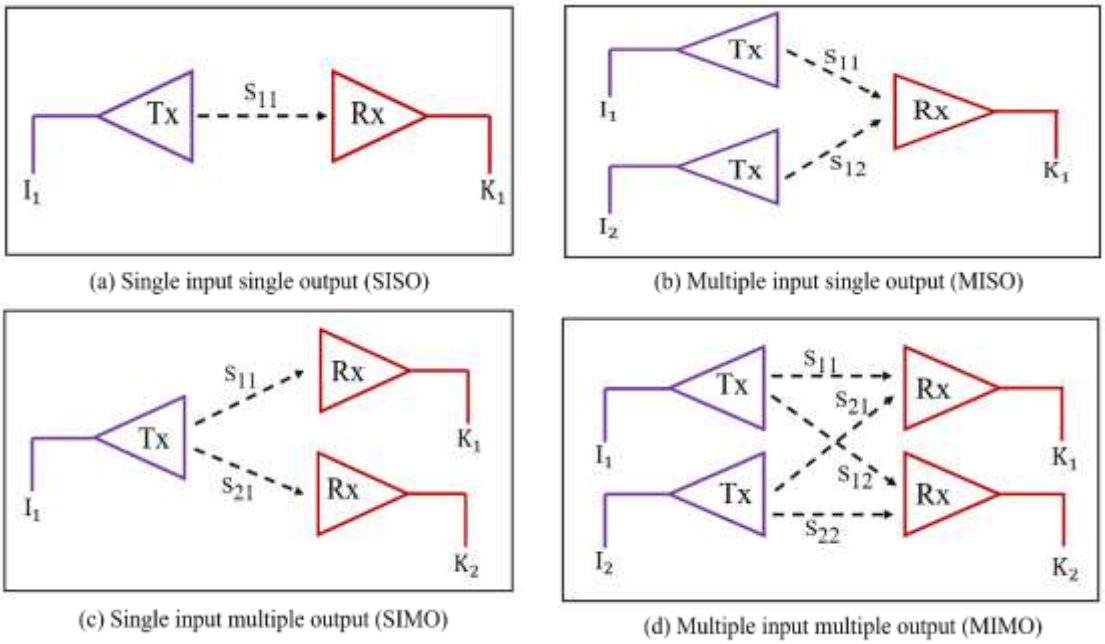


Figure 1.7 Different MIMO configurations [26]

According to Shannon and Nyquist's, the channel capacity rate in a multipath environment is proportional to the amount of trans-receiver antennas [25]-[26]

$$Cc = B \log_2(1 + m \times n \times SNR) \quad \text{----(1)}$$

Where, Cc represents the channel capacity; B indicates the bandwidth; m & n

indicates transmitter and receiver antennas, and SNR signifies signal to noise ratio. This provides insights into various MIMO antennas design and their inherent characteristics which makes MIMO technology as an important candidate for consumer electronics.

1.5 Necessities for sub-6 GHz 5G MIMO antenna

MIMO deploy its services on extensive scale for the cellular communication as well as for the base station antennas. This widespread deployment caters to numerous autonomous terminals globally. MIMO involves two or more antennas for trans-reception on transmission channel. This inclusion enhances performance through approaches like spatial multiplexing and diversity MIMO array antennas in 5G involve a substantial number of antennas at base station. Their functionality is designed to operate efficiently with numerous terminals, employing the principle of spatial multiplexing [27]-[28]. The fundamental requirements for a 5G antenna are outlined below.

1.5.1 Reflection Coefficient and VSWR

The FCC (federal communication commission) designated frequency spectrum for sub-6-5G band require the designed antenna to demonstrate excellent impedance matching characteristics to ensure a good impedance bandwidth. The impedance in terms of load (Zo) for antenna must match the source impedance (Zi), typically 50 Ω or 75 Ω for maximum power transfer. When the impedances are mismatched, some power is reflected back to the source, generating standing waves and resulting in energy loss. We calculate the energy loss in terms of reflected power using the reflection coefficient [29].

$$\Gamma = \frac{Z_o}{Z_i} \qquad \text{----(2)}$$

$$\text{VSWR} = \frac{1+|\Gamma|}{1-|\Gamma|} \qquad \text{----(3)}$$

The antenna broadcasts all the input power across the entire operational spectrum. Under the most demanding conditions, achieving a VSWR of unity within the operational range is the top challenge. The sub-6 GHz-5G band with 50-ohm impedance match throughout the spectrum poses a substantial challenge. Conversely, antenna impedance matching is accomplished through the utilization of impedance matching

networks. These networks effortlessly transform any impedance to 50 ohms. Nevertheless, as the bandwidth increases, the complexity of designing a matching network grows.

1.5.2 Spatial Multiplexing

Prior to transmission, the spatial multiplexing divides a data with high rate into several data low-rate streams as seen in figure 1.8. This process enhances the data transfer rate. using spatial multiplexing, multipath fading encounter is possible. The spatial multiplexing used in MIMO can serve many terminals for the integration of various application those are associated with 5G-IoT. MIMO technology enhances channel capacity by employing multiple antennas to allow simultaneous communication with a base station using the same frequency [30].

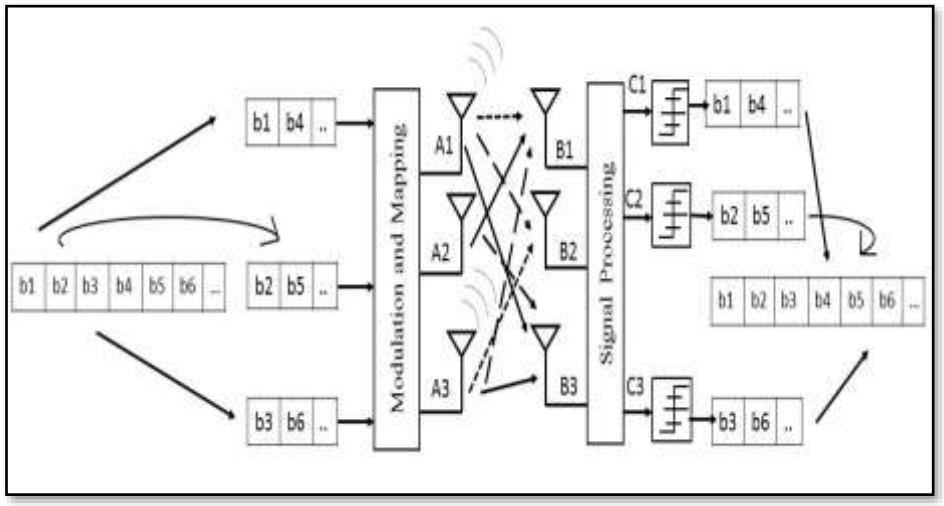


Figure 1.8 Data stream transmitted through spatial multiplexing

1.5.3 Multipath Diversity: Multipath propagation causes attenuation, phase delay, time delay, and other factors that result in multipath fading as shown in figure 1.9. The MIMO antenna can mitigate the effects of multipath fading in situations with substantial scattering [30].

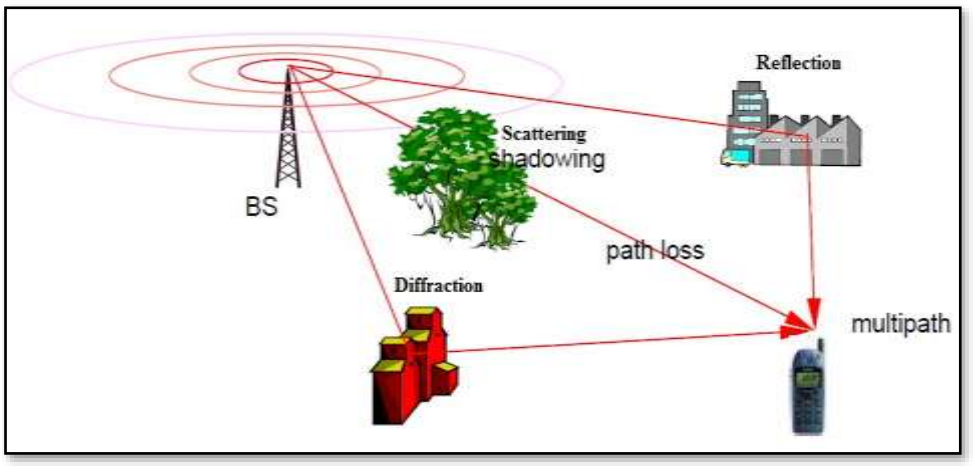


Figure 1.9 Multipath diversity [30]

1.5.4 MIMO Performance Parameters

The MIMO antenna performance is evaluated using Isolation, ECC, DG, TARC, CCL and MEG [31]. These characteristics are stated as follows.

I. The ECC provides the correlation between a practical MIMO antenna. Its computation involves the utilization of scattering parameters with the resulting value being dependent on the radiation efficiency. The ECC is considered as acceptable when it attains a value of 0.5, as required [31], [32].

II. Antenna coupling plays a crucial role in energy consumption, especially in MIMO systems where numerous antennas are positioned closely. For instance, when one antenna transmits a signal and the receiving antenna on the other side picks it up, the adjacent antenna may absorb energy. To achieve a sufficiently favourable ECC and robust MIMO diversity, it is imperative to maintain better isolation and correlation.

III. Diversity is calculated using 4×4 antenna combination, the transmitter obtains data in the form of streams from different paths. To achieve an improved SNR value, the signal must maintain a sufficient SNR at the receiving end. By lowering the correlation coefficient value, the diversity enhances.

IV. To calculate MIMO metrics like bandwidth and efficiency may not always be sufficient, particularly when several antennas are operating simultaneously. Then, it becomes a concern for the complete operational bandwidth and efficiency of the antenna systems. Hence, other/alternative methods are

necessarily required to obtain better results based on the antenna characteristics such as TARC [33].

V. The MEG is determined by considering propagation statistics and radiation patterns to estimate the actual power of each element in a MIMO system, particularly in a fading environment [31], [34].

VI. CCL measures the performance of an antenna array within a MIMO environment. For practical MIMO applications, CCL should remain below 0.5 bits/s/Hz across the operational bandwidth to be considered acceptable [31], [35].



Figure 1. 10. Various performance parameter of the MIMO antenna.

1.6 Motivation for the present research

- In recent years, the progress in 5G technology has significantly intensified the focus on creating high-performance MIMO antennas characterized by compact size and high operational frequencies. As a result, there is a substantial demand for devices that claim a modernized structure while remaining cost-effective.
- In the design of diversity antennas, to achieve the antenna miniaturization is critical concern in the given confined space for integration within portable devices like laptops and mobile devices and to expand bandwidth serves as a foremost task for researchers.
- The motivation of this work, revolves around exploring and designing sub-6 GHz 5G MIMO antennas to address complex demands. Therefore, the primary

objective is to broadly investigate the wideband performance of 2-element and 4-element diversity antennas along with packaging. These standards include high data rates, enhanced channel capacity, efficiency, and reduced absorption of electromagnetic waves (EMW) due to their close proximity.

1.7 Research gaps/ Challenges in the Antenna Design

The difficulties associated with designing the antenna are as follows:

1. Current 5G devices require compact antennas, but limited space for multiple elements affects radiation patterns and increases antenna correlation (ECC), impacting performance.
2. The key challenge in the sub-6 GHz band is designing compact MIMO antennas with high isolation (> -15 dB), reduced mutual coupling in 2×2 and 4×4 arrays, and broad impedance bandwidth using advanced decoupling techniques.
3. Another challenge in wideband antenna systems for sub-6 GHz and WLAN 5G applications is electromagnetic interference (EMI). This interference can be reduced using mitigation techniques such as Defected Ground Structures (DGS), ground plane optimization, and Antenna-in-Package (AiP) design.
4. Achieving multi-resonant functionality in compact antennas, which are naturally narrowband, remains a significant challenge. This is often tackled by modifying the ground plane with defected structures like slots or stubs to create multiple resonances without increasing antenna size.

1.8 Research Problem Statement

The objectives of the research are stated as follows:

To design and develop

1. Two element MIMO antennas for 5G (5^{th} generation) applications.
2. Four element MIMO antennas for 5G (5^{th} generation) applications.
3. Antenna-in-package in 5G communication band based on low temperature co-fired ceramic technology (LTCC).

1.9 Design methodology

In this section, the methods employed for designing, fabricating, and evaluating the proposed antennas are explored and the design flow for obtaining desired result is shown in figure 1.11

A variety of approaches have been deployed to address the electromagnetic challenges which includes techniques such as analytical techniques (e.g., by the separation of variables, series expansion, conformal mapping, integral solutions and more) as well as numerical methods (such as the transmission-line modelling (TLM), finite element method (FEM), and finite difference method (FDM)).

To solve the EM field problems at high frequencies presents greater difficulty when using analytical techniques in comparison to numerical methods. While, integral equation and differential equation approaches are typically used to solve electromagnetic (EM) wave problems. Researchers commonly use FDM, MoM, and FEM due to their systematic approaches, precision, and ability to tackle complex problems. Nevertheless, the finite difference approach is not well-suited for situations that include complex geometries.

On the other hand, MoM can effectively handle arbitrary structures, even those with highly intricate features. It proves valuable in addressing a wide range of electromagnetic problems, including radiation from slender wire antenna elements and their array configurations, scattering phenomena, and the analysis of microstrip antenna components and lossy structures. Despite its capabilities, MoM generates dense matrices, demanding additional storage resources and extended computational time. While MoM and FDM are more straightforward and easier to program than the FEM and FEM emerges as a potent, widely used, and versatile numerical technique for tackling intricate problems such as large and complex structures within inhomogeneous media.

In FEM, the extensive computational structure is divided into smaller finite element structures, which may include triangles, rectangles, tetrahedrons, and hexahedrons. As a result, FEM provides greater accuracy when compared to methods like MoM and FDM. Among these, FEM excels in terms of precision and systematic approximation of complex structures [36]. Accordingly, in this thesis, all structures are simulated and optimized using the FEM-based EM simulator known as High-Frequency Structure Simulator (HFSS).

The HFSS simulator simplifies the calculation of proposed antenna parameters, including VSWR, radiation efficiency, peak gain, radiation parameters, surface current distributions, S-parameters, and many more. Moreover, it allows for the easy extraction

of other parameters like Admittance (Y), impedance (Z), and 3-D EM near/far-fields. Additionally, the tool provides access to different port which helps in accurately simulating coplanar and microstrip lines. The HFSS simulator includes an optometric feature that proves highly useful for antenna designers, allowing them to optimize antenna designs for desired results.

The procedure for designing the HFSS simulator's structure is described in the stages as follows.

- Select the solution type and establish prototype units (cm, mm, etc.).
- Utilize the available drawing tools to sketch the proposed structure.
- Allocate boundaries to the created objects.
- Employ a suitable port excitation scheme to stimulate the design structure.
- Construct a radiation boundary filled with air, typically used for radiating structures. The size should align with a quarter of the wavelength.
- In analysis setup, specify frequency and number of passes. Moreover, configure a frequency sweep and set the start-stop frequencies.
- Authenticate the structure and conduct analysis within the specified range.
- At last, generate simulation output for different parameters including efficiency, S-parameters, VSWR, peak gain, efficiency etc.
- At microwave range of frequencies, a high-precision antenna fabrication is crucial. As a result, we employed the photolithographic method, milling machine techniques, and the MITS Eleven PCB prototype machine is used to create the proposed antennas. The front patch and ground plane are fabricated on a substrate (FR-4 material), with thickness of 1.6 mm. The antenna characteristics are then computed by a Rohde & Schwarz ZVL series VNA. We observed several parameters including S-parameters, gain CCL, radiation efficiency, MEG, TARC, diversity gain, ECC etc. in the frequency band of 9 kHz to 13.6 GHz.

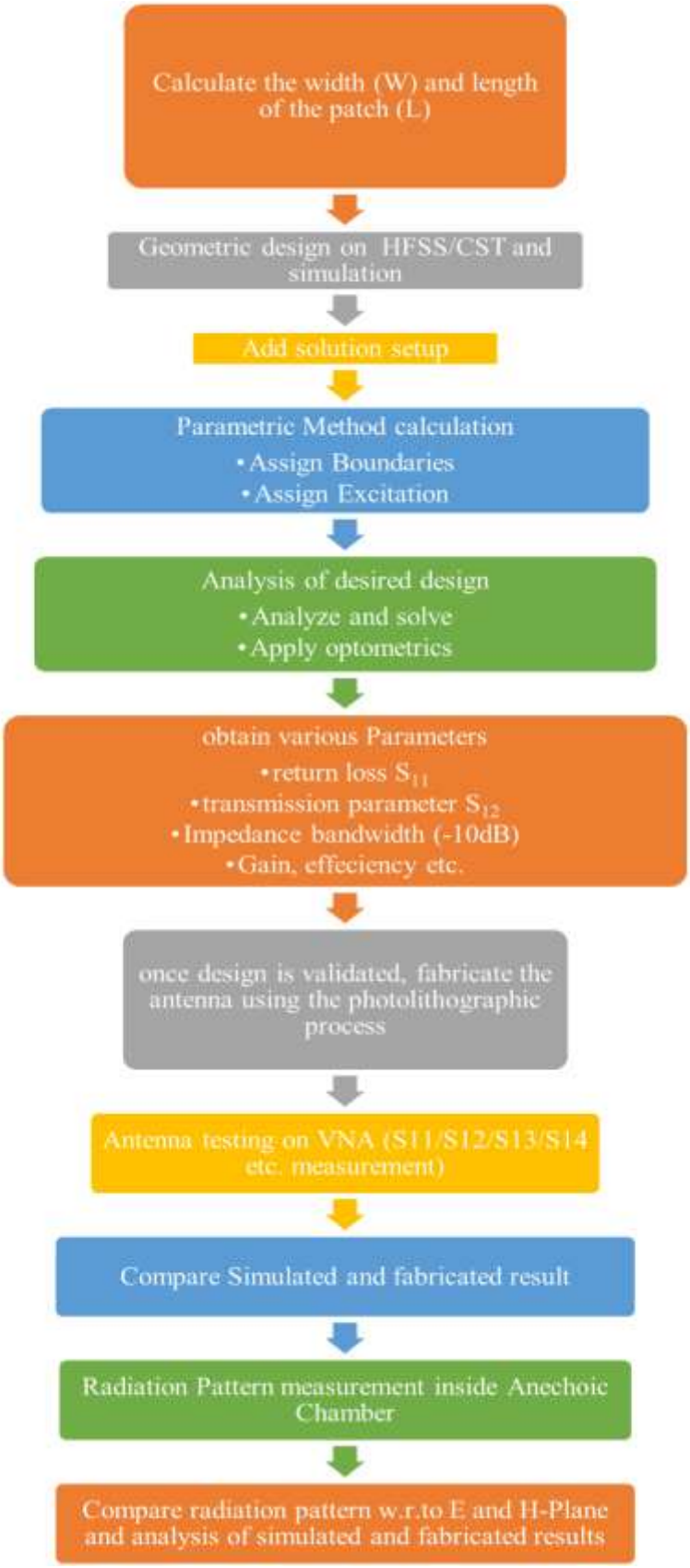


Figure 1.11 Process design flow for obtaining desired result

1.10 Thesis Organisation

The work of this thesis has been divided into the following six chapters:

Chapter1 presents the introductory section of the thesis and concise overview of 5G MIMO technology outlines the motivation for the study and provides an outline of the thesis structure.

Chapter 2 delves into the current state of the art in this field. In this literature review on various 5G narrowband and wideband MIMO antennas with multiple element antennas for 5G NR band and wide band is presented and summarized.

Chapter 3 introduces a compact and effective 2-element MIMO antenna built for the sub-6 GHz 5G (NR) frequency spectrum. The proposed antenna has dual element with ground of an inverted T-typed. We conduct an analysis on various antenna attributes like S-parameters, ECC, efficiency, DG, TARC, realized gain, current distribution, and radiation patterns.

Chapter 4 discusses the quad element patch MIMO system arranged in face-to-face method with adequate spacing between antennas so as to progress necessary mutual coupling. The enhanced structure consists of inverted T-shape partial ground and square type patch with stub elements on both sides to enhance impedance matching. Also, the role of twin stub and rectangular notch on top right corner of patch is discussed.

Chapter 5 discusses the implementation of a modified rectangular U-shape radiating element in a microstrip-fed antenna system. The MIMO antenna utilizes an asymmetrical strip line to enhance isolation, together with a partially grounded and parallel metal strip line on the ground side to enhance mutual coupling. This quad-port MIMO device functions in the sub-6 -5G bands, as well as the 5 GHz WLAN bands. We evaluate many characteristics like ECC, reflection coefficient, mutual coupling, DG and TARC. Moreover, the investigation to validate the housing effect by utilizing a diverse range of materials was carried out.

Chapter 6 summarizes the thesis work done through comprehensive research carried under three different work chapters as well as explores the potential avenues for future research.

1.11 Summary

This chapter provided a concise overview of 5G technology, followed by a detailed examination of several MIMO antenna. This chapter also summaries the motivation and challenges underlying the current investigation. Essentially, this chapter presents a comprehensive and exhaustive overview of the thesis. The next chapter provides a concise overview of 5G monopole and MIMO antennas.

2

Literature Review

" Effective antenna design demands careful impedance matching and minimal losses."
David M. Pozar

2.1 Introduction

This chapter includes a comprehensive exploration of various and widely adopted 5G antenna technologies intended for deployment in 5G mobile devices, WLAN, and diverse IoT applications like smart devices and smart houses, etc. Adding 5G to the IoT is the most difficult communication systems because it has its specific regulations about fast data transfer, more efficient channels, and reducing the effects of electromagnetic (EM) waves. To boost performance during transmission and reception, the use of MIMO technology involves many antennas at one or both ends of a communication link. This technology provides spatial multiplexing diversity and also helps to increase communication range. As the numerous wideband MIMO designs are available, incorporating both omnidirectional and directional patterns. The chapter presents 5G MIMO design approach to improve diversity gain and provide sufficient data rate. Further, a widely used printed design is surveyed, which includes tapered, circular, hexagonal, semi-circular, and elliptical shapes, as well as tuning stub antenna design, including T-shaped, fan-shaped, rectangular, and DRA-type structures [10].

In the year 2020, Kumar et al. [37] presented the various substrate materials used, as listed in figure 2.1. The antenna design includes a printed and planar monopole, a square monopole, and other types, such as circular, elliptical, trapezoidal, and PICA (planar inverted cone type antenna). Another popular approach to design is to use slot-on patches, periodic structures, stub lines, and hybrid techniques. Generally, 5G, WLAN, and WiMAX are compatible with these techniques. The antenna's primary requirement is a wide bandwidth with an improved radiation pattern and efficiency, but the antenna design confronts difficulties in terms of size, integration, and shape, making it unique. Choosing materials with lower loss tangent and permittivity values enhances gain, efficiency, compactness, and bandwidth [38]-[39]. Therefore, by utilizing a quarter-wavelength line, we examine conventional microstrip configurations, such as

monopoles and dipoles. These devices are simple to design and manufacture, but they require a large ground plane. However, opting for materials with low permittivity might be expensive and dependent on their availability. The high-permittivity materials greatly enhance the return loss. Additionally, the antenna specifications, substrate material, and dimensional restrictions are the key factors for the development of the compact antenna [40, 41].

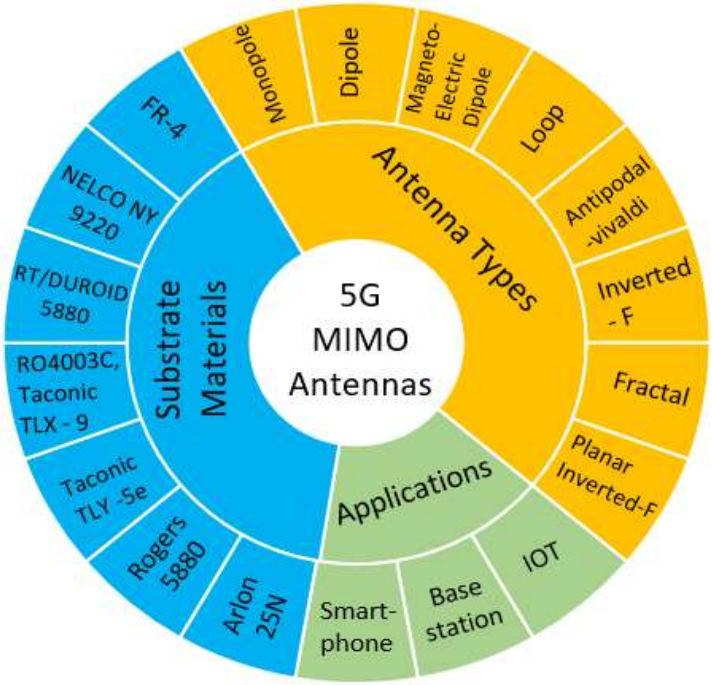


Figure 2.1 Pictorial representation of 5G MIMO antenna with substrate materials, antenna types and application

2.2 Review on performance enhancement technique of MIMO Antenna

Nadeem and Choi [42], presented a survey consisting of diverse techniques for enhancing isolation and mutual coupling. The minimum mutual coupling requirement between closely located antennas ranges from -17 dB to -20 dB. Below this value, the mutual impedances can cause antenna mismatch, thereby affecting radiation efficiency. Techniques such as DGS and CSRR can produce a broad frequency band with lower ECC. The neutralization lines (NL) provide significantly enhanced isolation, and the use of parasitic or slot elements reduces antenna size while improving ECC and efficiency [43]. Additionally, the decoupling networks use simple structure but advanced performance. As the DRA is considered inefficient in terms of area and

complexity compared to printed antennas, but metamaterial-based antennas offer superior performance with the drawback of costlier fabrication [44- 46].

Ullah and Tahir [47] presented the planar monopole array with a feeding network consisting of T-typed junctions. The array is constructed using a Rogers RT/Duroid 5880 substrate with dimensions of 40 × 15 mm^2. The helical monopole antenna array and hexagonal parasitic patches are used to reduce inter-element coupling and surface waves; the overall bandwidth performance gets better. This leads to a peak gain of 11.5 dBi and radiation efficiency of 83%.

Azim et al. [48] developed an LTE-based planar antenna using stepped patch and slots within patch, has a broad frequency range from 3.15 to 5.15 GHz. The resulting antenna demonstrated an impressive 80% radiation efficiency and maintaining an omni-directional pattern. However, the antenna's peak gain of 2.6 dBi falls short compared to antenna proposed by Li et al. [49], which meets the requirements for optimal performance in wireless applications for the frequency range of 1.68 to 3.92 GHz (SWR ≤ 1.5) and high isolation (> 25 dB), but the challenge lies in the design requiring a smaller and better feed-network integration to stay competitive in future deployments.

Ling & Li [50] proposed an antenna with minimal mutual coupling that covers WLAN and portable wireless device bands 5.8 GHz and 2.4 GHz. This MIMO consists of dual-band, two element monopole antennas connected back-to-back and fed with a transmission line suitable to cover WLAN and portable wireless device bands at 2.4 GHz and 5.8 GHz, but isolation was not adequate enough.

Wang et al. [51] recommended building a MIMO with a decoupling system to enhance isolation through a back-to-back connected slot. To obtain the WLAN band, a microstrip and a meandered branch structure feed a folded monopole onto a substrate. However, the challenge was to reduce size and improve isolation. Further, Yi et al. [52] presented dual-band monopole antennas working at 2.5 and 5.5 GHz that have applications in WLAN and WiMAX. Further, with the use of the miniature double circular split ring slot DGS approach, the port isolation has improved in a printed dual-band monopole array. The findings show a substantial reduction in the mutual coupling.

To improve isolation, Niu et al. [53] suggested an antenna that could separate signals by 34.2 dB at 3.7 GHz and 36.3 dB at 4.1 GHz. It would achieve this by utilizing

a modified antenna decoupling surface (MADS) and an H-shaped defected ground structure (HDGS). The antenna has an overall size of 48.5 × 60.6 mm^2.

According to Tang et al. [54], the antenna has a wide range, a favourable TARC, a wide impedance bandwidth, and acceptable radiation efficiency, gain, and ECC. It has a notched band that covers WiMAX, WLAN, and X-band. The staircase-shaped element is used for decoupling and has slits and radiating slots, resulting in favourable isolation and diversity. The MIMO antenna is 39 × 39 mm^2, has an FR-4 substrate with a constant of 4.4. The ECC is below 0.01, and the CCL is less than 0.4 bits/Hz.

Zou et al. [55] propose an eight-element array with an L-type slot and a U-type monopole, operating in the LTE band of size 150×75 mm^2. The frequency bands FR-1 (2400-2600) MHz and FR-2 (3400-3600) MHz come under the wideband MIMO antenna with good correlation, i.e., < 0.02, and acceptable isolation of ≤ -15 dB with a maximum efficiency of 63% and isolation better than 12.5 dB, operates in the LTE 42/43/46 band. Furthermore, the channel capacity at 20 dB SNR is 38.8 bps/Hz and 39.7 bps/Hz, respectively.

For the wide range of antennas available for 5G-MIMO applications, a compact handheld gadget in limited space, as deliberated by Zhai et al. [56], becomes more challenging. The close connection is susceptible to mutual coupling, which limits the use of array antennas with close-profile elements. Thus, Su et al. [57] proposed an antenna consisting of a compact two-inverted-F-antenna (IFA) system that can integrate a small "Π-shaped" structure cover (2.4/5) GHz WLAN bands by IFAs. The isolation between the IFAs in the 2.4 GHz band exceeds 16 dB in both bands by selecting the appropriate capacitance and inductance.

Xu et al. [58] created a planar monopole with low gain and low radiation efficiency, which they accomplished by attaching U- and T-shaped stubs to the patch. The shared ground feed line enhances mutual coupling. Zhang and Pederson [59] designed MIMO antennas that effectively span a band of 3.1-5 GHz, and achieves mutual coupling below -22 dB. The planned NL placement above the ground plane allows for a small clearance, resulting in a compact antenna area of 35 × 16 mm2 without the need for ground plane modification. A robust microstrip antenna (MSA) is presented by Yue et al. [60] with improved isolation. Furthermore, Tiwari et al. [61] suggested that a narrow strip with isolation enhancement works best with an ideal value

of -22 dB for multiple types of wireless communication. A square-shaped composite right- or left-handed cell is proposed by Sharma et al. [62], also recognized as a composite right or left-handed (CRLH) structure, which offers a level of isolation of at least -15 dB. Despite its enormous size, a hybrid dielectric resonator antenna (DRA) achieves an isolation value of approximately -25 dB in triple bands. Thus, better isolation of an additional -4 dB was provided by Sharma and Pandey [63], who developed the 2×2 antenna with a fractal electromagnetic bandgap (EBG). Additionally, Liu et al. [64] proposed that the design involves numerous IFAs. The antenna's overall dimensions are 140 × 70 × 0.97 mm^3, with an operational range of 3.4 to 3.8 GHz, an efficiency greater than 50%, and the ECC remaining below 0.2 across the band.

2.3 Literature based on performance parameters of MIMO antennas for 5G and WLAN

Gao et al. [65] proposed a 2-element slot-strip array for smartphones and base stations. Today's need for a compact antenna prompts the exploration of large-size antennas using a variety of techniques that ensure moderate coupling. Also, we need diverse antennas like antipodal vivaldi (AV), inverted-f (IF), fractal, planar inverted-f (PIF) and dissimilar loop antenna configurations to meet these 5G needs. We too need antennas that have higher gain and better channel capacity [66]-[67].

With improvements in bandwidth and gain, Chattha H. [68] proposed the two-element 4-port inverted-F antenna design for 5G-IoT applications, which covers a band from 2.7 to 3.6 GHz. The ground plane design includes a rectangular slot under the top plate to improve the antenna's impedance matching and coupling. This stops current flow between ports and boosts mutual coupling, but it covers only partial 5G (NR) bands.

Soltani et al. [69] presented a dual-band MIMO working on WLAN at a frequency of 2.4-5 GHz with two back-to-back slots and a second pair of slits added to achieve better isolation above -14 dB, and in the range from 4.9 to 5.75 GHz, the isolation is above -12 dB. This prototype antenna measures 46×20×1.6 mm^3, achieves isolations greater than 10 dB, and has an efficiency above 50%. The recent development in MIMO antenna design configurations has focused on unique and complex approaches, as discussed in [70]–[73]. The inductor-decoupled high-isolated inverted F antenna introduced by Chen et al. [70], featuring a T-shaped substrate for 5G

applications. This antenna requires improvement in the correlation between antenna elements; also, it is suitable for dual-band operation with an efficiency exceeding 35%. It incorporates the substrate height of 1.4 mm, providing an advantage in terms of display-to-body ratio, isolation over 10 dB, and ECC < 0.3.

A compact antenna is designed by Khalid et al. [71], with a size of 39 × 30 mm^2 for 5G communication, using a Rogers R04350B substrate with an identical dipole and single slot. The four-port antennas use a CSRR with the DGS method. Pattern diversity based on a T-junction improves isolation and correlation. The 4.1 GHz bandwidth and a gain of 8.3 dB, with a channel capacity loss of < 0.4 and an outstanding correlation of < 0.01, are the properties of the projected antenna.

Ullah et al. [72] proposed a monopole L-shaped structure for the 5G antenna in the C band. An L-shaped metallic strip on top of the FR4 substrate is placed, allowing the strip's length and width to be tuned to the desired frequency. The antenna has a peak efficiency of 82%; it deteriorates to 19% in the multiband. According to Chen et al. [73], a circularly polarized antenna with an EBG structure and a partially truncated DRA has a maximum impedance bandwidth of 25.9% and works well over a wide axial ratio. Although the projected design attains excellent isolation (> -15 dB).

For 5G applications, Saurabh and Meshram [74] designed a compact MIMO antenna that operates within the sub-6 GHz frequency range, specifically between 3.34 and 3.87 GHz. The MIMO system radiating part is made up of two identical rhombus-shaped parts that are linked together by a tapered microstrip feed line. The structure integrates with the U-shaped stub on the bottom plane to enhance isolation and achieve impedance matching. As a result, there was a noticeable improvement in isolation of -20 dB within the specified frequency range.

Jiang et al. [75] introduced the hybrid decoupling neutralization line (NL) with a ground slot to enhance the complexity of the design. The surface wave coupling and inductive coupling were effectively decreased by the hybrid decoupling structure. The overall efficiency degrades performance depends on the hand effect in close proximity, as the hand is acting as a lossy medium. As a result, due to the various hand and head models, the isolation becomes weaker. The electromagnetic absorption causes a 30% reduction in efficiency and a 40% decline in radiation efficiency.

The antipodal-vivaldi antenna designed by Dixit and Kumar [76], consists of an upper and lower conductor act as a radiator and ground on substrate material. The antenna requires more space [77]-[78] but also provides a wider bandwidth and stable radiation pattern. Comparatively, with good impedance matching and sufficient bandwidth, Darimireddy et al. [79] proposed a densely packed fractal antenna using repetitive behaviour and consistent performance, but design complexity is one of the major constraints.

Parchin et al. [80] proposed an orthogonally placed microstrip antenna using an FR-4 substrate to simplify the design and minimize mutual coupling among elements. Additionally, the mutual coupling between the four pairs of double-fed circular-ring resonators reduces due to the inclusion of rectangular slots beneath each microstrip feedline. This has resulted in an impressive frequency bandwidth ($S_{11} \leq$ -10 dB) covering the range of 3.3 GHz to 3.9 GHz for the smartphone antenna array. The eight uses an L-shaped microstrip structure was suggested by Abdullah et al. [81]. It has an ECC of less than 0.2 and an efficiency of 45–65% in the 2.4–3.6 GHz band. Thus, Ghannad et al. [82] suggested the design with -40 dB of isolation and 9.7 dB of DG with ECC of 0.15. Further, it is stated that a linear array construction with two basic patch antennas demonstrated superior isolation and impedance matching without the need for traditional matching networks.

Ban et al. [83] demonstrated a novel method by utilizing high-permittivity glass (4.4) material for the display. This methodology allows for the observation of the reflection coefficient with and without a display panel. Nonetheless, the technique continues to encompass the operating frequency range that is beneficial in 5G applications, specifically within the 3.3 to 3.8 GHz frequency band. We obtained a correlation coefficient below 0.05 using far-field measurements, which suggests that there is a strong diversity and multiplexing capability among the antenna parts.

Kaushal et al. [84] suggested a better antenna design that uses a ring slot-based CSRR and an L-shaped parasitic element. This gives isolation > -20 dB in the sub-6 GHz band and an efficiency of 82.6%. The only problems are that it is bigger (75 × 150 mm^2) and only covers 3.4-3.8 GHz. Additionally, Jayant and Srivastava [85] said that to get the right antenna performance, ground etching and polarization diversity are used

from a 4 by 4 proximity-coupled microstrip feed MIMO antenna in order to get enough efficiency.

Raheja et al. [86] proposed fractal Koch geometry and CSRR with an elliptical shape loaded with orthogonally placed MIMO and two notched bands. CSRR techniques improve the operating range and eliminate undesired bands (3.5 and 5.5 GHz). The isolation achieved is approximately -22 dB, which indicates strong performance at an operating frequency of 3-13.5 GHz, was enhanced by the use of a slotted edge substrate. However, the cutting slot raises concerns for inter-element isolation.

A group of researchers led by Wu et al. [87] suggested a four-port antenna with a 3×3 EBG structure that can block bands from 5 to 9 GHz and possess diversity properties, with isolation of -17.5 dB. The fractal geometry incorporates a 4-element crescent ring-type slot to achieve sufficient impedance matching, while the FR-4 material with a profile dimension of $60 \times 60 \times 1.6$ mm^3 is employed by the notched band at 4.6 GHz.

For wideband operation, Tirado-Méndez et al. [88] proposed the multilayer drop-type 4-element Kraus method with a photonic band gap (PBG) structure for improved inter-port isolation. A wideband MIMO antenna configuration has four drop-shaped slot antennas that are placed in different layers and perpendicular to each other. They are paired up to stop surface currents from spreading to other radiators.

Srivastava and Mohan [89] showed a wideband MIMO antenna with a staircase-shaped element and many slits that has good TARC but poor isolation. Hence, to improve the isolation, Tiwari et al. [90] suggested a compact neutralisation technique-based MIMO antenna that can work with wireless networks up to 10.08 GHz and has a size of 39×39 mm^2 with -23 dB of isolation. Furthermore, the advancements in MIMO have led to the exploration of numerous methods to improve patch coupling and address the resonance condition. Additionally, Kulkarni et al. [91] proposed wideband MIMO for the NR (n77/n78/n79) 5G band using an EL slot and a protruded UPMS isolation technique. The isolation attained is 17.5 dB with a gain of 3.5 dBi and an efficiency of 85%. But the mathematical modelling is limited, which does not justify the slot width and length.

Keshri et al. [92] proposed the orthogonally placed quad element 30×30 mm^2 compact and high-performance MIMO. The isolation of $S_{12} < -22$ dB and $S_{13} < -23$ dB

is considered excellent performance for MIMO antennas. In the MIMO environment, we expect an arc on the radiator and a modified staircase-shaped ground structure with improved isolation. Amin et al. [93] proposed the semi-elliptical structure using FR-4 material. The four-element UWB antenna can be put together more easily with the help of parasitic resonators and a stub network. Among the various techniques, one of the most effective is the open-slot-based technique, whose length varies with compact shape and size. The various methods discussed by Megahed et al. [94], such as EBG (electric bandgap), DGS (defected ground structure), and NL (neutralisation line), are used in the construction of 5G antennas. The stated EBG provides better isolation due to the capacitance effect, which led to high DG (diversity gain) and efficiency.

For the sub-6 GHz 5G band, Desai et al. [95] proposed a transparent, dual-element MIMO antenna. Here are two scenarios to elucidate the isolation mechanism: In the first scenario, the radiating elements align in the same direction using an unconnected ground plane, and in the second scenario, the antennas are vertically oriented facing each other with a shared ground. We present dual-element MIMO antennas that achieve, a bandwidth of 300 MHz (4.65 - 4.97 GHz) and isolation beyond 15 dB, and it do not utilise any decoupling elements. furthermore, the proposed antenna has an efficiency of 45% and gain of only 1 dBi. However, it still performs well enough for MIMO diversity in both situations. But the limited band was covered. Thus, to improve the coverage, Xi et al. [96] designed the dual-band MIMO antenna tailored for operation within the 5G sub-6 GHz frequency range, specifically covering n7, n38, n41, and n79. A DGS and a slotted stub were strategically employed to mitigate coupling currents between adjacent ports. The measured S_{11} varies from 2.34 to 2.71 GHz and 3.72 to 5.10 GHz, with an improved isolation of 20 dB across the frequency band. However, a peak gain of 3 dBi and radiation efficiency of 62% is attained by the proposed antenna.

Chattha et al. [97] proposed the 5G antenna for handheld applications, which operates in the frequency range of 2.4 to 3.8 GHz. The ground plane etched the slots to reduce mutual coupling among elements, ensuring 30 dB of isolation within the desired frequency band. Additionally, the proposed MIMO antenna demonstrates an improved gain of 5 dBi, and the ECC value remains within acceptable limits.

Rekha and Jino [98] presented the MIMO antenna featuring a four-element design for 5G and WLAN operating within the frequency band of 4.5 to 5.8 GHz. This antenna incorporates parasitic elements to enhance isolation, achieving a notable increase from 20 dB to 45 dB. Experimental testing of the prototype validates the antenna's performance, with measurements corroborated by simulations. This antenna has a notable efficiency of 96% and an average gain of 4 dBi.

Gao et al. [99] presented a 2-port high-gain MIMO antenna designed for 5G applications with dimensions of 190.46 × 56.65 × 0.254 mm^3. The ground plane integrates a hollow T-shaped branch to enhance antenna isolation. With a hybrid series-parallel feeding technique, the achieved gain of 25.75 dBi with nearly 90% efficiency in the designated band. The maximum diversity gain value attained by the antenna is 10 dB and the minimum of 9.89 dB, while, the ECC peaks at 0.022. Furthermore, ECC and CCL verify the MIMO antenna's diversity performance, both falling within the optimal value range as described in [100]-[101]. For outdoor long-range point-to-point wireless relay communication systems, the developed MIMO antenna is used.

Sun et al. [102] proposed a dual-mode decoupling; two meticulously spaced open-slot antennas introduce a connecting line between them. The combined slot antenna pair offers a wide operational bandwidth from 3.3 to 5.0 GHz with S_{11} < -6 dB and S_{21} < -10 dB. The total efficiency varied from 62% to 81%, with an ECC below 0.15. Comparatively, a compact MIMO system with four identical magnetic dipoles housed in a metallic handset has a bandwidth of 3420 - 3500 MHz and a calculated ECC of about 0.31 dB [103].

A study by Addepalli et al. [104] suggested an asymmetrically fed MIMO antenna to increase the bandwidth. It uses a 4 × 4 MIMO with a Calendula radiating patch and a rectangular stub to improve isolation. The antenna works in 3.26-5.18 GHz band and exhibits excellent diversity characteristics, including an ECC below 0.005, a diversity gain close to10 dB, a CCL under 0.05 b/s/Hz, a MEG around -3.0 dB, a TARC lesser than -10 dB in the specified band, a radiation efficiency of 90%, and a gain ranging from 2.50 to 4.50 dBi. Additionally, the same author presented both a 2/8-element and a 2-element antenna, each using a unique approach. The first approach used fractal-loaded patch and protruding T-shaped stub with partial ground for enhanced isolation. The antenna proves better impedance matching and high isolation

>15 dB between ports in 5G sub-6 GHz bands. The key performance metrics comprise ECC < 0.005, TARC <−10 dB, peak gain over 2.5 dBi, and radiation efficiency over 95%, making it an excellent choice for 5G wireless services [105]. In later approach, the antenna consists of two improved V-typed radiators interconnected with feeds and T-typed ground. The 4-element crescent ring type slot and fractal geometry are utilized to create a notched band and an impedance matching at 4.6 GHz with a profile dimension of 60×60×1.6 mm^3. The design reaches over 18 dB of isolation across the entire operational WLAN and 5G-NR band [106].

The current scenario requirement is to develop a miniature MIMO antenna that can support several bands to enable the independent use of 5G NR bands in indoor networks, ensuring smooth transitions. Maintaining isolation between nearby deployed radiators is a significant difficulty for antenna designers since it adversely affects the MIMO's performance metric. Improvements in the isolation between closely spaced antenna radiators have been reported using various methods [107-113].

Table 2.1 Performance Comparison of the Multiple-Input Multiple-Output Antennas for 5G

Ref. No.	Type of antenna technique used	Impedance bandwidth (GHz)	Isolation (dB)	ECC	Max. Efficiency (%)	Channel capacity (bps/hz)
[16]	Dual polarized with compact ring slot	3.4–3.8	> −25	< 0.5	60	-
[55]	L-shaped slot and U-shaped monopole	5–6.08	> -12.5	< 0.15	63	40
[74]	Rhombus-shaped monopole with microstrip line feed	3.34 - 3.87	> -20	< 0.012	92.9	--
[77]	Inverted-F antenna (IFA)	2.4 - 2.48 GHz 5.15 - 5.82 GHz	> -15	< 0.2	Upto 85	-
[80]	Circular ring slot	3.3–3.9	< -18	< 0.005	60–80	35

[81]	Unit monopole open-end slot antenna	2.5 - 3.6	≤ -15	< 0.2	65	34.25
[83]	Coupled fed loop	3.3–3.6	> -15	<0.15	<40	40
[100]	Using quad-element antenna linear array	3.4-3.6	> -12	< 0.3	53	36
[101]	Asymmetrically mirrored gap- coupled loop antennas	3.4-3.6	> -10	< 0.15	52	36
[102]	Closely-spaced open-slot antennas	3.3 – 5	> -10.8	<0.14	52.5 - 83.1	--
[102]	Inverted L-shape monopole	3.3 – 3.7	> -15	<0.1	50 - 75	38.1
[114]	Four element microstrip dipoles	3.45-3.55	>-15	<0.31	40 - 50	15
[115]	Side Edged Framed MIMO	3.25 - 3.75	>-13	0.1	58-72	38.5
[116]	Crown shape radiator with DGS	--	≤ -15	< 0.05	upto 90	--

In table 2.1, the performance characteristics of diverse MIMO works in 5G band is carried out with acceptable isolation and sufficient ECC. In the given table, the respectable isolation obtained in around 20 dB, and the ECC below 0.05, indicating acceptable diversity performance in the case of compact MIMO.

2.4 Inferences drawn from the literature survey:

- The literature review discussed above covers traditional approaches such as electromagnetic bandgap (EBG) cells, dielectric resonators antenna (DRA), complementary split ring resonators (CSRR), and neutralization lines (NL) to suppress mutual coupling in various MIMO antennas for sub-6 and above 6 GHz band. The availability of compact and innovative MIMO array antenna

designs for 5G NR (n77/n78/n79) and WLAN (Wi-Fi 5/6/6E) frequency bands are still limited, which consequently restrict the required bandwidth coverage.

- Designing an efficient broadband antenna for the IoT, and 5G applications remains challenging as achieving broadband coverage without compromising MIMO performance parameters is difficult. While many antennas cover the sub-6 GHz spectrum, often suffer from poor isolation. Additionally, ensuring stable MIMO parameters such as ECC, DG, TARC, MEG and CCL across the entire operating band remains a significant challenge.
- The key issue in MIMO system is the mutual coupling, which refers to the unwanted interaction between closely spaced antenna elements. Although, employing various decoupling structures with different orientation can reduce coupling, but these techniques often tend to occupy additional space and an increase the complexity of the design. Therefore, there is growing need for compact, wideband planar antenna structures that can inherently mitigate mutual coupling without compromising the antenna performance.
- To meet the stringent requirements of the 5G communication system, this work presents a design and development of compact 2-element and 4-element wideband rectangular truncated-corner patch antennas employing an asymmetrical feed along with a staircase U-shaped quad-element MIMO configuration. The proposed structures exhibit wide impedance bandwidth covering n77/n78/n79 and WLAN bands. Further, an enhanced isolation is achieved through a simplified ground plane integrated with stub-based decoupling, thereby eliminating the complex/bulky decoupling networks. The compact design ensures broad coverage and stable performance across desired frequency range, confirming its suitability for next-generation 5G and WLAN applications.

2.5 Summary

In this, we delve into various MIMO configurations and schemes utilized in 5G. It has been observed that the number of antennas at both transceiver end can significantly boost channel capacity. This principle holds promise for integrating diverse applications of 5G and IoT. For 5G, the aim is to achieve sufficient isolation, improved correlation between antennas, maximum efficiency, and ample bandwidth and for the same a

comparative analysis of different antenna techniques is discussed. This literature chapter explores several innovative MIMO antennas designed specifically for Sub-6 GHz applications. However, there remains a notable necessity for further research to develop and refine compact 5G-MIMO antennas with enhanced isolation, aligning with the requirements of modern wireless applications.

This research primarily focuses on investigating, developing, and presenting the analysis and design of novel two- and four-element MIMO antennas operating within the wideband 5G spectrum (under 6 GHz) in the subsequent chapters.

3

High Isolation Compact Two Port 5G MIMO Diversity Antenna with Asymmetrical Feed and Partial Ground Structure

"Antenna design is a balance between performance and practicality."

Constantine A. Balanis

3.1. Introduction

The 5G of portable communication devices is increasingly necessary to meet the demands of the growing traffic on the internet. This reason has led to the installation of cellular systems 1's within a few hundred meters, and wireless local area networks (LANs) have been installed almost everywhere to cater for this need. The devices are attractive, as they have a number of desirable characteristics, such as low delay, a wide spectrum bandwidth, and low power requirement in scattering environments. Also, they offer high trans-reception of data in gigabits per second (Gbps). According to ITU-R, a 5G network is said to have two primary spectrums: millimeter waves and sub-6 GHz. Using 5G networks, mobile networks will be capable of transferring data at faster rates, while they will also be able to scale, be connected to other networks, and be more energy-efficient.

Developing a popular smart-phone and smart IoT device using 5G requires MIMO antennas. Mobile devices of the 5th generation utilize multiple-element MIMO/massive MIMO for wireless communication for base stations and other applications. This scenario occurs due to the increase in capacity gain by using more antennas on the transceiver. The 3rd generation partnership project (3-GPP) has spectrum ranges from (n77: 3.3 to 4.2) GHz, (n78: 3.3 to 3.8) GHz, and (n79: 4.4 to 5) GHz [37]. Designing a compact handheld gadget in limited space becomes more challenging due to a wide range of antennas available for 5G-MIMO applications, and array antennas are close-profile elements restricted by close connections, and the close connections are prone to mutual coupling [56]. Different decoupling techniques (mutual

coupling reduction) have been examined for enhancing isolation between closely located antennas, which improves MIMO performance parameters like ECC, MEG, DG, and TARC [42].

In [55], the proposed 8-element array working in dual-band (LTE 42 and 46) of size 150 × 75 mm^2 with an L-type slot, and a U-type monopole and isolation of >12 dB for 5G smartphones is discussed. The operating frequency ranges from 3.4-3.6 GHz with maximum efficiency of 56% and ECC of 0.1. In [32], the proposed MIMO structure have open ended slots of varying length ranges from 2.40-2.67 GHz and 5.46-5.73 GHz with isolation 20 dB. In [114], two elements symmetric microstrip antenna (MSA) developed on T-type ground and I-type parasitic element for good mutual coupling for sub 6 GHz application. In [69], dual band MIMO slot antenna with two back-to-back slots was designed to operate from 2.4 to 2.5/4.9 to 5.725 GHz. Further, in [53], high isolation antenna with modified H-type defected ground structure (DGS) and array decoupling structure was proposed. In [58], parasitic element-based planer monopole was proposed with low gain and low radiation efficiency. The U and T shape stubs were connected to the patch and feed line with shared ground to improve the gain, efficiency, and the mutual coupling [82]. In [63], the 2 × 2 antenna with fractal electro-magnetic bandgap (EBG) provides additional 4 dB better isolation with simple structure. In [64], the proposed low-profile 8- element Inverted-F antenna (IFA) has repetitive behaviour and orthogonality results in complexity and poor efficiency. To achieve sufficient efficiency, the ground etching and polarization diversity is used for necessary antenna performance [85]. Further, the complementary split ring resonator (CSRR) improves isolation and correlation by pattern diversity [71]. In [60, 115], the robust microstrip antenna (MSA) with improved isolation is presented but it is not suitable for 5G. With the use of narrow strip, the isolation enhancement is achieved with ideal value of -22 dB is used in diversified wireless communication [90]. In [116], the proposed design consists of square shape composite right/left-handed cell i.e., CRLH structure which gives the isolation ≥15. Additionally, the isolation value of < −25 dB in triple band is achieved by using hybrid dielectric resonator antenna (DRA) but, it is enormous in size [62].

The MIMO antenna design is linked with many features of smartphones, base stations, and MIMO communication. As the Compact antenna is today's need but in

[59, 65, 68, 119], large-size antennas are deliberated using various techniques, with moderate coupling and low-frequency coverage. The design and simulation are carried out on the Ansys HFSS, used for optimizing the size and finding results of the antenna with a wideband operation that covers the sub-6 GHz 5G band.

In this chapter, a compact high-performance two-element MIMO diverse antenna for wireless-LAN 5 GHz band and sub-6 GHz 5G(NR) band is presented. The structure comprises of two identical radiating elements with an inverted T-shaped modified ground plane as shown in figure 3.1. This antenna has sufficient bandwidth ranging from 2.92 to 5.72 GHz. The measured and simulated result illustrates that the proposed antenna is suitable for 5G wireless communication.

3.2. Antenna Design configurations and simulated Results

3.2.1. Antenna Design

Figure 3.1 illustrates the design of a 2-element MIMO system. It consists of two identical rectangular radiators placed on the top side and a modified inverted T- shaped common ground structure for isolation improvement. The total size of the designed antenna is only 34 x 20 mm^2. It is composed of a microstructure that fabricates on a FR-4 substrate. This material has relative permittivity, tan-σ and a thickness (t) of 4.4, 0.0025, 1.6 mm, respectively. The two identical patches have square shaped whose length (L_p) and width (W_p) with truncated corners of length (L_1) and width (W_2+W_3+W_4) to enhances the working frequency band. The rectangular stubs attached on both sides of the patch having width (W_3) and length (L_1+L_2) are connected below the patch in order to increase the path of the current by reducing capacitive reactance. The coupling between ground and rectangular stubs helps to shift the frequency band towards the lower side. The ground plane involves a simple rectangular strip of length and width of (L_g x W) and an I-shape strip of width (W_{g1}) and length (L - L_g) attached in the center, which leads to an inverted T-shaped ground. Further, to cover partial 5G bands, a U-shape slot is etched on the rectangular ground of length (L_g - L_{g1}) and width (W_g). To cover all 5G-NR bands, an asymmetric feed principal is used, wherein, the radiating elements are kept aside by (W_{g3}) with reference to the U-type slot. The optimized feed of length and width (L_f x W_f) is considered to attain characteristic impedance (Z_O) of 50 Ω. The table 3.1 shows the optimized dimension.

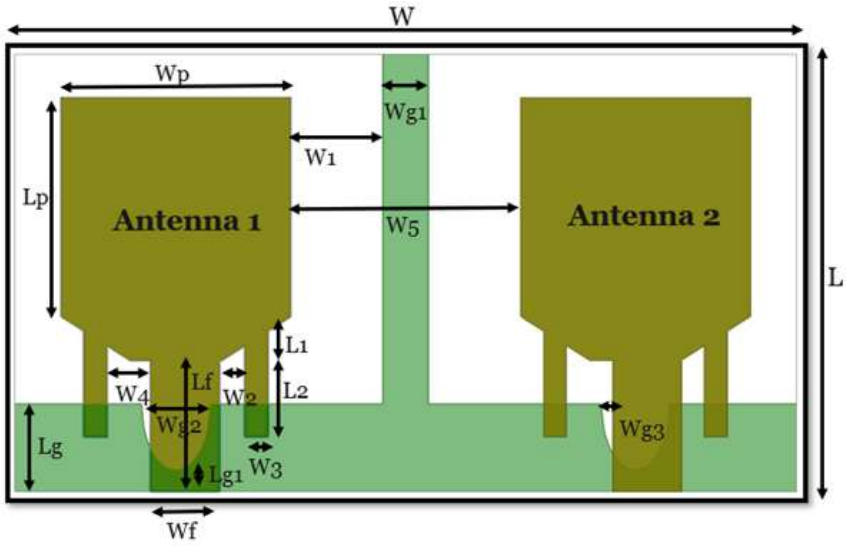


Figure 3.1 Configuration of 2-element MIMO with optimized parameter.

Table 3.1 Design parameter of the two-element antenna.

Parameters	W	L	h	L_g	W_p	L_p	W_{g1}	W_1	W_f	L_f
Unit	34	20	1.6	4	10	10	2	4	3	6
Parameters	W_{g2}	L_1	L_2	W_2	W_3	W_4	L_{g1}	W_{g3}	W_5	
Unit	3	2	3.5	1	1	2	1	0.5	10	

3.2.2. Simulation Results (Scattering Parameters)

The design steps of the antenna transformation from a single to a two-element array are shown in Figure 3.2, which shows a significant increase in bandwidth. Initially, the optimized square shaped monopole fed with a microstrip-line consists of partial ground with dimensions (10 × 10) mm^2 with an asymmetrical feed line. In design-I, the simulated -10 dB impedance bandwidth of a rectangular patch radiator with a partial ground has a reflection coefficient (S_{11}) from 3.04 to 3.54 GHz. In design-II, the modification in a rectangular patch is presented, where the lower ends are truncated, providing a reflection coefficient (S_{11}) from 3.11-3.28 GHz. In both cases, the frequency band covered is insufficient for developing the sub-6 GHz 5G antenna. Further, the design-III consists of an improved antenna structure with rectangle stub lines connected at the bottom side of the patch, and partial ground improves the frequency range which occupies impedance bandwidth from 2.92 to 5.72 GHz suitable for 5G wireless communication. The parameters are the same as listed in Table 3.1.

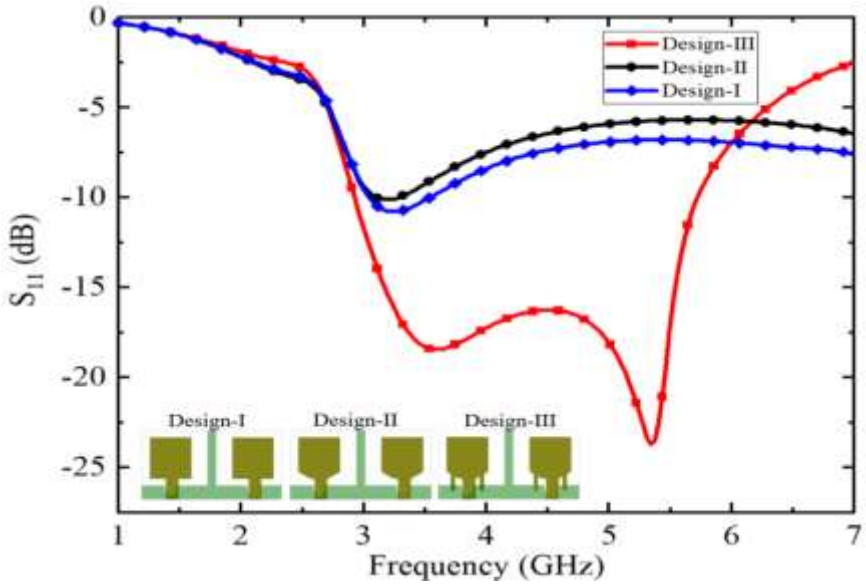


Figure 3.2 Simulated Reflection coefficient (S_{11}) of design-I, design-II and design-III.

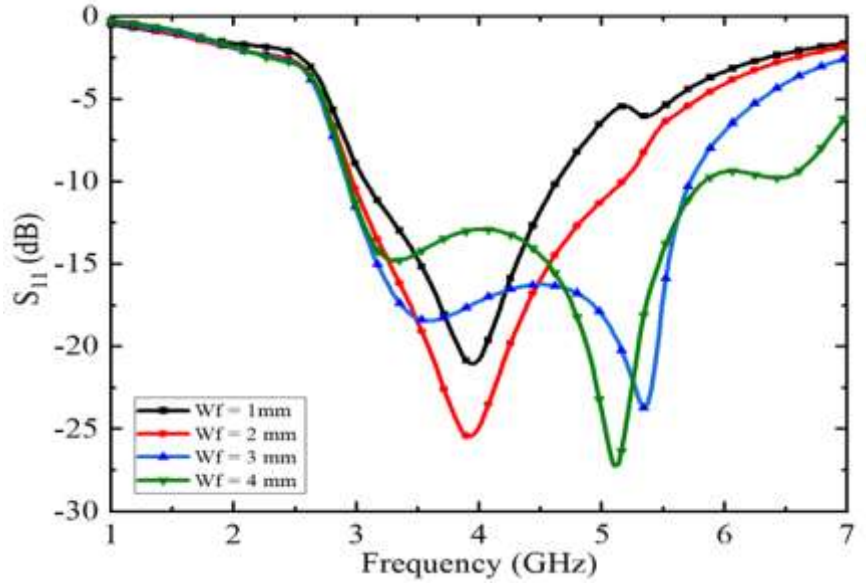


Figure 3.3 Simulated S_{11} versus frequency for different values of Wf.

Figure 3.3. depicts the effect of the width of the feedline on the S_{11} of the designed antenna. It is observed that the change in feedline width from 1 mm to 4 mm mainly improves the impedance matching between 4.5 and 6 GHz bandwidth. Thus, the optimum value Wf is chosen at 3 mm for good impedance matching in the whole band.

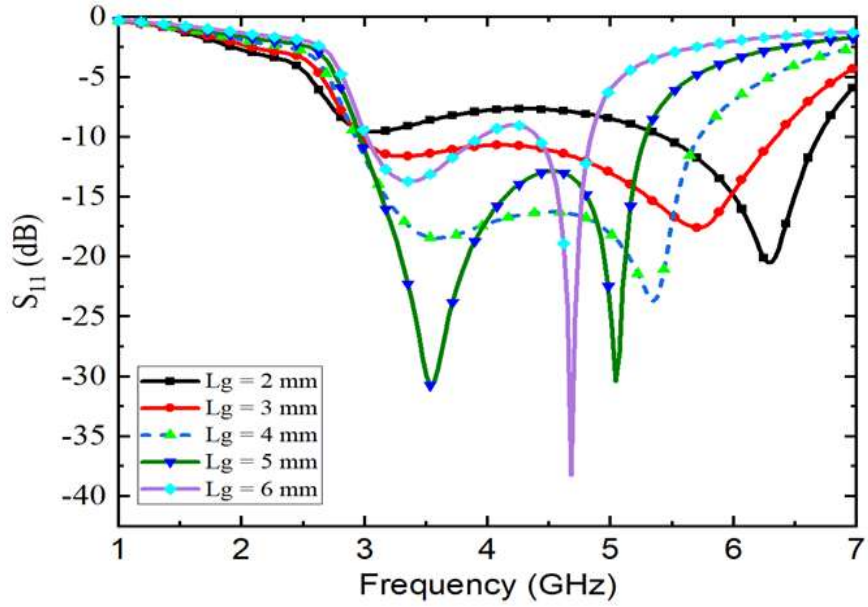


Figure 3.4 Simulated S_{11} against frequency for different values of L_g

Figure 3.4 depicts the variation in the length of the ground (Lg). It is observed that there is unfortunate impedance matching at 2 mm and 3 mm. Further, at 5 mm and 6 mm, a partial coverage of the 5G (n77, n78, and n79) band is obtained. After optimization, for Lg = 1mm, the antenna covers all 5G bands along with the frequency range used for WLAN.

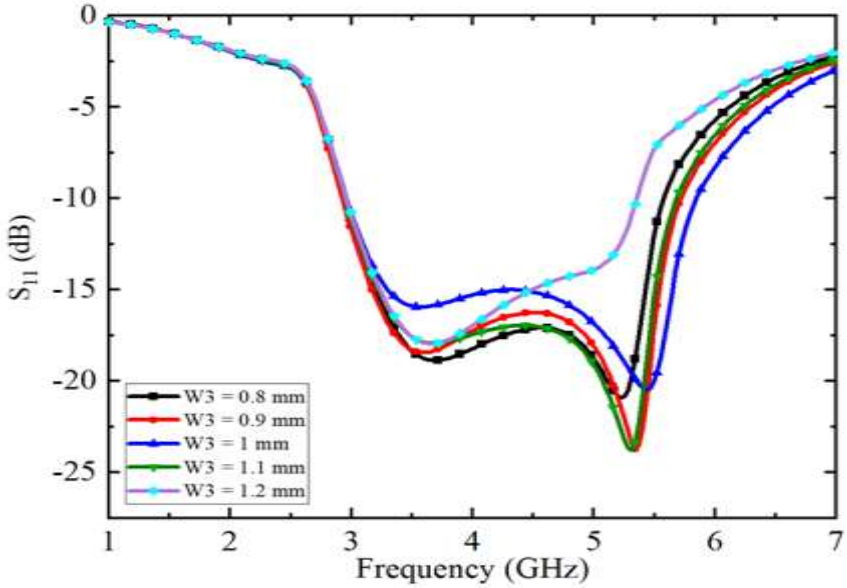


Figure 3.5 Simulated S_{11} against frequency for different values of W_3

From the figure 3.5, it is notable that the width of the rectangular stub line (W_3) designated on either side of the antenna varies from 0.8 mm to 1.2 mm, which provides

a slight deviation in S_{11}. Therefore, W_3 is set to 1 mm, it offers appropriate matching of the impedance and works for sub-6 GHz 5G NR bands. In this way, a wider bandwidth can be accomplished by enhancing the ground length (L_g) and the stub-line width (W_3).

3.2.3 Current distribution

To further realize the effectiveness, the circulation of current on the antenna surface is studied. At the resonant frequency of 4.5 GHz, the distribution is observed with and without an I-shaped stub when port 1 is terminated with a 50 Ω load and port 2 is excited, as depicted in figure 6. The fundamental of this design is to decrease the coupling between neighbouring elements with the help of a rectangular stub connected at the bottom side of the patch so that the generated field will get cancelled between adjoining patches and maintain current integrity by reducing interference using an inverted T-shaped element and hence direct coupling between two antennas is reduced.

Further, the impedance characteristics of the antenna depend on field strength cancellation, which improves isolation among two-element antennas. It is observed from Figure 3.6 (b) that without an I-shaped stub, strong current is coupling between the two ports, resulting in high mutual coupling between the ports.

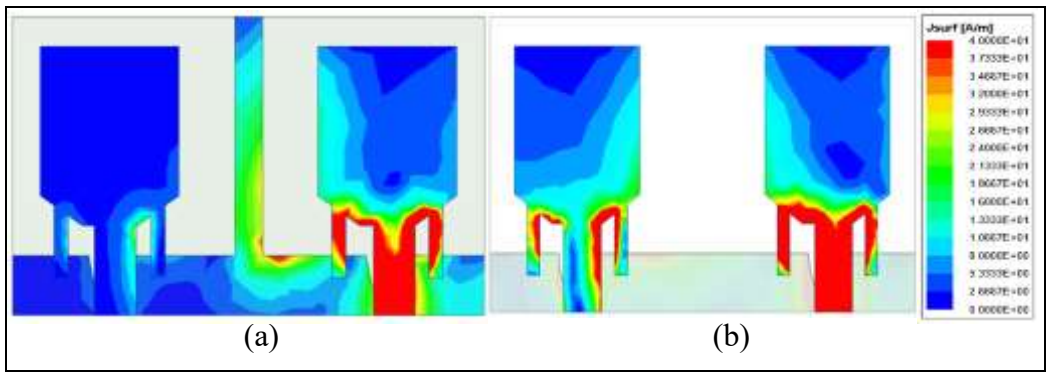


Figure 3.6 Current distributions of the designed antenna, with and without an I-shaped stub, with port 2 excited at 4.5 GHz

With an I-shaped stub, the flow of current is intense on the port 2 feed line accompanied by two rectangular stubs on both sides of the radiating patch, resulting in high impedance and improved isolation, with port 1 match terminated, as observed in figure 3.6 (a). Hence, with the help of an I-shaped stub on the ground, suppresses the coupling current from port 2 to port 1.

3.3 Experimental Results and Discussion

3.3.1 S-Parameters

As antenna's front patch and ground plane are constructed on a 1.6 mm thick FR-4 substrate and using a Rohde and Schwarz ZVL series vector network analyser (VNA), antenna parameters were measured as shown in Figure 3.7.

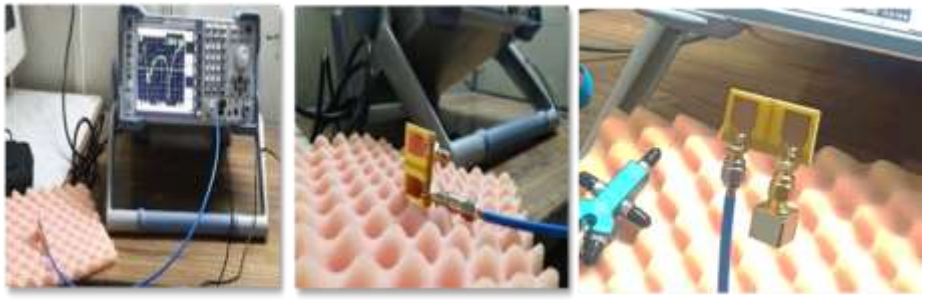


Figure 3.7 Two element MIMO measurement using Rohde and Schwarz vector network analyser

The S-parameter results are obtained as shown in fig. 3.8. The S-parameters show almost similar characteristics with little deviation in the simulated and measured values. The measured impedance bandwidth (3.08–5.72 GHz), i.e., 2.64 GHz is about 5.7% less than the simulated bandwidth (2.92-5.72 GHz), i.e., 2.8 GHz. Consequently, by using an I-shaped structure, the transmission coefficient ($S_{12} = S_{21}$) is measured at port 1, with port 2 match terminated, and vice versa. Moreover, the antenna elements are successfully isolated from one another, with a minimum isolation value of -15 dB obtained throughout the band, which satisfies the 3GPP requirement for sub-6 GHz communication and 5 GHz WLAN. The minimum isolation value of -15 dB was obtained throughout the band, but there is a slight deviation in the simulated and measured value due to manufacture and soldering imperfections, including sub-miniature version A (SMA).

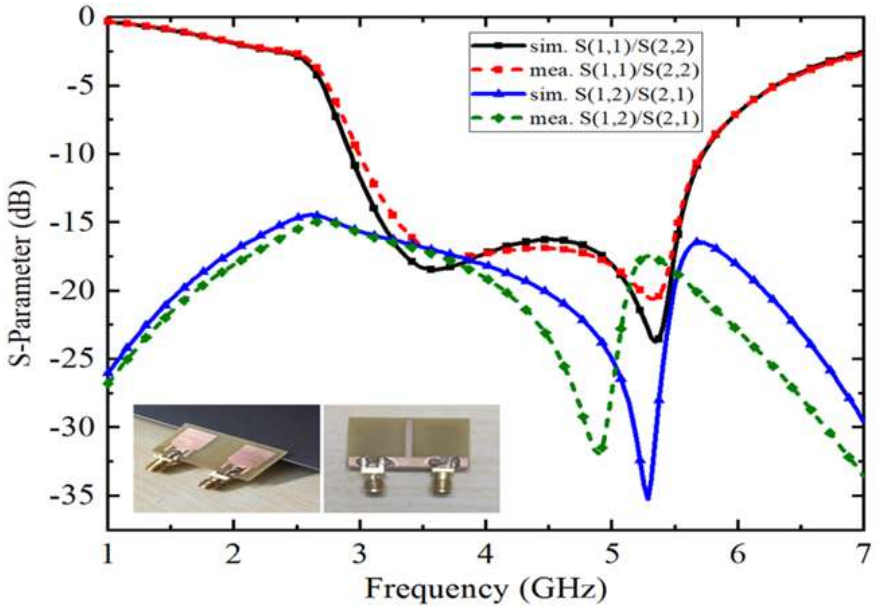


Figure 3.8 Simulated and measured s-parameter of developed 5G MIMO antenna

Table 3.2 Comparison of developed MIMO antenna with recently reported design.

Ref. No.	Antenna Electrical size	Frequency band (GHz)	Isolation (dB)	Design complexity	ECC	Type
[32]	0.20 λ_0 × 0.21 λ_0	2.35-2.69/ 5.4-5.68	< -20	medium	< 0.5	Dual band slot antenna
[53]	0.598 λ_0 × 0.747 λ_0	3.7/4.1	< -20	medium	< 0.01	Improved ADS and H-type DGS
[57]	0.04 λ_0 × 0.30λ_0	2.4-2.48/ 5.15-5.82	< -15	medium	Not given	π-shaped structure with IFA
[59]	0.341 λ_0 × 0.3616 λ_0	3.1 - 5	< -22	medium	0.1	Use of NL with metal strip and circular disc.
[62]	0.3683 λ_0 × 0.5893 λ_0	1.5–2.55/ 3.21–4.0/ 4.59–5.98	< -25	simple	< 0.186	Hybrid antenna with

						circular ring and CDRA
[63]	0.3056 λ_0 × 0.7675 λ_0	2.43–2.50	< -24.67	simple	0.008 7	fractal shaped EBG
[65]	1.01 λ_0 × 1.01 λ_0	1.256-1.272	< -30	medium	< 0.005	a novel decoupling slot-strip array (DSSA)
[68]	0.900 λ_0 × 0. 360 λ_0	2.7 - 3.6	< -25	medium	< 0.009	Two diagonally opposite PIFA
[69]	0.368 λ_0 × 0.16 λ_0	2.4-2.5/ 4.9-5.75	< -14	simple	< 0.3	Series feed with m monopole slot
[82]	0.73 λ_0 × 0.55 λ_0	5.15–5.92	< -30	medium	< 0.15	T type stub and via less structure
[90]	0.245 λ_0 × 0.396 λ_0	3.60–9.35	≤ -22	simple	0.084	Symmetric antennas with neutralization line
[114]	0.55 λ_0 × 0.46 λ_0	3.11–3.78	< -20	medium	< 0.005	Monopole parasitic element
[115]	0.277 λ_0 × 0.253 λ_0	5.9–7.1	< -20	complex	0.005	Mushroom-type EBG with E type decoupling

[118]	0.35 λ_0 × 0.35 λ_0	3.2-3.9	< -20	complex	< 0.0045	Orthogonal bow-tie dipoles and U shape slot
[119]	0.2075 λ_0 × 0.3735 λ_0	2.37-2.64/ 3.39-3.58/ 4.86-6.98	< -15	complex	0.012	Modified square loop with I-shaped slot
[120]	0.312 λ_0 × 0.552 λ_0	3.7 - 4.2	< -21.5	medium	0.003	Hyper NL and DGS
proposed	0.30 λ_0 × 0.51 λ_0	2.92-5.72	> -15	Simple	< 0.02	Asymmetric feed with rectangular stub lines

As, λ_0 is free space wavelength.

Table 3.2 presents an evaluation of various MIMO prototype antennas, taking into account factors such as size, frequency band, isolation, complexity of the design, ECC, and diverse MIMO types. Thus, the designed profile is a miniature-sized two-element antenna compared to other antennas, except [32, 57]. Further, the bandwidth coverage is limited in [32, 53, 57, 59, 62, 63, 65, 68, 69, 82, 90, 114, 115, 118, 119, 120], as the obtained results shows, the presented MIMO operates from 2.92 to 5.72 GHz and covers sub-6 GHz NR bands for 5G communication. The presented antenna has isolation of > -15 using asymmetric feed structure which is greater than other antennas except [82, 65]. In practical case, an uncorrelated antenna must have ECC < 0.5 which is followed in all the above listed antennas and in this design, the desired values of ECC < 0.02, indicating acceptable diversity performance.

3.3.2 Radiation Performance of two element MIMO

The 2-D pattern of designed MIMO in the E and H plane is observed in figure 3.9. During the analysis of radiation pattern, initially, port 1 is excited and port 2 is terminated with 50 Ω load.

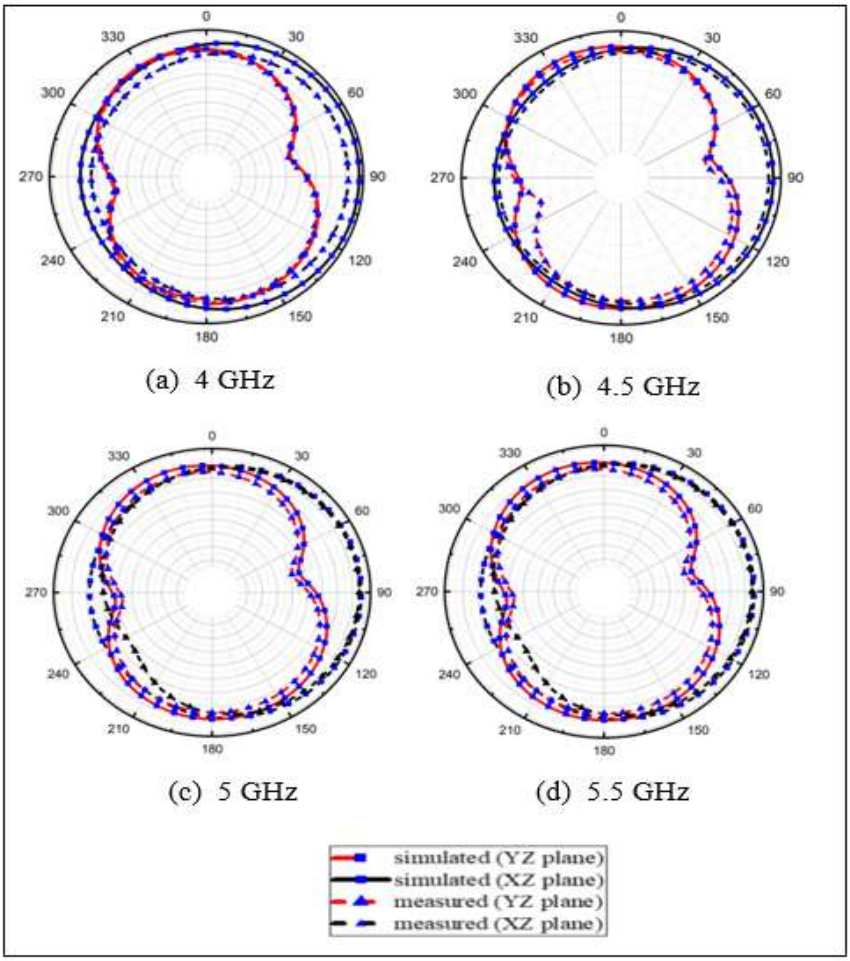


Figure 3.9 Measured and simulated radiation characteristics of 2-element MIMO antenna.

The E plane pattern is out of phase with each other and the H plane pattern is slightly quasi omnidirectional at low frequency, and with high frequency, little deviation is observed due to the interaction of higher modes. Omnidirectional antennas are used in broadcast applications due to electromagnetic (EM) signal radiation/reception from any desired direction. In the radiation pattern plot, the strength of signal at various angles is observed in figure 3.9., typically in the shape of doughnut. The extreme peak gain of 3.11 dB and minimum efficiency of around 86 % is attained. The E plane pattern has attained pattern diversity and is almost bidirectional in nature, proving there is no outside intrusion occurring during reception.

Figure 3.10 shows the realized gain and efficiency of the two-element MIMO antenna. In the entire frequency band, it is observed that the realized gain varies from 0.25 to 3.118 dB and radiation efficiency differs between 86 % to 95.005%.

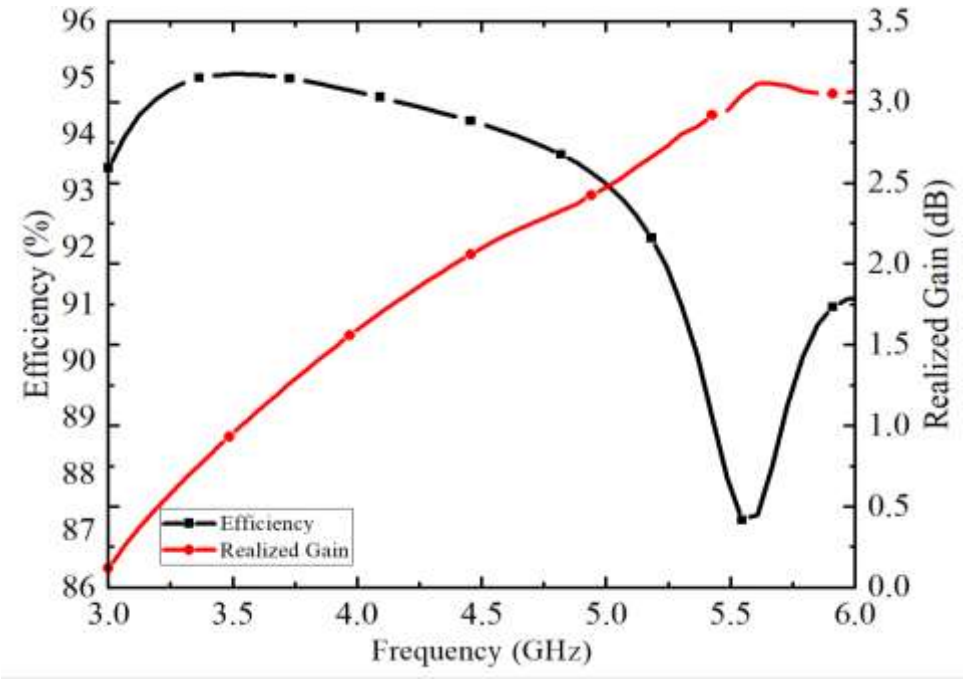


Figure 3.10 Realized gain and radiation efficiency of the 2-Element MIMO antenna.

3.4 MIMO Performance Parameters

We assess MIMO antenna performance according to several criteria, including ECC, DG, TARC, CCL, and MEG. We will examine these characteristics below.

3.4.1 Envelope correlation coefficient (ECC)

The ECC measures the correlation between closely spaced MIMO antennas and it is calculated using scattering parameter and radiation efficiency. As coefficient of correlation is denoted by Greek letter ρ_{kl} and envelop correlation coefficient as ρ_e[48].

If $|\rho_{kl}|^2 = \rho_{ekl}$ i.e., the magnitude of square of correlation coefficient which is equal to the envelop correlation coefficient of k^{th} and l^{th} element therefore,

$$ECC = \rho_e = \left| \frac{|S_{kk}^* S_{kl} + S_{lk}^* S_{ll}|}{\sqrt{(1-|S_{kk}|^2-|S_{lk}|^2)(1-|S_{ll}|^2-|S_{kl}|^2)\eta_{radk}\eta_{radl}}} \right|^2 \quad \text{----- (4)}$$

Where, η_{radk}, η_{radl} are the radiation efficiency and S_{kl} is S-parameter of k^{th} and l^{th} antenna elements respectively. Antenna coupling is a significant performance parameter which gives the idea about consumption of energy in the MIMO due to many antennas that are placed in closed proximity. From the equation 4, it is verified that in order to reach sufficiently good MIMO diversity performance, we must have better isolation and correlation. However, ideally the ECC is zero, but in practical case an

uncorrelated antenna must be < 0.5. The simulated and measured ECC is less than 0.01 and around 0.02 respectively as given in fig. 3.12.

3.4.2 Diversity Gain (DG)

The DG is calculated for n x n combination of antenna, in which the data is obtained in the form of the stream from the various transmitter path. The signal must follow a sufficient SNR value at the other end to get an improved signal strength with minimum attenuation. From equation (5), it is concluded that, the minor value of the correlation coefficient enhances the DG.

The DG of the 2-element MIMO is calculated using,

$$DG = 10\sqrt{1 - ECC^2} \qquad \text{---- (5)}$$

It is seen from the figure 3.12, that the simulated and the measured value of the DG is almost identical and greater than 9.99 dB.

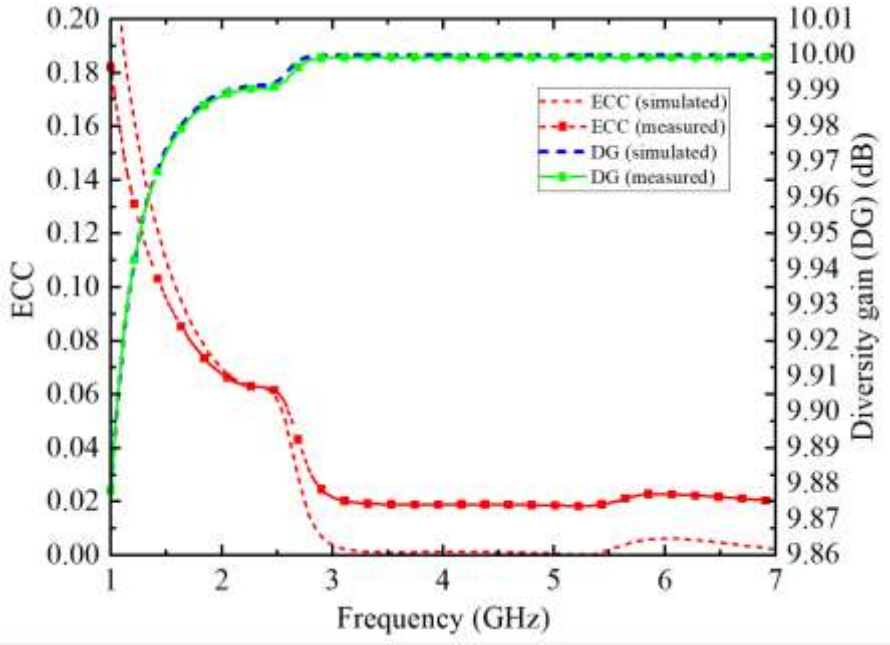


Figure 3.11 Simulated and measured results of ECC and DG versus frequency for a two-element MIMO antenna.

3.4.3 Total Active Reflection Coefficient (TARC)

The TARC is the ratio of the incident (*Ii*) to reflected power (*Ri*) in the antenna system. As, it is not always enough to compute the parameters like bandwidth, and efficiency of MIMO using scattering parameters while we have multiple antennas working simultaneously and the entire operational bandwidth is utilized by the antenna systems.

Therefore, we need to use efficient methods for understanding the behaviour of antenna on the basis of performance characteristics such as TARC.

If antenna has two ports, then TARC is given as,

$$T^R = \sqrt{\sum_{j=1}^{2}|R_i|^2} \,/\, \sqrt{\sum_{k=1}^{2}|I_i|^2} \qquad \text{----- (6)}$$

$$\begin{pmatrix} R_1 \\ R_2 \end{pmatrix} = \begin{pmatrix} S_{11} & S_{12} \\ S_{21} & S_{22} \end{pmatrix} \begin{pmatrix} I_1 \\ I_2 \end{pmatrix} \qquad \text{----- (7)}$$

$$\text{TARC} = \sqrt{\frac{(s_{11}+s_{12})^2 + (s_{21}+s_{22})^2}{2}} \qquad \text{----- (8)}$$

Given that, *Ri* is a total reflected and *Ii* is a total incident signal at Port 1 and Port 2 of the antenna. Where, S-matrix for 2-Element MIMO is represented by, S_{11}, S_{12} S_{21} S_{22} and Finally, R_1, R_2 and I_1, I_2 is the reflected and incident signal at port 1 and port 2 and S_{11}, S_{12}, S_{21} and S_{22} are the reflection and transmission parameter of 2-element antenna. Figure 3.13 shows the graph of the simulated and measured result of the TARC. The desired value of the TARC is calculated in reference to impedance bandwidth and the simulated and the measured values are almost identical and covers sub-6 5G bands.

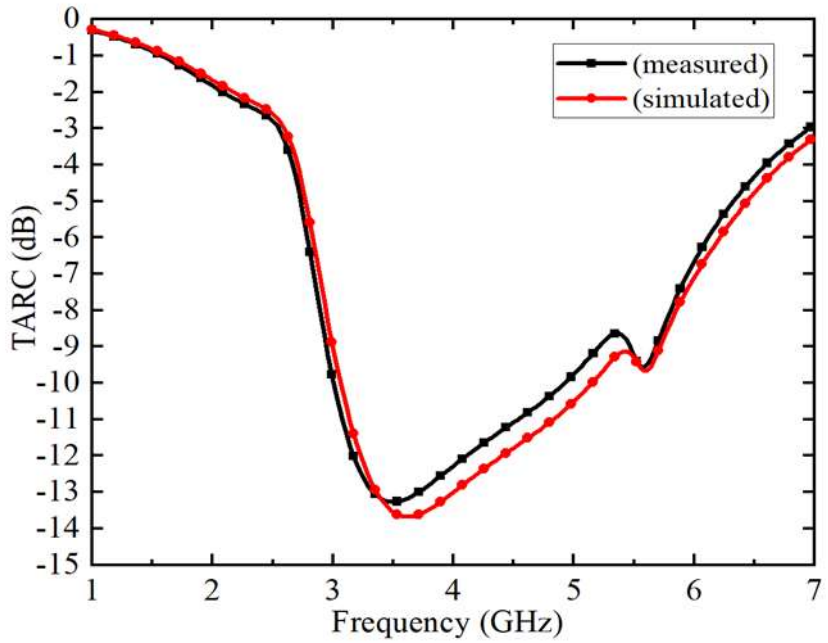


Figure 3.12 Simulated and measured result of the TARC for the two-element MIMO antenna.

3.4.4 Mean Effective Gain (MEG)

MEG, is the ratio of mean power accepted to the average incident power with reference to an isotropic antenna, and is used to calculate gain performance in rich fading scenarios. Evaluating the effective power of each i^{th} component of a MIMO may be done using propagated statistics and radiation patterns [50]

$$MEG = \frac{P_r}{P_i} = \int_0^{2\pi} \int_0^{\pi} [\frac{XPR.F_\theta(\Omega).P_\theta(\Omega) + F_\phi(\Omega).P_\phi(\Omega)}{1+XPR}] \, d\Omega \qquad \text{-----(9)}$$

In equation (9), XPR stands for the cross-polarization power ratio, where Ω represents the solid angle. For a uniform propagation environment, the values of XPR = 1 and $P_\theta = P\phi = 1/4\pi$ are taken into account. The power gain patterns of MIMO are measured w.r.t to F_θ and F_ϕ.

For good MIMO performance, MEG_j / MEG_k should be near to unity and the desired value of MEG vary from -3 to -4 dB as shown in figure 3.14. The table 3.3 explain the two-element antenna has MEG values within specified limit, and the ratio of MEG, i.e., MEG_1/MEG_2, is close to unity which shows that the antenna is built with exceptional performance.

Table 3.3 MEG at various frequencies of the 2-element MIMO

Frequency [GHz]	**MEG_1**	**MEG_1 in dB**	**MEG_2**	**MEG_2 in dB**	**MEG_1/ MEG_2**
3.0	0.49579	-3.04702	0.49861	-3.02231	1.0081
3.5	0.49958	-3.01392	0.49926	-3.01670	0.99907
4.0	0.49971	-3.01276	0.49791	-3.02843	0.99482
4.5	0.49976	-3.01237	0.49458	-3.05754	0.98522
5.0	0.49990	-3.01113	0.48800	-3.1157	0.96641
5.5	0.49941	-3.01537	0.48972	-3.10044	0.97256

3.4.5 Channel Capacity Loss (CCL)

CCL, is the important element while evaluating an antenna array's effectiveness in a MIMO system. In figure 3.15, the proposed MIMO design is able to achieve a CCL value of less than 0.2 bits/sec/Hz, which is the required value for the 5G band, and allows a maximum wireless throughput capability. In two element MIMO

configuration, correlation between antenna pair which defines the impact of antenna 1st on 2nd Antenna. Clearly defined mathematically in [90] as,

$$C_{loss} = - \log_2 \det (Y^R) \quad \text{----(10)}$$

$$\text{as, } (Y^R) = \begin{bmatrix} Y_{11} & Y_{12} \\ Y_{21} & Y_{22} \end{bmatrix}$$

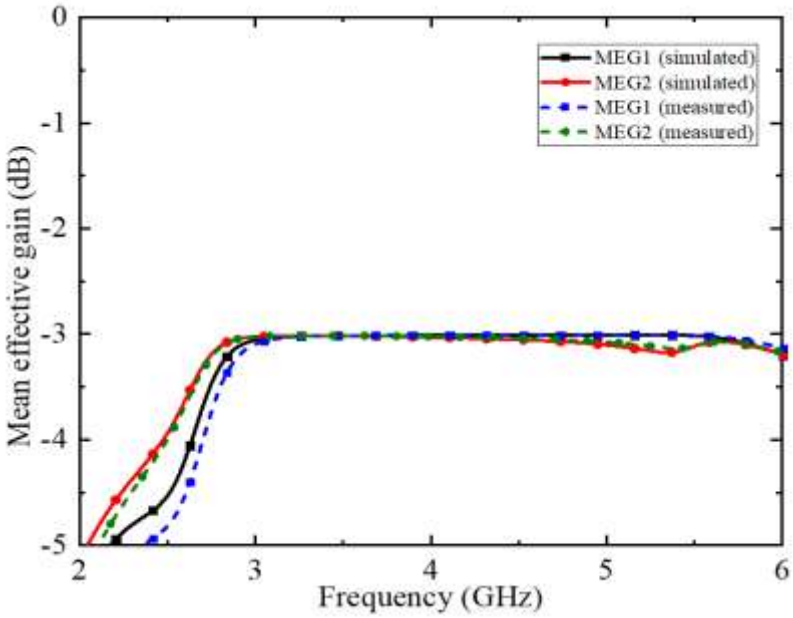


Figure 3.13 Simulated and measured MEG versus frequency for the 2-element MIMO antenna.

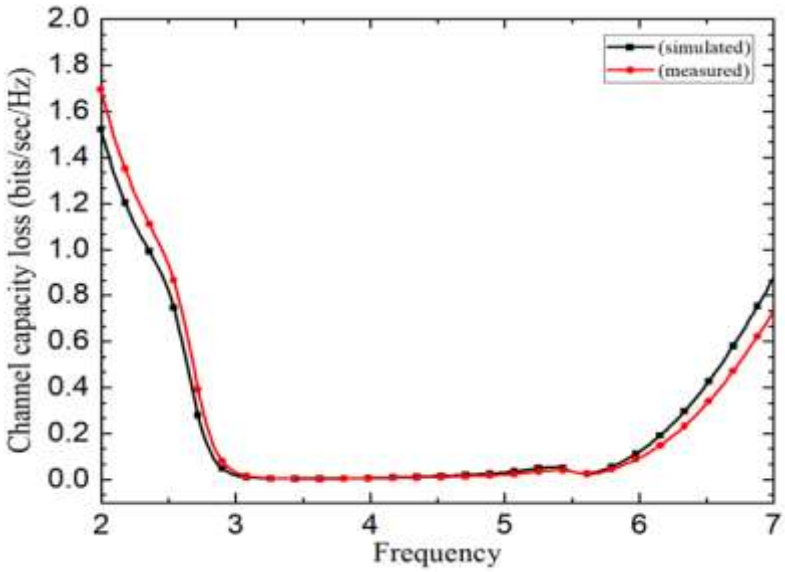


Figure 3.14 Simulated and measured CCL versus frequency for the 2-Element MIMO

3.5 Summary

In this chapter, an improved two-element compact MIMO antenna with close spacing, maximum impedance matching, and a high level of isolation is presented. The result shows that the sub-6 GHz 5G MIMO operates within a frequency range of 2.92 to 5.72 GHz, with a minimum isolation value of -15 dB. The diverse MIMO performance parameters are calculated and the desired values are obtained as ECC < 0.02, DG > 9.999 dB, $MEG_1/MEG_2 \cong 0.95$, and CCL ≅ 0.2 bits/sec/Hz. These values are within acceptable range for optimal MIMO performance.

In nutshell, this chapter presented an efficient antenna design approach that can be used to achieve high isolation 2-element MIMO antenna for WLAN/sub-6 GHz (n77, n78, n79) 5G application. The presented work unveils the ongoing research in antenna design and provides valuable insights into the performance parameters of 2-element MIMO antenna. In the next chapter, a quad port MIMO for WLAN and sub-6 GHz applications is explored, achieving maximum isolation, ECC and DG within acceptable ranges.

4

Quad-Radiator MIMO with Asymmetric feed line for (n77/n78/n79/WLAN) 5G-Wireless Applications

"The wave is nothing without the antenna to guide it."

- Heinrich Hertz

4.1. Introduction

In a 5G wireless communication system, the major challenge is to develop a small-sized microstrip patch antenna (MSPA) with adequate channel capacity, high spectrum efficiency, and a wideband system. Currently, high-speed transmission speeds are crucial for connectivity, which contributes to both economic growth and social digitalization, as the global network will connect billions of subscribers in the coming years, necessitating high bandwidth and low latency due to the growing user base. To achieve a higher data rate, the 5G-MIMO network will fulfill the need as expected by researchers. It will not only accelerate mobile data but also improve network compatibility, efficiency, and scalability.

Furthermore, the use of substrate material in diverse antennas is the utmost criterion for 5G communication. With the use of smaller loss tangents and the permittivity constant values, these substrate materials allow extensive bandwidth and efficiency [10]. Recently, there have been significant advancements in MIMO technology, and researchers have been exploring various mechanisms to improve mutual coupling. In [50], the proposed antenna with minimized mutual coupling covers the 2.4/5.8 GHz wireless local area network (WLAN), useful for portable wireless device bands. However, the isolation achieved was not sufficient by using a back-to-back connected dual-range array [52]. As a result, an improved antenna design was introduced that incorporates a ring slot-based CSRR and an L-shaped parasitic element, which provides isolation of greater than -20 dB in the sub-6 GHz band with an efficiency of 82.6%. However, the disadvantages include its size (75×150 mm^2) and limited bandwidth coverage (3.4-3.8 GHz) [84].

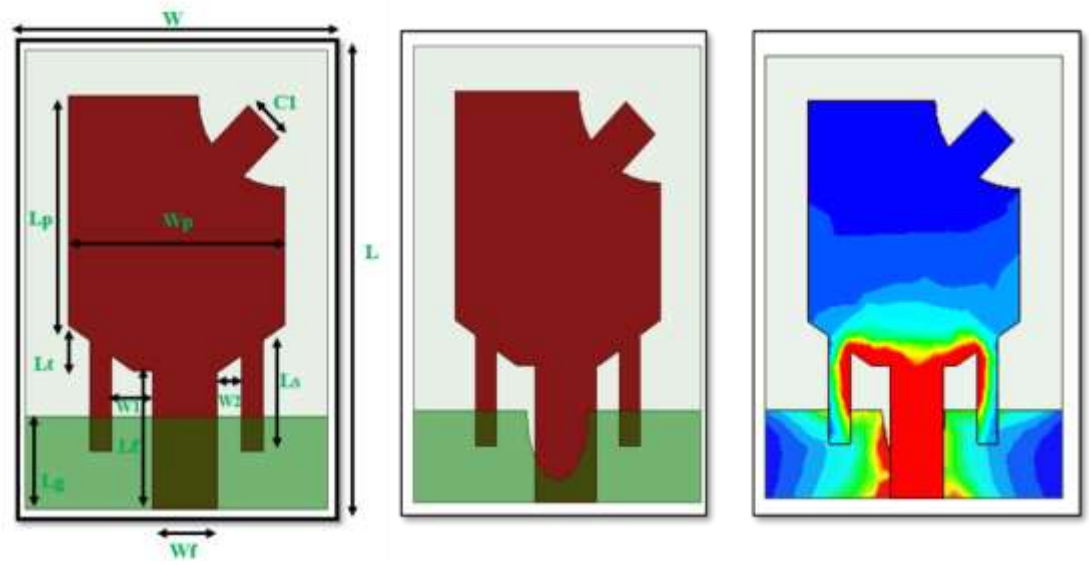
In [53], the proposed compact antenna with overall dimensions of 48.5 × 60.6 mm² consists of improved decoupling and defected ground in the shape of H with excellent isolation values of 34.2 and 36.3 dB. In [86], the fractal Koch geometry and CSRR with elliptical shape are loaded with orthogonally placed MIMO with the highest isolation of -22 dB and two notched bands, but inter-element isolation is another concern due to the cutting slot. In [87], a quad-port antenna with a 3×3 EBG (electromagnetic-bandgap structure) is implemented with band rejection and outstanding diversity characteristics with minimum isolation of -17.5 dB. In [62], using a circular ring and metallic strips on the ground, respectable isolation above -25 dB is attained by utilizing a hybrid approach combining MSPA and DRA. However, the larger area requirement is a drawback of the dielectric resonator antenna (DRA). In [88], the multilayer drop type 4-element Kraus method is employed for wideband operation, and the use of a photonic band gap (PBG) structure improves inter-port isolation; however, this approach has the disadvantages of a larger size and insufficient impedance bandwidth. For various wireless networks, a wideband MIMO antenna is presented in [89] and [91]. The wideband coverage in the 5G band with the use of the EL slot and the UPMS isolation technique is explained, but the proposed method has low gain. In [54], the proposed 39 × 39 mm² size antenna has wide coverage, sufficient TARC, high gain, and enhanced bandwidth. The design introduced notches to cover multiple wireless applications. The multiple slit and decoupling structure are followed by a staircase-shaped element used for isolation enhancement and diversity performance. But the isolation between ports is the problem. Further, in modern wireless communication, wideband MIMO antennas play a vital role in enhancing data and overcoming challenges such as multipath fading. By utilizing MIMO technology with diverse array combinations, it is possible to increase channel capacity without demanding extra bandwidth. By effectively addressing multipath propagation, this technology enables the achievement of high data rates. However, in recent studies, the correlation value was found to be less than 0.001, and other performance parameters like DG, MEG, and TARC were within the desired value.

The chapter presented the U-shaped etched slot on defective ground with an asymmetrical feed line structure for the operation of the quad-port antenna design within the compact size of 31 × 40 mm² and achieves significant isolation. Additionally,

the twin-stub-based quad-element antenna with a rectangular patch and inverted T-type partial ground with a face-to-face patch arrangement is conferred. The goal of this work is not only to attain wider bandwidth but also to offer a high data rate with a nearly omnidirectional-type radiation pattern and the unique design approach.

4.2. Proposed single and quad element system with asymmetric feed line

The proposed model consists of a single-element patch antenna built on a FR-4 substrate material, as depicted in figure 4.1. The constant ($\in_r$) of material is 4.4 and the loss tangent is 0.0025. The optimized structure includes a partial ground dimension (Lg × Wg) of 14 × 4 mm² and a substrate of 20 × 14 mm² (L × W). Additionally, a 2.5 mm wide feed line (W_f) is implemented to attain 50 Ω characteristic impedance (Z_0). The surface current distribution at 5 GHz deep when port 1 is excited is depicted in Fig. 4.1 (c). The feed is associated with more concentrated current at the center and it is moderate in other parts of the patch.



(a) (b) (c)

Figure 4.1. (a) Antenna geometry of a single element (b) With U-shape cut on ground (c) Current distribution of a single element MIMO at 5 GHz

The optimized dimensions are in millimetres: W=14, L=20, Lp=10, Wp=10, Lf=2.5, Lt=2, Lg=4, Ls=4.5, W1=2, L2=1, C1=2, Wf= 2.5

The single element reflection coefficient (S_{11}) is depicted in figure 4.2 (a) without U-shaped etched ground and (b) shows and with the U-shaped etched ground.

The bandwidth obtained in single element is below -10 dB before making U-Slot. After the slot is made, the bandwidth varies from 4.97 to 5.21 GHz. The effect of U-type slots on bandwidth is depicted in [100] for 5G and WLAN applications. Enhancing the bandwidth for 5G wireless applications is of prime importance. The twin-stub-based quad-element antenna with a rectangular patch and inverted T-type ground with a face-to-face patch arrangement is shown in figure 4.3. The U-shaped etched slot is formed on defective ground, and resonant frequency is obtained at 4.2 GHz. The optimized structure (L × W) has an overall size of 40 × 31 mm². The four-element stub-interfaced antennas are placed with dense spacing of (d_2) 0.129 λ_0 and (d) 0.06 λ_0 between antenna elements to keep the justified geometry for the desired band coverage. By using a partial ground plane, the mutual coupling and isolation among antenna elements are kept efficient with the help of a thin-thick parallel line. This parallel line behaves like a resonant circuit consisting of a capacitor and inductor. The gap between strip lines is maintained in such a way that the resonant frequency should be as close as possible to get extremely good isolation among antenna elements as depicted in figure 4.3(b).

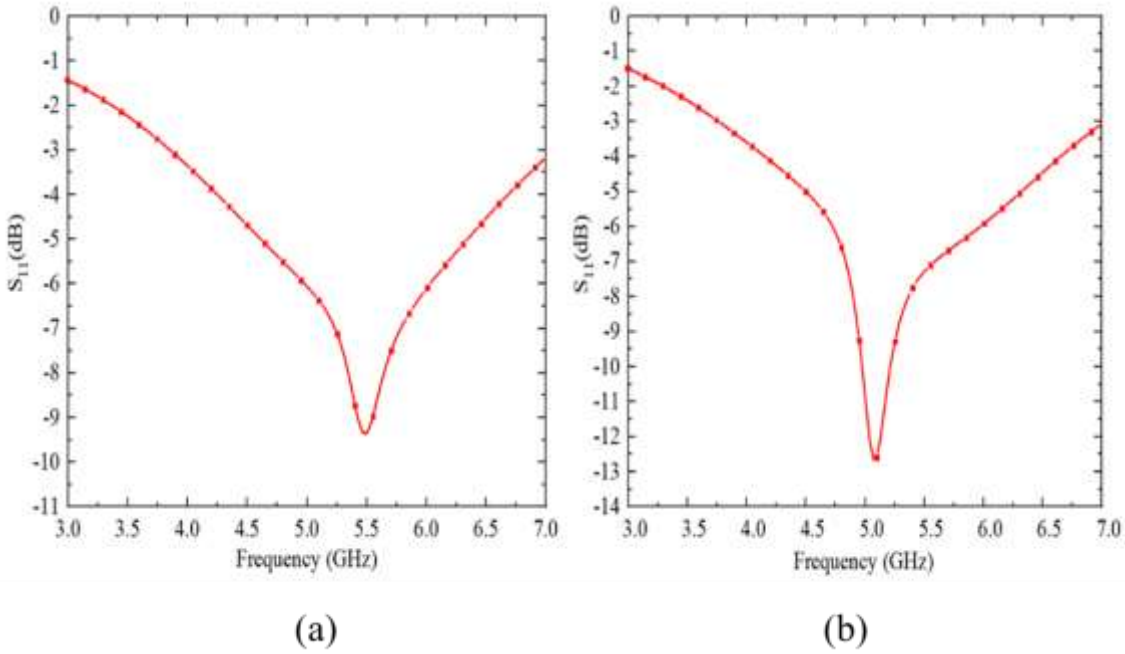


Figure 4.2. Reflection coefficient (S_{11}) of 4- element MIMO (a) Without U-shaped Slot on ground (b) With U-shaped slot on ground

In optimized form, all the antenna dimensions are given in (mm) millimeter. L=40, W=31, d=4, d1=1.2, d2=8.6, R1=6, R2=4, R3=18, R4=3, R5=3.2, R6=4, S1=S3=S4=S5=0.25, S2=1, S6=0.5, S7=0.5.

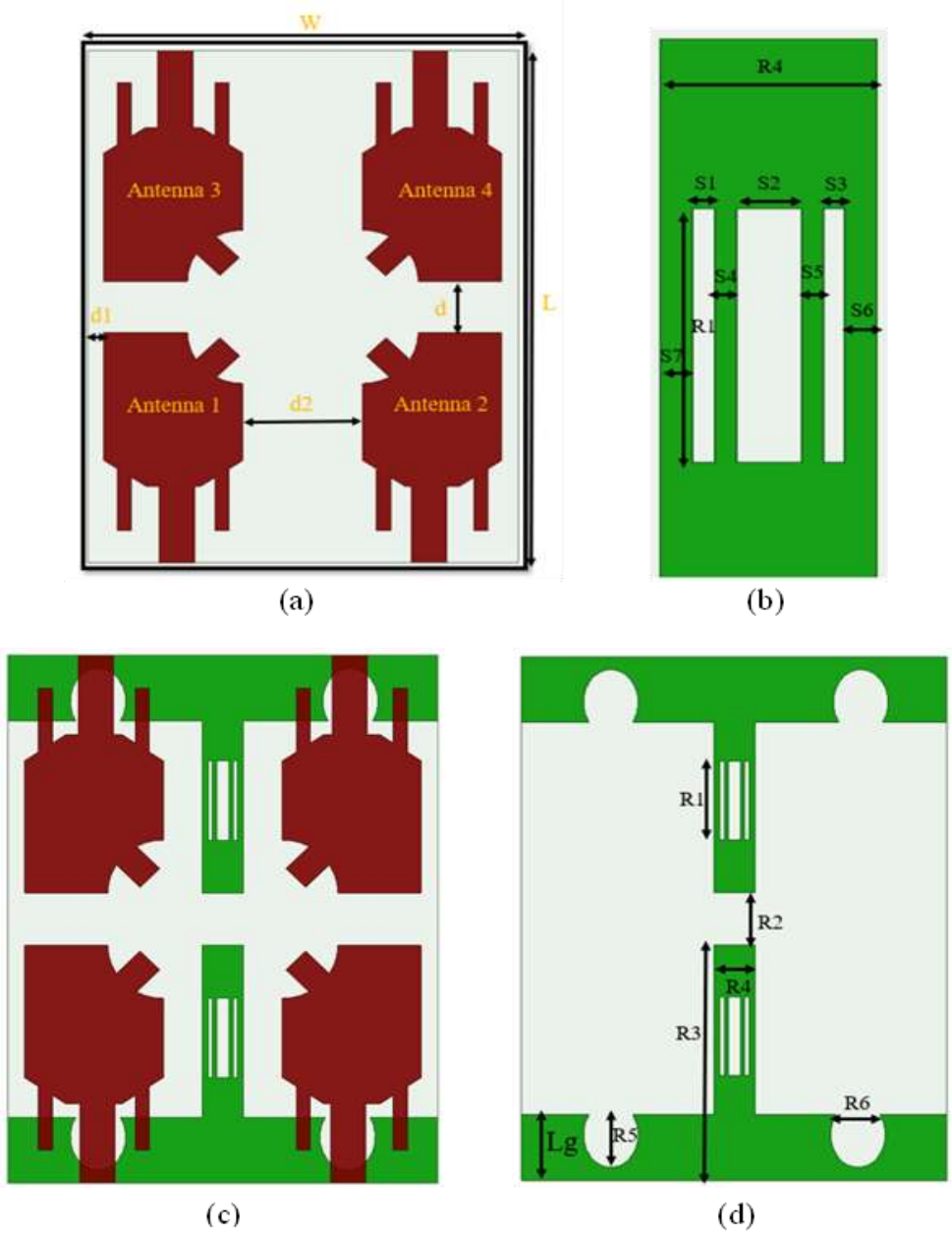


Figure 4.3 Configuration of 4-element asymmetric feed antenna (a) Geometry of patch (b) Parallel strip line for mutual coupling reduction (c) Combined geometry of 4-element antenna (d) Antenna with U-shape slot on the ground

In case of 4-element design, firstly the feed width is taken as 2 mm forming the symmetric feed design and the antenna provides the bandwidth from 2.92 GHz to 5.16 GHz, with a single resonance point and poor isolation. But, in an asymmetric feed line,

the width of the feed line was taken at 2.5 mm. The structure exhibits asymmetric behaviour, and achieves a bandwidth from 2.7 to 5.34 GHz with dual resonance. The minimum isolation is better than -15 dB at 4.5 GHz, which is the highest value among both cases. Additionally, the radiation characteristics provides more directional behaviour with the implementation of asymmetric feed. In order to improve necessary mutual coupling, the quad patch elements are arranged in face-to-face method with adequate spacing between antenna elements of MIMO system.

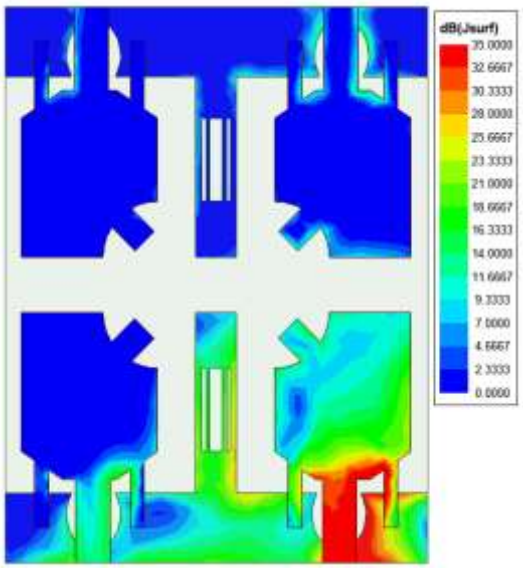


Figure 4.4. Current distribution of quad radiator MIMO at 4.5 GHz

Figure 4.4 displays the surface current distribution at the resonant frequency. When the input excitation is applied to port 2, the coupling current is concentrated on the feed line, and port 2 is coupled to an EM wave that does not radiate into free space. This phenomenon highlights the efficiency of the resonant structure in directing the energy along the feed line and minimizing unwanted radiation. Consequently, the antenna system remains highly effective in maintaining signal integrity and optimizing overall performance.

4.3 Results and Discussion

The figure 4.5 shows the S-parameter analysis of the proposed quad-radiator MIMO with asymmetric feed line 4-element MIMO antenna. In figure 4.5 (a), the impedance bandwidth is 2.7 to 5.34 GHz with resonating frequency is obtained at 4.5 GHz. Also, isolation among other ports i.e., $S_{11}/S_{12}/S_{13}/S_{14}$ is justified well in figure 4.5 (b) and the return loss among same port is observed in figure 4.7 (c).

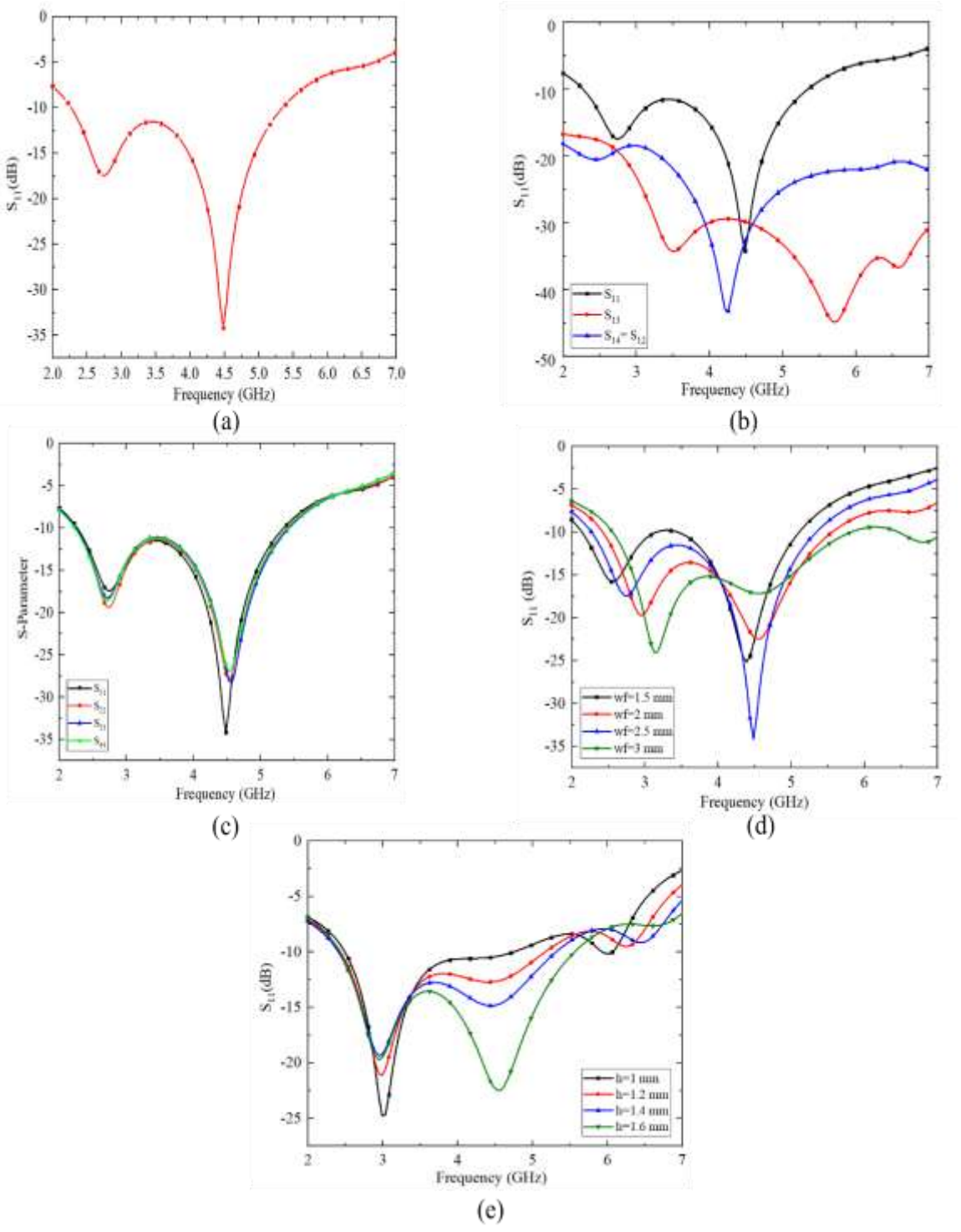


Figure 4.5 S-parameter results for quad-radiator MIMO with asymmetric feed line (a) Plot of S_{11} (b) Plot of $S_{11}/S_{12}/S_{13}/S_{14}$ (c) Plot of $S_{11}/S_{22}/S_{33}/S_{44}$ (d) Plot of varying width of feed line from 1.5 mm to 3 mm (e) Plot of S_{11} for varying substrate thickness

The optometric analysis is done with respect to feed line and substrate thickness as shown in the figure 4.5 (d) and (e). In the plotted curve it is observed that the feedline

with width of 2.5 mm covers entire 5G band with maximum return factor in comparison with other feedline width. Also, with varying substrate thickness from 1 mm to 1.8 mm there is frequency shift and narrow band coverage except 1.6 mm. At 1.6 mm, antenna operates over wide frequency range which in turn use for 5G wireless communication.

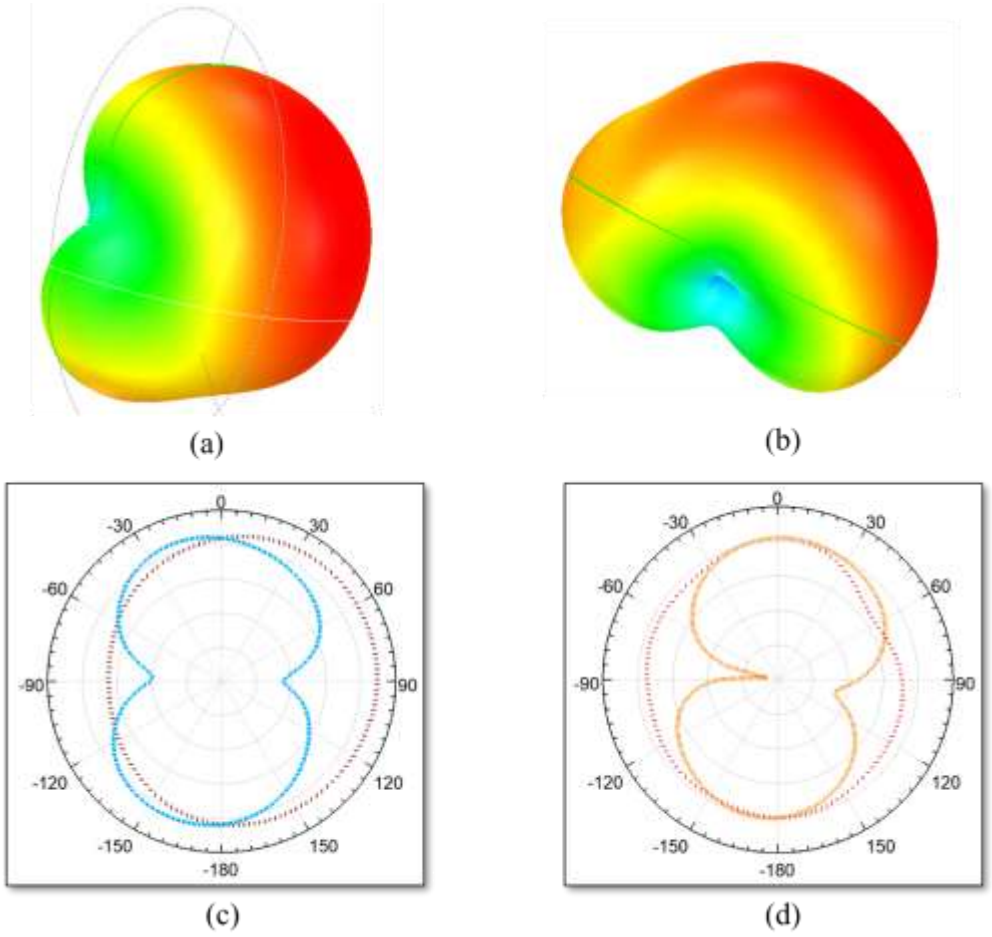


Figure 4.6 (a), (b) 3-D radiation pattern and (c), (d) 2-D radiation pattern of quad-radiator MIMO with asymmetric feed line at center frequency

The 3-dimension radiation pattern for the antenna-1 at resonant frequency of 4.5 GHz is depicted in figure 4.6. In the far field test, theta varies from -180° to +180° and phi varies from 0 to 90° to obtained the XZ and YZ plane radiation pattern. The obtained results give omnidirectional pattern with maximum gain of 3 dB and the designed antenna proves it works well for MIMO wireless applications.

To verify the simulated result, a prototype of the proposed four-element antenna is fabricated for practical measurements as shown in fig. 4.7 (a) the front and (b) back views of this prototype. Since all four antenna elements are identical, ports 1, 2, 3, and

4 exhibit nearly identical reflection coefficients. Hence, our comparison between simulated and measured results focuses solely on the reflection coefficients S_{11} and S_{22} as shown in Fig. 4.8. The variance in outcomes could be obtained from fabrication tolerances or measurement procedures conducted within a scattering environment.

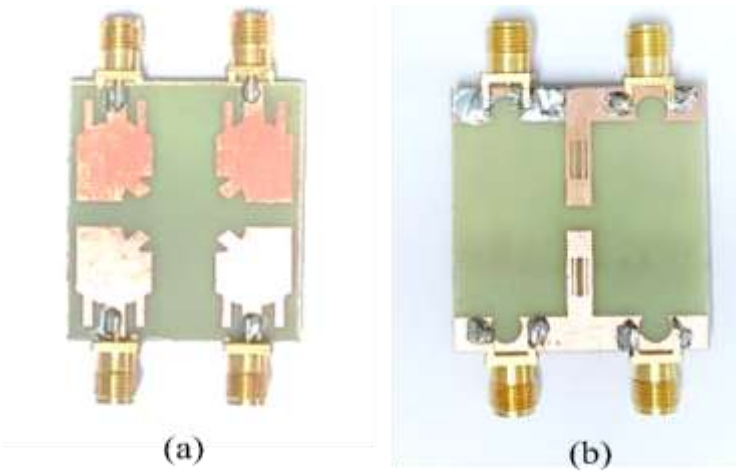


Figure 4.7 Four element MIMO antenna fabricated for measurements (a) front view (b) back view

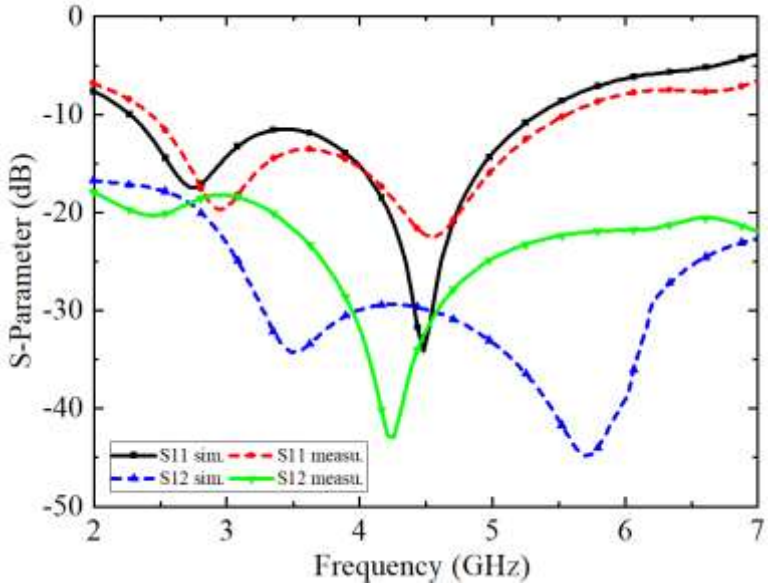


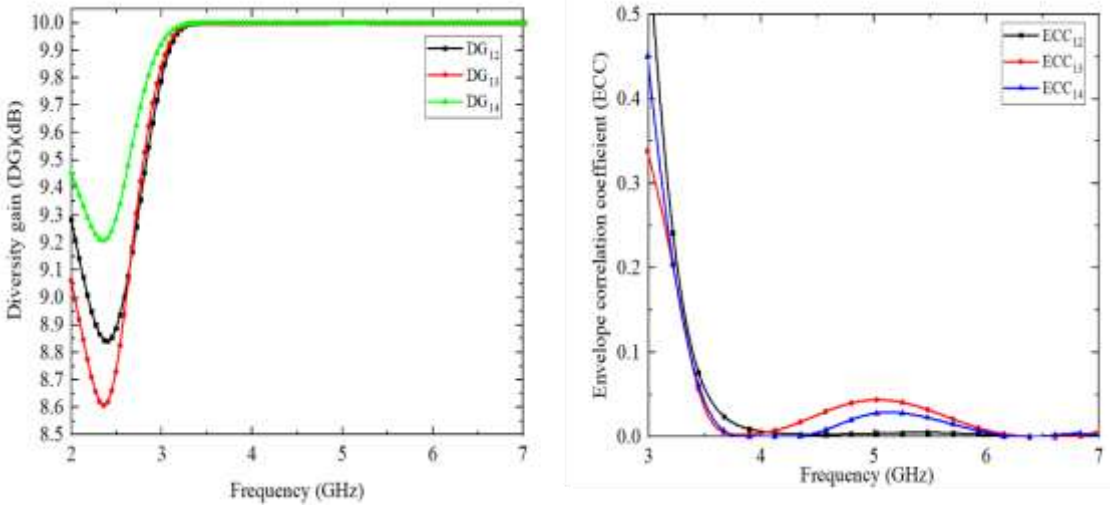
Figure 4.8 S-parameter of fabricated four element MIMO antenna

4.4 Diversity Performance

In DG, diversity performance characteristics shows how much power loss happens while transmitting power for 4×4 elements [123-124]. The DG can attain maximum value of 1 and in dB, it can reach up to 10 dB as shown in fig. 4.9 (a). ECC gives

correlation among 4×4 antenna elements as shown in figure 4.9 (b) and correlation among antenna element [125], calculated using following equation,

$$ECC = \frac{\left[\iint_{4\pi}\left(\overrightarrow{B_i}(\theta,\emptyset)\right)\times(\overrightarrow{B_j}(\theta,\emptyset))d\Omega\right]^2}{\iint_{4\pi}\left|(\overrightarrow{B_i}(\theta,\emptyset))\right|^2 d\Omega \iint_{4\pi}\left|(\overrightarrow{B_j}(\theta,\emptyset))\right|^2 d\Omega} \quad \text{------(12)}$$



(a) (b)

Figure 4.9 (a) Diversity gain (DG) and (b) ECC of quad-radiator MIMO of asymmetric feed line

Table 4.1. Comparative study of various diversity antennas

Ref. No.	Size (mm^2)	Substrate	Type of MIMO	Working frequency Range (GHz)	Isolation (dB)	ECC
[50]	50 x 80	FR-4	Novel dual band	2.45/5.8	≥ 20	< 0.01
[53]	48.5 × 60.6	F4B	Dual Band closely coupled Patch MIMO	3.7/4.1	NA	< 0.01
[68]	50 × 100	FR-4	Inverted-F antenna (IFA)	2.7-3.6	> -25	< 0.3
[84]	75 x 150	FR-4	Four-element CSRR structure	3.4 – 3.8	> -40	0.005

[86]	58 x 58	FR-4	Four element elliptical monopole with Koch geometry	3–13.5	> -22	< 0.008
[87]	60 x 60	FR-4	Quad port circular monopole and EBG	3-16.2	> -17.5	< 0.3
[88]	110 x 110	CER-10	4-element Drop shaped slot antenna	1.7 - 7.2	> -30	0.0025
[91]	30 x 40	FR-4	Four ports with EL slot and UPMS isolation	3.20-5.85	> -20	< 0.05
[104]	60 × 60	FR-4	Calendula patch with rectangular stub	3.26-5.18	> -15	<–0.005
[114]	47.5 × 40	FR-4	Two element arrays with parasitic element	3.11–3.81	> -42.9	0.001
[122]	145 × 70	FR-4	Integrated quad-element MIMO	3.3 – 7.2	> -10	< 0.2
[125]	73 x 120	Taconic's TRF-43	Four element microstrip dipoles	3.45 to 3.55	>-15	< 0.15
Proposed	31 x 40	FR-4	Rectangular patch and parallel strip line structure	2.27 - 5.34	> -15	< 0.001

In the table 4.2, the comparative analysis is shown. In comparison to the previously reported designs, the proposed design offers more viable solution for the wireless communication. The presented design is highly compact and exhibits a wider bandwidth with improved isolation, and ECC is compared to the antennas reported in [50, 68, 86, 87, 91, 104, 122, 125]. In most of the reference work the isolation achieved is around -20 to -25 dB with ECC < 0.5. In contrast, the proposed 4-element MIMO

antenna achieves high isolation exceeding -30 dB particularly in WLAN/Sub-6 GHz (n77, n78, and n79), along with an ECC of 0.001, indicating acceptable diversity performance.

4.5 Summary

In this chapter, the quad-port high-isolation MIMO antenna using an asymmetric feed line is presented, and the performance parameters, such as correlation coefficient, diversity gain, and isolation among antennas, were investigated. The achieved isolation > -15 dB indicates the bandwidth is suitable for 5G communication. The findings show that the ECC value is 0.001, and the DG value remains around 9.99 throughout the band. These values fall within acceptable ranges, indicating optimal MIMO performance. Essentially, the chapter presents a design approach to achieve high isolation in 4-element MIMO antennas for WLAN and sub-6 GHz 5G applications. This contribution advances the use of ongoing research in antenna design and provides important information regarding the performance parameters of MIMO antennas. The next chapter explores a wideband staircase U-shaped 4-port MIMO antenna for sub-6 GHz & WLAN applications, along with the low-temperature cofired ceramic (LTCC) technology and device housing.

5

Quad-port Staircase U-Shaped Wideband MIMO Antenna for 5G New Radio Applications

"Electromagnetic waves, though invisible, govern the unseen world of communication."

James Clerk Maxwell

5.1 Introduction of quad-port MIMO Antenna

In today's wireless networks, MIMO antennas are essential for increasing data throughput and resolving signal problems. MIMO systems enable more effective data transmission, improve signal quality, and suppress interference and multipath fading. It also progresses the efficiency and dependability of today's wireless communication networks. Further array configurations with MIMO technology increase channel capacity without requiring more bandwidth. Systems that demand low latency, high performance, or increased capacity can all benefit from the 5G network's improved service quality. The current scenario requirement is to develop a miniature MIMO antenna that can support several bands to enable the independent use of 5G NR bands in indoor networks, ensuring smooth transitions. Maintaining isolation between nearby deployed radiators is a significant difficulty for antenna designers since it adversely affects the MIMO's performance metric.

Improvements in the isolation between closely spaced antenna radiators have been reported using various methods [43-90]. In [43], with a dual-band capability antenna, the two-port MIMO with asymmetrical T-shaped monopole and inverted E-shaped radiators meets the bandwidth requirements of the sub-6 GHz. In [82], it is stated that a linear array construction with two basic patch antennas demonstrated superior isolation and impedance matching without the need for traditional matching networks. In [98], the parasitic structures between the radiators efficiently minimized mutual coupling, increasing the isolation by 45 dB. In [106], a 4-element crescent ring-type slot and fractal geometry are utilized to create a notched band and an impedance matching at 4.6 GHz with a profile dimension of 60×60×1.6 mm^3. The operational

range was increased using the complimentary split ring resonators (CSRR) approaches, and undesirable bands (3.5 and 5.5GHz) were eliminated by using the elliptical CSRR approach [86]. In [105], the operational band, the coupling between components has increased by more than 22 dB by employing a substrate with a slotted edge. In [85], more than 23 dB of isolation was found for the tiny proximity-type microstrip antenna in isotropic radiation wireless applications. Moreover, antennas were positioned on both levels using the kraus technique to increase bandwidth [88]. A staircase-shaped modified ground structure and an arc on the radiator followed the orthogonally positioned quad-element MIMO antenna, which showed the isolation of $S_{12} < -22$ dB and $S_{13} < -23$ dB [92]. In [93], using parasitic resonators and stub placement, a semi-elliptical structure was used to construct a four-element UWB antenna that isolated more than 20 dB. Additionally, the different techniques including an electromagnetic bandgap (EBG), neutralization line (NL), and defective ground structure (DGS), are often employed. However, the maximum isolation is mostly attained in the EBG because of the increased capacitance, which leads to high efficiency and diversity gain [94]. In [62], the suggested hybrid strategy produced an adequate isolation value of 25 dB. In [71], high isolation was attained using the NL approach, which has a bandwidth variation of 3.52-10.08 GHz and 23 dB of isolation. However, the above structure has minimal isolation, poor coupling and covers only partial sub-6 GHz 5G band. The coupling can be improved further by introducing metamaterial and CSRR structures and the isolation can be improved by using numerous tuning elements and the involvement of improved feedline which improves efficiency [131]. Further, some array structure has very narrow bandwidth coverage of 5.35% at 5.5 GHz. Additionally, the gain is major concern which can be improved by using low loss material and diverse gain enhancement techniques.

In this chapter, we have designed a quad-port MIMO antenna with a modified ground plane. A captivating feature of this structure is its miniaturization and high isolation. The staircase U-shape radiating element and an I-shaped stub etched with rectangular strips between radiating elements provide enhanced isolation. It limits the amount of current flow from one element to another one to limit surface current. This configuration covers the requisite bandwidth of 5G NR. The fig. 5.1 shows the structure of the designed MIMO antenna.

5.2 Antenna Configuration and Analysis

In this, a 4-port MIMO is developed using an inexpensive FR-4 substrate, and we evaluate the design as an optimized four-port MIMO antenna with a staircase configuration on the bottom side and a U-shaped etched ground. Four unique radiating elements are kept on the top in this design, while a modified ground structure is located on the bottommost side of substrate. The designed MIMO antenna has a total dimension of 52 × 31×1.6 mm^3 with constant of 4.4 and tangent value of 0.0025. The feeding mechanism comprises of 50 Ω microstrip fed in each radiator with a dimension of L_f and W_f. Here, four face-to-face closely arranged U-shaped rectangular radiators with a partial ground are implemented with the use of a symmetric feed line to further enhance the bandwidth and gain. The design is studied in two portions, a single-element antenna and a modified four-port MIMO antenna. Optimization of antenna parameters is done with the help of HFSS simulator. The subsequent part discusses all of the important MIMO configuration results, including bandwidth, diversity performance, and far-field outcome.

The four-element MIMO configuration covers requisite bandwidth and higher isolation with improved impedance and also accounts for acceptable diversity performance in 5G bands. As per our findings, the proposed antenna without any hindrance will work in multipath surroundings, which brings the practicability. The designed antenna layout is presented in figure 5.1.

(unit: mm, L=52, W=31, Wp= 10, Lp =12, Wf =1.8, Lf =9, Lg12=2.12, Lg= Lg3= Lg2=7, Wp1=4, Lp1=5, Wp3= Lg5= Lg10=6, Lp2=2, Lp3=Wp4 = Wp7= Lg8= Lp4=1, Wp5 = Wp6 =2, Lg1 =38, Wg1=3, h=1.6, Wp2=8, Lg4 = Lg9=5.5, Lg6 =10, Lg7= Wg4=4.5, Lg11 =0.5, Wg2 = Wg3=0.3).

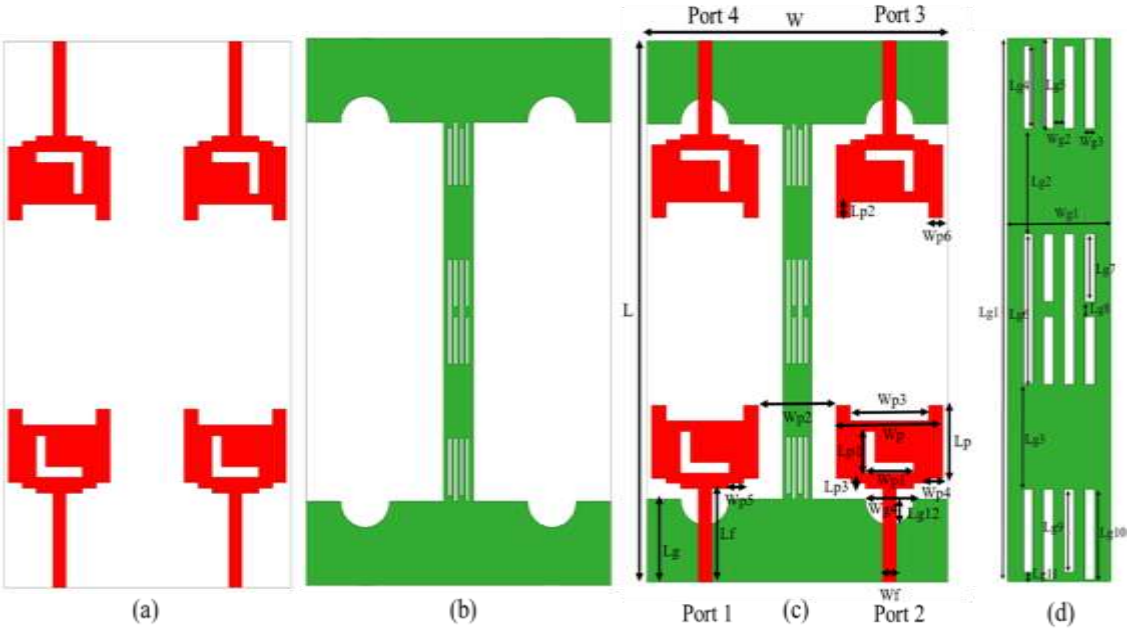


Figure 5.1 (a) front view, (b) back view, (c) Layout of the suggested MIMO antenna (d) modified I-shaped structure dimension

5.2.1 Single Element MIMO Antenna

In this section, the evolution steps of the unit element antenna with a U-shaped patch along with an improved ground are discussed. A single radiating element with an overall dimension of 26 × 14 × 1.6 mm^3 situated on an FR-4 material is presented. The step-by-step procedure to get a single-element is shown in fig. 5.2. The antenna-1 originates with a simple rectangular patch radiator with a partial ground excited by a 50-ohm microstrip feed line shown in fig. 5.2 (a). The fig. 5.3 shows the antenna resonates at 6 GHz & 9 GHz due to a partial ground plane. In step 2 (Antenna 2), the radiator is modified by etching uniform steps on the lower side due to which the band occurs at a lower frequency of around 4.5 GHz. In step 3 (Antenna 3), the radiator is reformed with U shape slot on the upper side with a partial ground. The antenna impedance improves and covers the band from 4.7 to 9.46 GHz.

Further, in step 4 (Antenna 4) an L-shaped was etched in the center of the radiator, and a semi-circular slot in the partial ground as represented in fig. 5.2. With these transformations designed antenna covers the frequency from 3.73 to 9.46 GHz and attains partial 5G frequency bands with resonance at 5.6 GHz resonant frequency depicted in fig. 5.2.

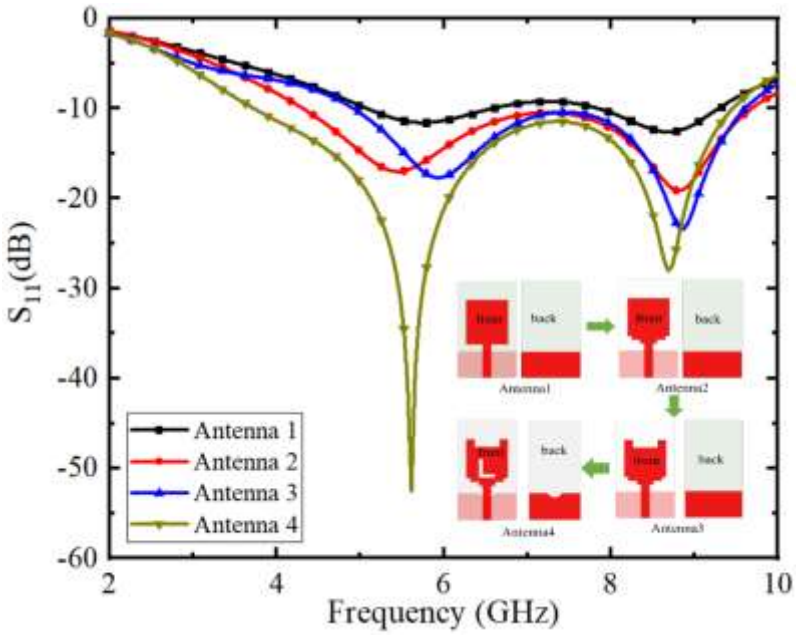


Figure 5.2 Effect of S_{11} due to development steps of single-element antenna.

5.2.2 Mathematical Modelling of Single Element Rectangular Patch

According to [126-127], the rectangular patch antenna dimensions are given by equation (13) as,

$$W = \frac{c}{4fr\sqrt{\frac{\epsilon_r+1}{2}}} \qquad \text{-----(13)}$$

The substrate's constant is considered from equation (14) as,

$$\epsilon_{reffp} = \frac{\epsilon_r+1}{2} + \frac{\epsilon_r-1}{2} \times \left[1 + 12 \times \frac{H_S}{W}\right]^{\frac{-1}{2}} \qquad \text{-----(14)}$$

Accordingly, equation (15 and 16) calculates the antenna's length L.

$$\frac{\Delta L}{H_S} = 0.412 \times \frac{(\epsilon_{reffp}+0.3)\left(\frac{W}{H_S}+0.264\right)}{(\epsilon_{reffp}+0.258)\left(\frac{W}{H_S}+0.8\right)} \qquad \text{-----(15)}$$

$$L = \frac{c}{2f_r\sqrt{\epsilon_{reff}}} \qquad \text{-----(16)}$$

Where, fr is the resonant frequency,
ϵ_{reffp} is the substrate effective constant,
ϵ_r is the substrate material constant,
ΔL is the extended length,
W is the slot width,
H_S is the substrate height,
ϵ_0 is free space permittivity,

c is the speed of light (3×10^8 m/sec),

S_{11} is the return loss,

W_s is the substrate width,

L_s is the substrate length.

5.2.3 Quad Port MIMO Antenna

A single port antenna may be transformed into a quad port MIMO antenna with an expanded substrate and connected ground, as illustrated in Figure 5.1. The size of the suggested MIMO antenna is $52 \times 31 \times 1.6$ mm^3. The feeding mechanism comprises a 50 Ω microstrip-line feed in each radiator with a dimension of L_f and W_f. Here, a symmetric feed line creates four closely spaced, face-to-face, U-shaped rectangular radiators with a partial ground to increase the gain and bandwidth.

5.2.4 Effect of Ground Plane on Four-Element MIMO Antenna

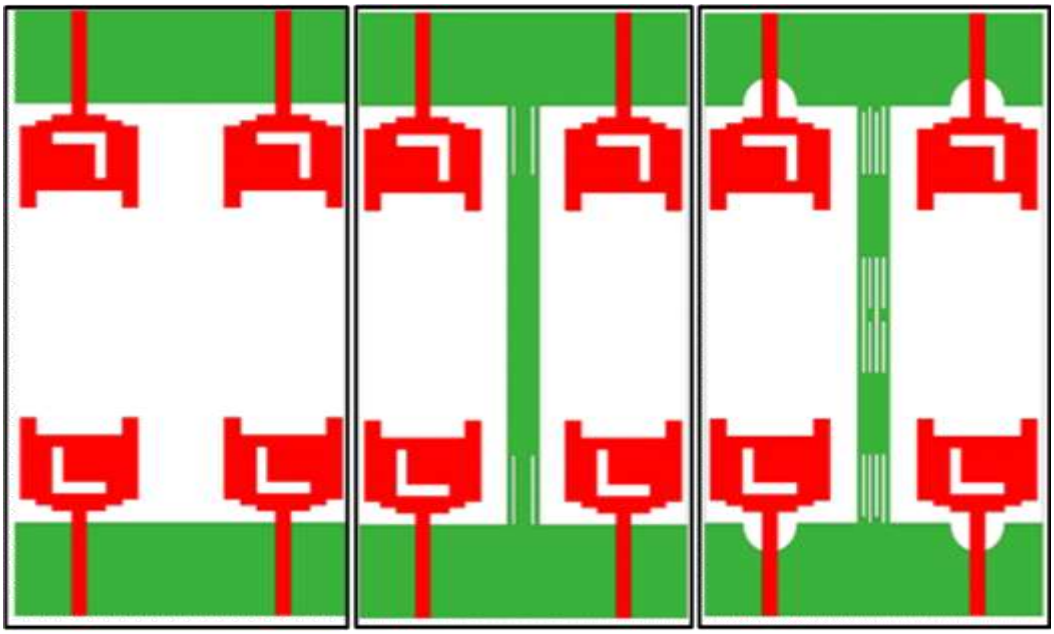


Figure 5.3 Evolution of Isolation structure (a) without I-shaped (b) with I-shaped and corner slit (c) Modified I-shaped.

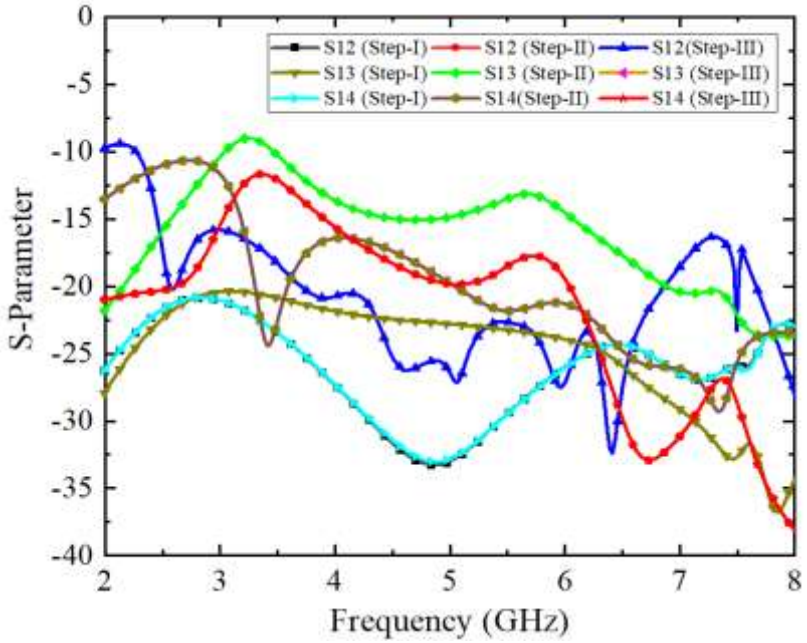


Figure 5.4 S-parameters against frequency for different isolation structures.

The requirement of today's era is a compact, improved close-spaced four-element MIMO with improved matching and isolation. Here, the performance of three distinct ground structures is analysed as depicted in fig. 5.3, while the optimal isolation characteristics are illustrated in fig. 5.4. Four identical radiators are set up on one side of the FR-4 substrate layer, whereas a partial ground plane is situated on the other, as shown in figures 5.4 (a), (b), and (c). The antenna bandwidth is increased by using partial ground. To enhance the isolation, four rectangular strips and an I-shaped isolation structure is introduced on the ground plane, resulting in improved mutual coupling as shown in figure 5.4. An I-shaped stub impedes the current flow between elements.

Additionally, high isolation is attained by etching I-shaped stub, as illustrated in figure 5.4 (c). With the introduction of this modified structure, isolation between antenna elements (S_{12} < -15 dB, S_{13} < - 20 dB, S_{14} < -15 dB) was attained across the obtained band, as shown in figure 5.5.

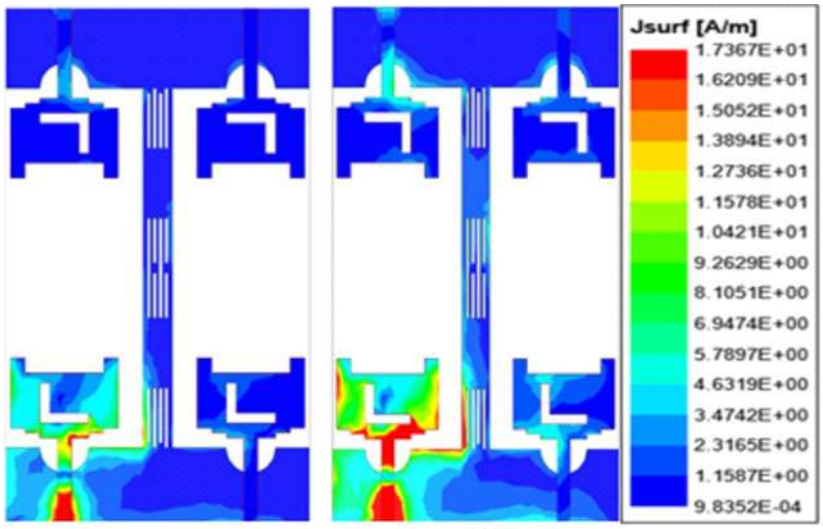


Figure 5.5 Surface current of quad-port MIMO at (a) 3.4 GHz (b) 5.2 GHz

With the partial ground plane, the surface currents tightly couple with all four antenna elements. Introducing a modified I-shaped slot between antenna elements on the ground plane reduces surface current across the radiating elements. The current circulation on the patch surface at 3.4 and 5.2 GHz is illustrated in fig. 5.5. As per observation, the surface current occurs across the feeding line, and a small amount of current exists on the radiating patch and ground at 3.4 GHz resonant frequency. A high surface current density occurs at 5.2 GHz because of the U-shaped slot etched on the radiating patch. When Port 1 is excited, and the other ports are matched with 50 Ω, no portion of the current is reached on the other elements. Hence, it shows that all the ports are isolated from each other's.

5.3 Experimental Analysis of MIMO Antenna

The quad-port MIMO antenna's fabricated prototype is illustrated in fig. 5.6. The measured and simulated S-parameters are illustrated in fig. 5.7. The suggested MIMO antenna operates in the 5G NR bands range 3.06 GHz to 7.56 GHz, with a bandwidth of 4.5 GHz, and the percentage of impedance bandwidth is 84.75%. The minimum isolation achieved was -15 dB in the operational band. The simulated and the measured result shows suitable agreement. The measured value exhibits slight deviation, which is attributed to the cabling effect and the SMA connector. The overall radiation efficiency of the suggested antenna is around 82% and the gain varies from 2 to 7 dBi, respectively, in the operational band, as illustrated in Fig 5.8.

The design and development of the reported antenna on FR-4 is observed in fig. 5.6 (a) and (b). The Rhode and Schwaz VNA is used for the measurement purpose and the setup of measurement with VNA is shown in figure 5.6 (c). The radiation pattern in the H-plane and E-plane at 3.4 and 5.2 GHz is illustrated in fig. 5.9. The H-plane patterns show a 180◦ phase dissimilarity. The omnidirectional and directional patterns are achieved at 3.4 and 5.2 GHz, respectively.

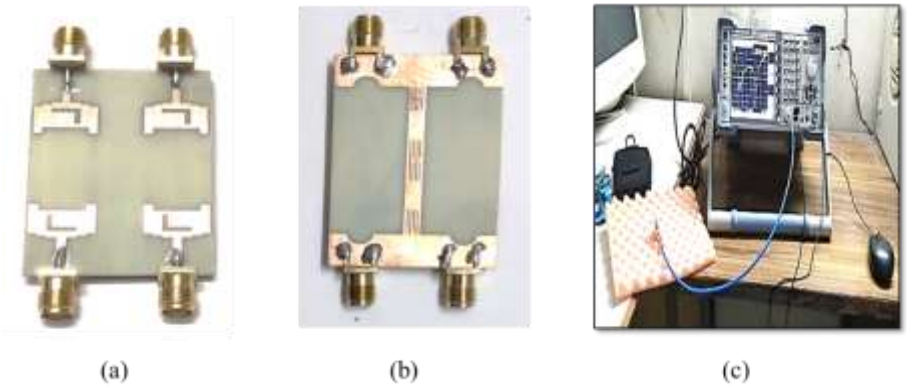


Figure 5.6 Fabricated photographs of 4-element MIMO(a) with top view (b) with bottom view and (c) Measurement environment.

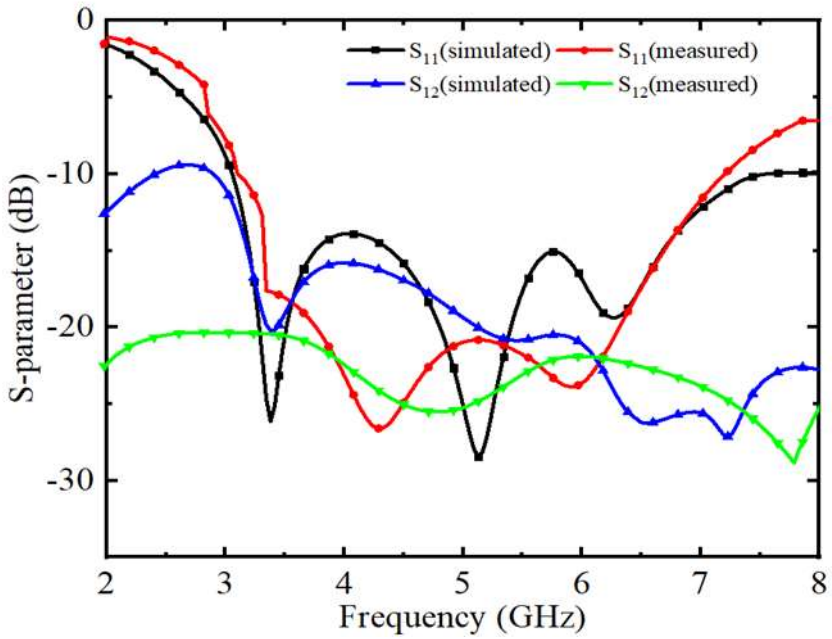


Figure 5.7 Measured and Simulated S-parameter of the suggested MIMO Antenna

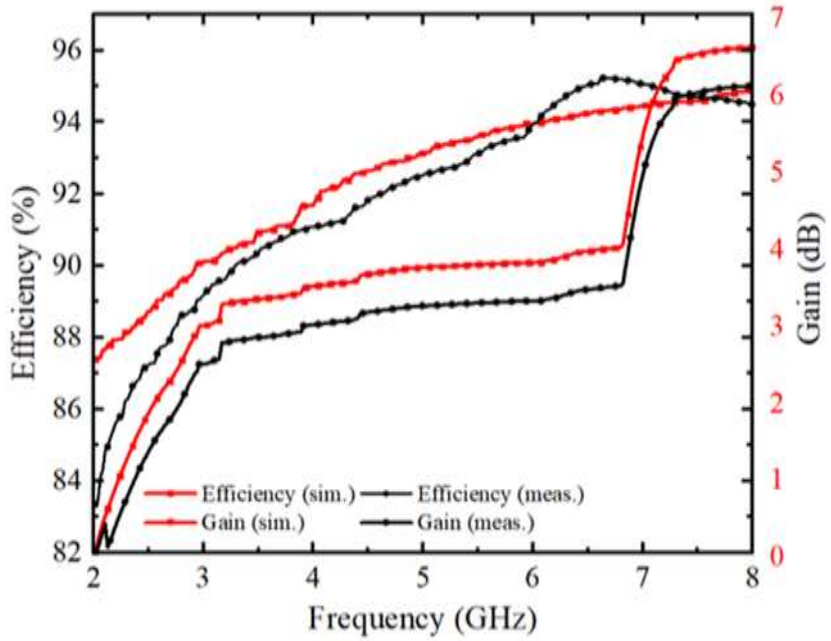


Figure 5.8 Measured and Simulated Efficiency and Gain of the suggested MIMO Antenna

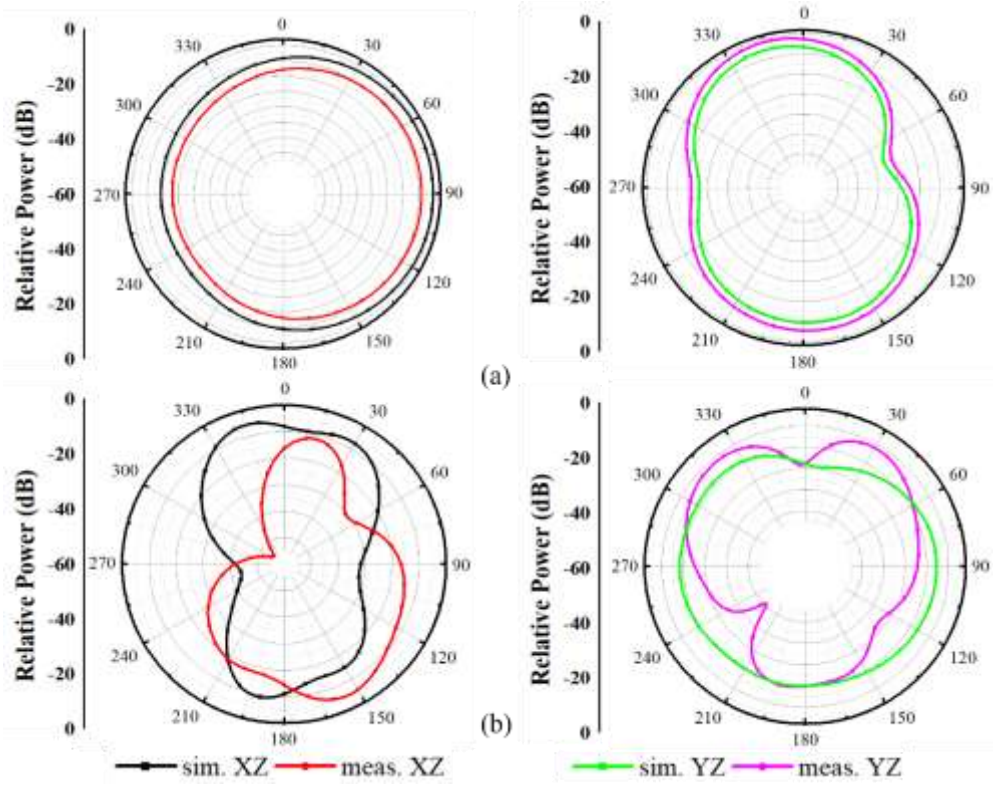


Figure 5.9 Simulated and measured pattern in YZ-plane and XZ-plane at (a) 3.4 GHz, and (b) 5.2 GHz.

Table 5.1 Comparison of the proposed work with other previously reported MIMO antennas

Ref.	Antenna Size (mm^2)	No. of Antenna elements	Bandwidth (GHz)	Isolation (dB)	Gain	ECC
[68]	50 × 100	4	2.7 to 3.6	>-13	>3	<0.009
[80]	75 × 150	8	3.3–3.9	>-18	3	<0.001
[84]	75×150	4	3.4–3.8	>-20	5.21	0.005
[93]	40 × 43	4	3.1–10.6	-20	4	<0.2
[94]	40 × 40	4	3.2-5.75	-22	9	<0.05
[104]	60 × 60	4	3.26–5.18	< -15	2.5 and 4.5	< 0.005
[131]	39 × 30	4	5.15-5.85	-20	2.8	--
[132]	150 × 75	4	3.4–3.6, 4.8–5.0	-17.5, -20	--	<0.14<0.12
[133]	70 × 160	4	5.6–5.67	>-30	--	<0.005
[134]	75 × 150	8	3.3–7.1	>-12	4.6–6.2	<0.07
[135]	80 × 150	8	3.6–3.8, 5.15–5.92	>-15	> 3	< 0.2
[136]	68 × 136	8	2.55–2.65	>12.5	3	<0.05
[137]	68 × 136	8	2.55–2.65	>-13	2.2–3	<0.1
[138]	136 × 68	8	5.15–5.92	> -10	12.6	< 0.005

[139] (Proposed)	52 x 31	4	3.06-7.56	> -15	Upto 7	< 0.0015

Table 5.1 provides a comparison between the proposed work and previous literature. In comparison to previously reported designs [68], [80], [84], [104], [132]-[139], the intended sub-6 GHz 5G antenna is highly compact with acceptable bandwidth ranging from 3.06-7.56 GHz with isolation above -15 dB. The analysis shows that, the fabricated prototype has compact dimensions with wide bandwidth coverage, sufficient isolation, and an excellent correlation coefficient useful for NR bands like n77, n78, and n79 as well as for WLAN bands (Wi-Fi-5 and Wi-Fi-6) applications.

5.4 Diversity Performance

The various diversity parameters of the MIMO antenna are analyzed through total active reflection coefficient (TARC), diversity gain (DG), channel capacity loss (CCL), and envelope correlation coefficient (ECC) [14], [128].

To understand the behaviour of MIMO antenna, it is always essential to first verify individual antenna element performance for the parameter like correlation coefficient and diversity gain, determined from S-parameter. For higher antenna efficiency, the appropriate correlation is obtained with the help of S-parameters as shown in figure 5.10. The value of ECC in the operational bands is less than 0.05. Further, in wireless antenna communication, signal travel through multiple path and results in the dissipation during power transmission through MIMO element without compromising loss of performance and thus, evaluated by diversity gain. The calculated DG from ECC is shown in figure 5.10 and the equation (21) and (22) shows the expression for ECC and DG.

$$ECC_{m\times n} = \frac{|S_{11}^{*}S_{12}+S_{12}^{*}S_{22}+S_{13}^{*}S_{32}+S_{14}^{*}S_{42}|^{2}}{(1-(|S_{11}|^{2}+|S_{21}|^{2}+|S_{31}|^{2}+|S_{41}|^{2}))(1-(|S_{12}|^{2}+|S_{22}|^{2}+|S_{32}|^{2}+|S_{42}|^{2}))} \quad \text{-------(17)}$$

$$DG_{m\times n} = 10\sqrt{1-ECC_{m\times n}^{2}} \quad \text{------(18)}$$

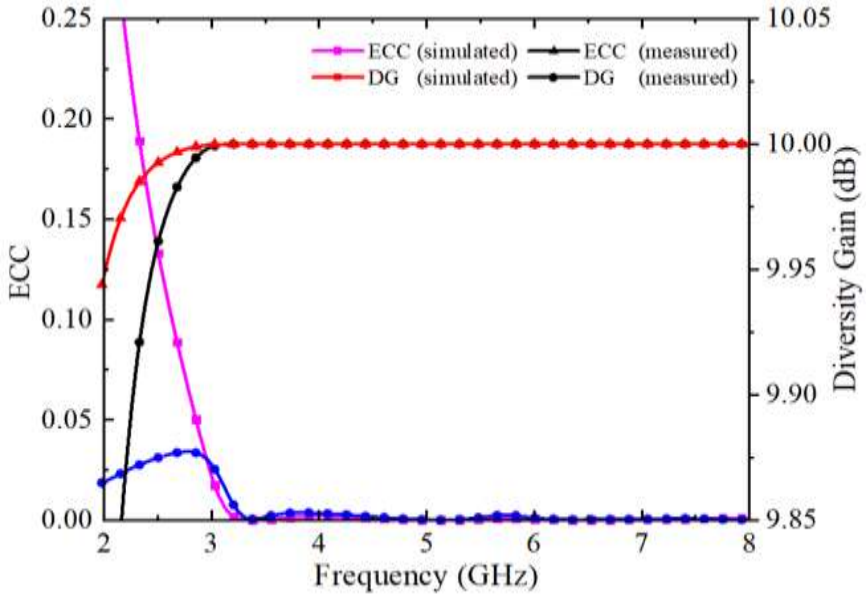


Figure 5.10 Simulated and measured diversity gain and ECC versus frequency

The TARC defines the radiation band of quad element MIMO and is calculated through equations (19) and (20) defined using s-parameters and is always ≤ 10 dB. The result shows shifting of frequency due to imperfection in measured and simulation result due to error during fabrication and input to one of the ports is linear and others are excited by deviation in phase angle. The CCL estimated in fading environment by considering appropriate signal to noise power and calculated by admittance from port 1 to port 4, and it is determined through equations (21) to (26). For the simplicity, the analysis of port 1 and 2 are taken here. The figure 5.10 and 5. 11 illustrate the MIMO's diversity measurement metrics performance.

$$\mathrm{TARC_{m\times n}} = \sqrt{\frac{(s_{mm}+s_{mn})^2 + (s_{nm}+s_{nn})^2}{2}} \quad \text{------(19)}$$

$$\mathrm{TARC_{14}} = \sqrt{\frac{(s_{11}+s_{14})^2 + (s_{41}+s_{44})^2}{2}} \quad \text{------(20)}$$

$$C_{loss} = -\log_2 \det\ (Y^R) \quad \text{------(21)}$$

$$\text{as, } (Y^R) = \begin{bmatrix} Y_{11} & Y_{12} \\ Y_{21} & Y_{22} \end{bmatrix} \quad \text{------(22)}$$

$$Y_{11} = 1 - |s_{11}|^2 - |s_{12}|^2 \quad \text{------(23)}$$

$$Y_{22} = 1 - |s_{22}|^2 - |s_{21}|^2 \quad \text{------(24)}$$

$$Y_{12} = -[S_{11}^* S_{12} - S_{21}^* S_{12}] \quad \text{------(25)}$$

$$Y_{21} = -[S_{22}^* S_{21} - S_{12}^* S_{21}] \quad \text{------(26)}$$

The environmental effects have impact on overall gain of antenna. The MEG is the ratio of average power accepted to the power incident. The MEG has considerable rage of < -3 dB and is shown in figure 5.12. The propagation statistics and radiation patterns can calculate a MEG to estimate the effective power of each ith element of a MIMO [126-127],

$$MEG = \frac{P_r}{P_i} = \oint \left[\frac{XPR.G_{\theta j}(\Omega).P_{\theta}(\Omega) + G_{\phi k}(\Omega).P_{\phi}(\Omega)}{1+XPR} \right] d\Omega \quad \text{------(27)}$$

For mth and nth antenna,

$$MEG_m = 1 - |s_{mm}|^2 - |s_{mn}|^2 \quad \text{------(28)}$$

$$MEG_n = 1 - |s_{nn}|^2 - |s_{nm}|^2 \quad \text{------(29)}$$

$$\frac{MEG_m = 1-|s_{mm}|^2-|s_{mn}|^2}{MEG_n = 1-|s_{nn}|^2-|s_{nm}|^2} \quad \text{------(30)}$$

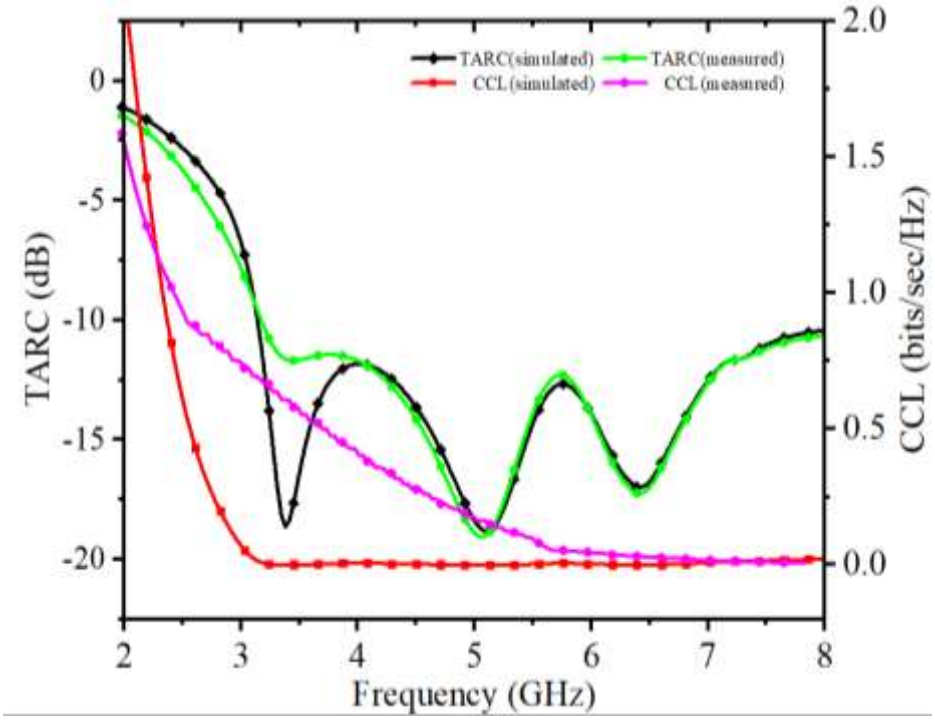


Figure 5. 11 Measured and simulated TARC and CCL

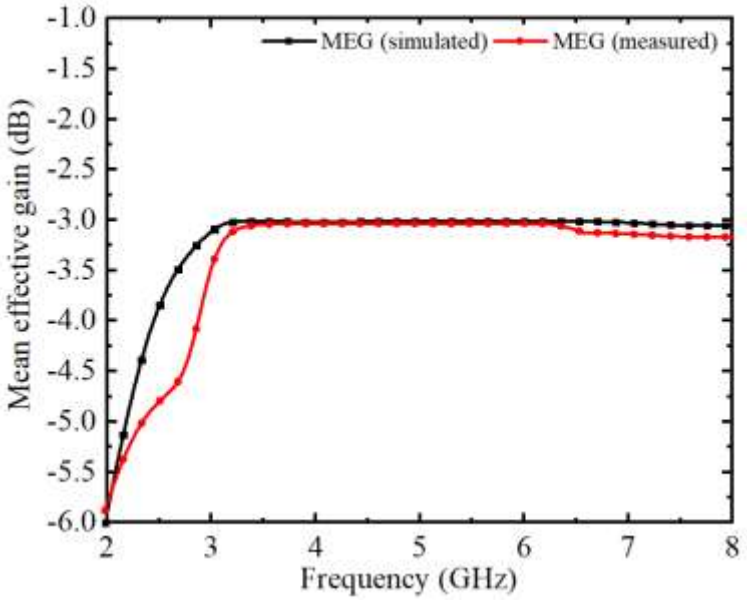


Figure 5.12 Measured and simulated mean effective gain (MEG)

As the expected value of ECC is below 0.5, in the proposed structure the obtained value of ECC is below 0.05 which is quite good. The DG > 9.999, MEG < -3 dB, and CCL < 0.2 bits/s/Hz, indicates the superior MIMO performance parameters used efficiently for the 5G application.

5.5 Device Enclosure and Packaging

The antenna proposed in this study is positioned within a plastic housing characterized by permittivity values of 2.2, 3, 4.4 and 4.8. The plastic housing is 52 mm × 31 mm in size. The box has height of 16 mm and thickness of 1 mm.

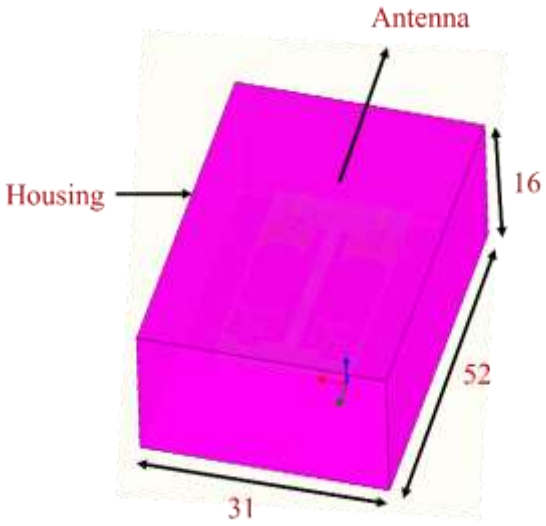


Figure 5.13 Housing of the designed MIMO antenna

The lower frequency band shifts down as the ε_r declines from 4.8-2.2. Additionally, S_{11} varies with ε_r, and isolation parameters S_{12} consistently maintained values less than -15 dB in the operating band as represented in fig. 5.13. This implies that the prototype MIMO can efficiently operate within various device housings [140-141].

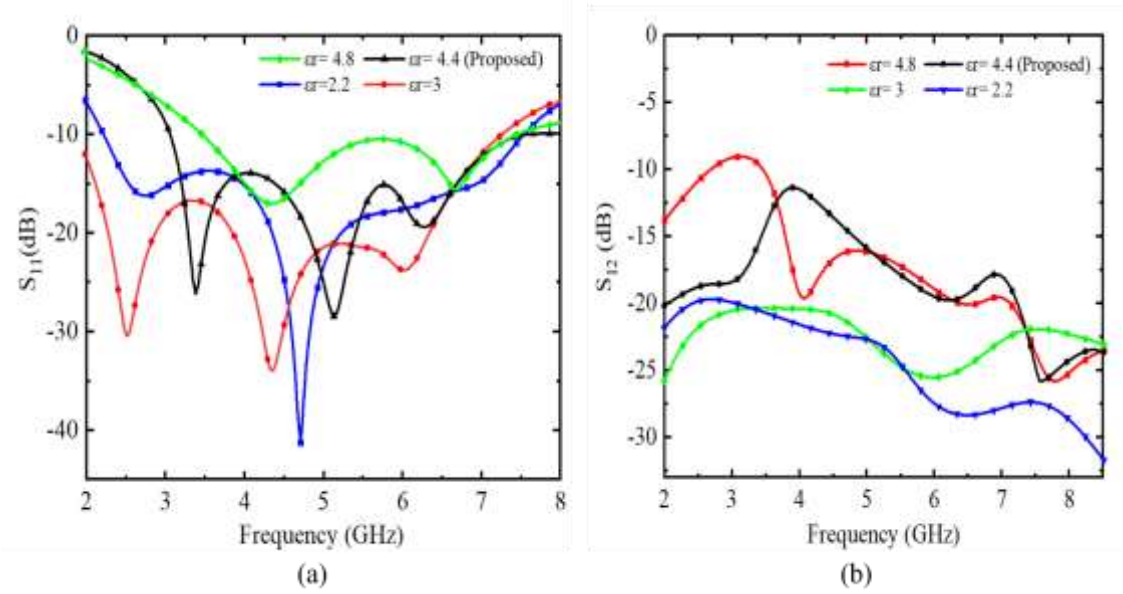


Figure 5.14 S-parameters for various materials with the designed MIMO antenna (a) Return loss (S_{11}), (b) Isolation parameters (S_{12}).

5.6 Implementation of 4-element MIMO using Low-temperature cofired ceramic (LTCC) Technology

5.6.1 Introduction of LTCC Technology

In the recent years, the substantial advancements have been made in wireless antenna models like MIMO, massive MIMO, and LTCC. The demand of LTCC antennas is increasing due to high 5G rollout and capacity to integrate into a miniature size. The LTCC based antenna will grow due to wide radio frequency spectrum which can integrate into a small module [142]. The LTCC module used for Internet-of-Things (IoT) applications, such as wearables, smart home-based systems, and connected vehicle needs reduced antennas size and multifunctional capabilities at high frequencies which include radar, vehicle-to-everything (V2X) communications and advanced driver-assistance systems (ADAS) in the automotive field. Currently, there are challenges such as cost and regulatory compliance but requires an innovation and strategic partnerships [143].

5.6.2 Geometry and Analysis of 5G-LTCC MIMO antenna

The geometric structure of the proposed 5G 4-element LTCC diversity MIMO antenna is depicted in figure 5.14. The substrate material used for the antenna is Ferro A6M with and overall dimensions of the prototype are 52 x 31 x 12 mm^3. The width of each layer of LTCC is 0.254 mm. At 4 GHz, the distance between elements is kept as λo/2 which reduces mutual coupling. The positioning involves a face-to-face arrangement between antenna elements 1 and 2 concerning antenna elements 3 and 4. The fig. 5.14 (a) depicts the antenna divided into numerous layers. We start with layer 1, which is on top. It is 1.2 mm thick and made of the ferro A6M LTCC material, 0.002 (loss tangent) and material constant of 5.9. The layer 2 encompasses the planar structure, situated between air gaps on both sides with thicknesses of hgs and hgr. The fig. 5.14 (b) shows the overall size and positioning on Layer 2. The conducting elements and ground plane are made of silver and have a conductivity of $\sigma_g = 7.4 \times 10^6$ S/m with thickness (hg).

The LTCC Ferro A6M material consists of five sub-layers, each with a thickness of 0.1277 mm. We denote the overall height of the LTCC layer as h_{LTCC}. As, layer 3 is the last layer, located at a specific height from layer 2's primary radiating elements. Silver is the chosen material for layer 3, with a thickness represented by h_{ref}. Furthermore, the LTCC material presents a distinct set of challenges because of its significant radiation losses, which exceed ε_r greater than 5. This makes it difficult to resonate an antenna in the required band of interest, specifically the sub-6 GHz 5G bands (n77, n78, n79).

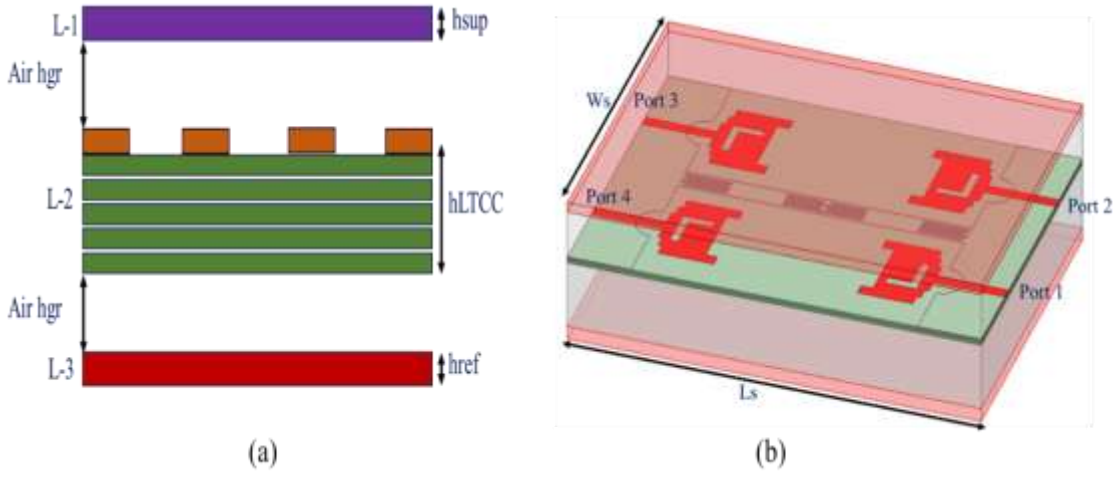


Figure 5.15 (a) Side perspective view (b) Front perspective view of prototype MIMO

Table 5.2 Optimized parameters with dimensions

L_s	h_{gr}	W_f	h_{sup}	h_{ref}
52	7	1.5	1.2	1.6
W_s	h_{LTCC}	L_f	h_{gs}	h_g
31	0.762	9	3.8	0.035

In this antenna design, from the layer 2 as the optimum configuration. With the use of LTCC sub-layers, this structure offers wide coverage across entire 5G spectrum. Additionally, compared with various LTCC antenna designs, it offers simplified fabrication with no need for unnecessary or complex cavities. Furthermore, the fact that this design includes layers 1 and 3 offers notable advantages for the targeted applications is another noteworthy benefit.

All 4 ports have identical placement on the LTCC substrate, so their return loss outcomes are all below -10 dB. Figure 5.16 displays the S-parameters of the 4-element MIMO antenna. The graph shows the frequency band from 2.69-6.86 GHz. However, the figure clearly indicates that the mutual coupling accounts for the increase in bandwidth. The use of a unique structure has improved the mutual coupling of -45 dB between 4-element design and attains a high-level efficiency.

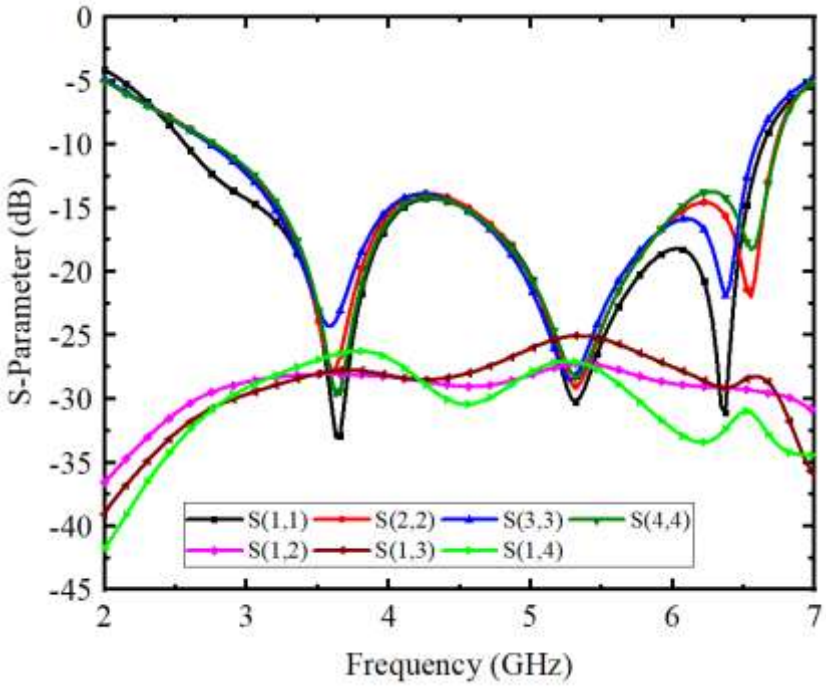


Figure 5.16 S-parameter of four-element MIMO with LTCC technique

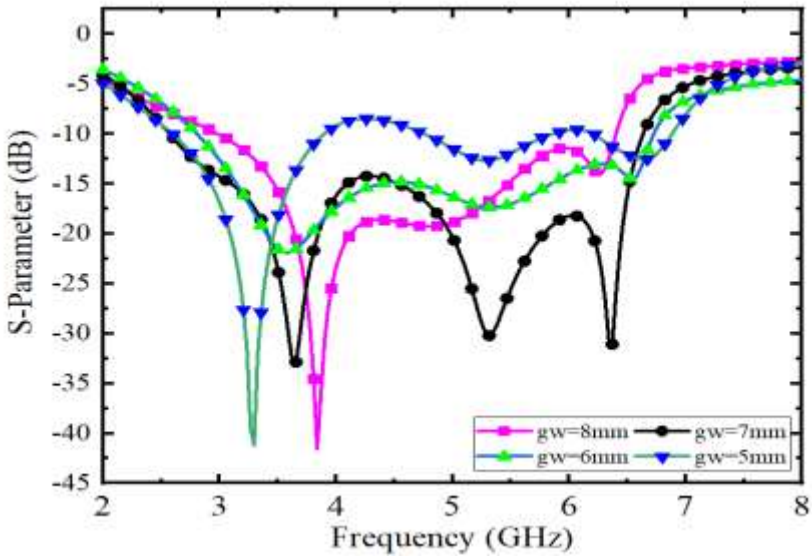


Figure 5. 17 S-Parameter of four-element MIMO-LTCC Antenna for varying ground width (gw)

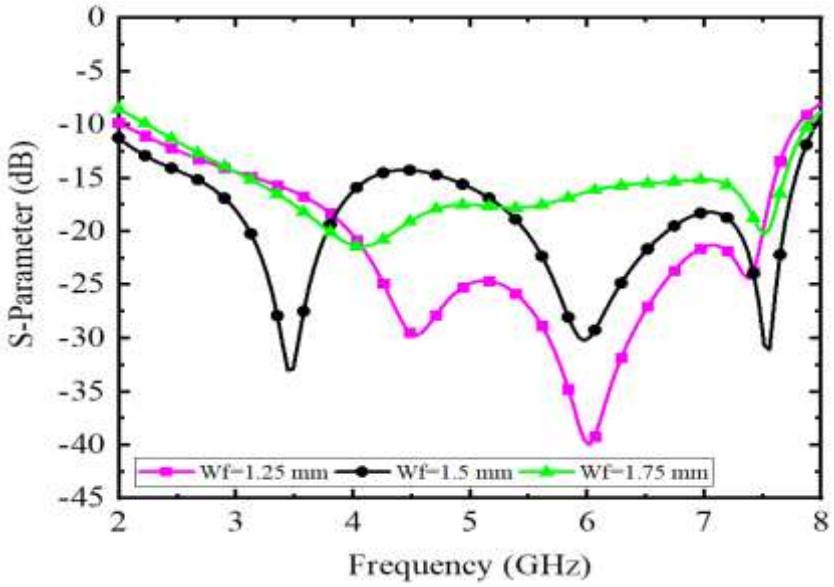


Figure 5. 18 S-Parameter of four-element MIMO-LTCC Antenna for varying feed line width (wf)

The fig. 5.16 shows the Scattering parameters of the 4-element LTCC based MIMO antenna. The graph shows a frequency band of 2.69-6.86 GHz. However, the graph clearly indicates that the suitable mutual coupling and the increase in the bandwidth. The use of a unique structure improved the mutual coupling of > -25 dB between the 4-element design. As observed in fig. 5.17 and 5.18, the optometric analysis is performed by varying ground length (gw) and feed line width (Wf). The corresponding

S-parameter for feed line width (Wf) at 1.25 mm, 1.5 mm ,1.75 mm and ground length (gw) 5, 6 7, 8 mm is plotted accordingly and the best values are selected as gw as -7 mm and Wf is 1.5 mm.

5.6.3 Radiation Performance of 5G-LTCC MIMO

The two-dimensional radiation pattern in the E and H Plane of the proposed four port antenna shown in the fig. 5.8 at the center frequency. The antenna in analysed in two principal plane (XY and YZ) which exhibits omnidirectional pattern used for practical 5G applications.

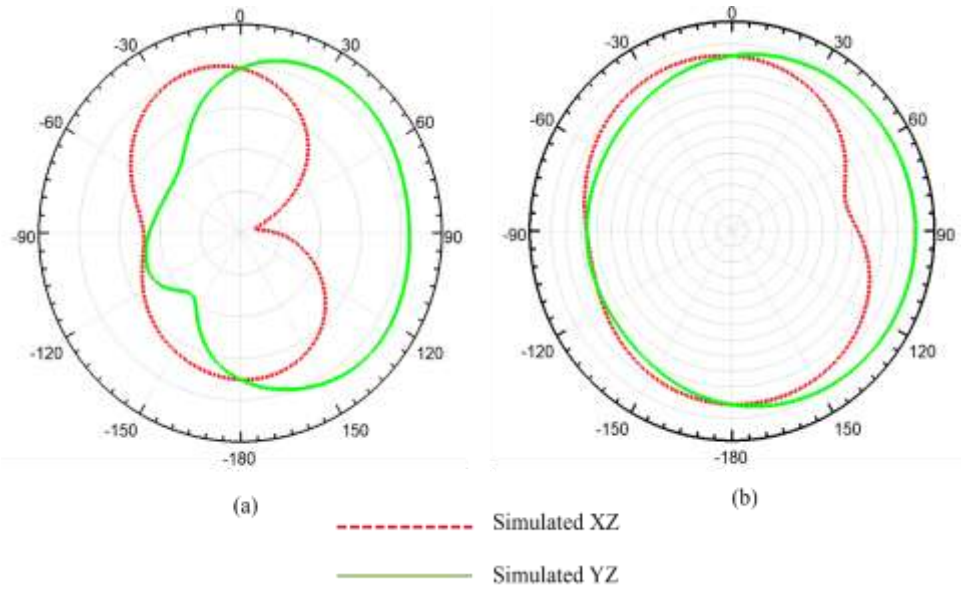


Figure 5. 19 2-D simulated radiation patterns of four port LTCC-MIMO along XZ and YZ Plane

Table 5.3 Comparative study with previously published Sub-6 LTCC planar patch

Sr. No.	B.W. (GHz)	Gain (dB)	Area (mm)	LTCC Tape	Constant ($\in_r$)	Loss Tangent	Firing Temp. (°C)
[144]	3.0-7.0	5	41×36	Ceramtec GC	8	0.002	900
[145]	2.5-2.54	5.22	116×55	DuPont 9K7	7.1	0.001	Not given

[146]	6.65-10.0	5	50×25	Ferro A65	5.9	0.0015	850
[147]	4.9-5.9	6	30×24	DuPont 951	7.8	0.002	850
[148]	3.0-5.0	4.5	19.25 ×12	Ferro A6M	5.9	0.0015	850
[149]	3.0-11.9	5	25×25	Ferro A6M	5.9	0.0015	850
[150]	2–11.8	10	75×78	GL-550	8.5	0.0003	900
[151]	25.5-29.5	5	12×12	DuPont DP943	7.8	0.002	850
[152]	4.35-10.5	4.7	66×50	DuPont 951	7.8	0.002	850
[153]	24-30	16	42.5× 42.5	Ferro A6M	5.9	0.0015	850
Propo sed	2.69-6.86	~ 7	52×31	Ferro A6M	5.9	0.0015	850

The comparative study shown in table 5.3 has diverse LTCC based antenna used for wide range of applications [144], [145]-[153]. The planar LTCC has less design complexity compared to proposed technique in terms of its stack layers and placement of MIMO but the presented antenna has effective broad bandwidth, higher gain and sufficient mutual coupling among 4-elements. The designed sub-6 GHz 5G antenna has the commendable -10 dB impedance bandwidth in the entire band of 2.69-6.86 GHz. Further, in this MIMO antenna technique, we achieve a sufficient reduction in the ECC and acceptable isolation, which makes this antenna suitable 5G-new radio (NR) and WLAN band wireless applications.

5.7 Summary

This chapter has suggested a quad-port staircase MIMO antenna for 5G-NR applications. High isolation and miniaturization, which are the crucial constraints for the MIMO system, have been attained only by the involvement of a staircase U-shaped radiating element and an I-shaped stub etched with rectangular strips in the ground plane. The beneficial part of this design is its compact size, which has a dimension of 52×31 mm^2. The design has progressed through fabrication accompanied by a testing phase to estimate the uniformity of simulated and measured results. The stated design exhibits the results such as the gain varies from 2 dB to 7dBi, 84.74% impedance bandwidth, isolation < -15 dB, ECC < 0.05, DG > 9.999, $MEG_1/MEG_2 \geq 0.95$, TARC ≤ - 10 dB, and CCL < 0.2 bits/sec/Hz. Hence, we can simply claim that this design is a suitable candidate for 5G NR (n77/n78/n79) application in the Sub 6GHz band as well as for WLAN (Wi-Fi 5 and Wi-Fi 6) band and imminent mobile communication.

Further, this chapter demonstrates a compact and low-profile 4-element LTCC-MIMO antenna optimized for sub-6 GHz 5G bands operating from 2.69-6.86 GHz which are highly suitable for 5G applications. The antenna exhibited impressive performance when incorporated into standard device dimensions using LTCC technology, affirming the robustness and practicality of the presented design. In the upcoming chapter, the future direction and its applicability in MIMO array for future generation with miniaturization is concluded.

6

Conclusions and Future Scope

"Antenna design is a balance between size, shape, and the desired radiation pattern."

- Warren L. Stutzman

6.1 Conclusion

In this thesis, sub-6 GHz wideband MIMO/diversity antennas are meticulously investigated in theoretical as well as practical aspects. Three miniature MIMO antennas for 5G new radio (n77/n78/n79/WLAN) are thoroughly evaluated through multiple simulations and measurements. These include a modified rectangular-shaped MIMO antenna, a Quad-radiator MIMO with asymmetric feed line, Quad-port staircase U-shaped MIMO/diversity antenna. To understand the broad-spectrum capability of the proposed antenna, we examine the design steps. Initially, we conduct simulation studies on software to examine the designed antennas and parameters like radiation patterns, return loss, and current distribution. Finally, we validated the designed antenna through fabrication and measurements. This chapter outlines the main outcomes of all the designed antennas.

In chapter three, a compact high-performance two-element MIMO diverse antenna is proposed for wireless-LAN (5 GHz) band and sub-6 GHz 5G (NR) band. The antenna consists of two symmetrical antenna elements with an inverted T-shaped ground structure. The antenna attributes such as S-parameters, realized gain, current distribution, and radiation patterns are studied. Additionally, MIMO performance was also investigated in terms of ECC, DG, TARC, and multiplexing efficiency. The antenna covers the entire 5G band for wireless communication, with an effective band (-10 dB) of 2.92 to 5.72 GHz (provides bandwidth of 2.8 GHz). The obtained values indicate that measured performance is in reasonable agreement with simulated performance. Additionally, efficiency and gain were above 80 % and upto 3 dB across the band of interest respectively.

Further, a compact quad port antenna using effective technique for sub-6 GHz 5G band is conferred in chapter four with broad bandwidth and nearly omnidirectional

radiation pattern. The face-to-face arrangement of quad patch elements reduces mutual coupling, while an inverted T-shape partial ground and stub elements enhance impedance matching. Twin stubs and rectangular notch on top right corner of the patch improves performance. The asymmetrical feed line structure of Quad port antenna with dimensions 31 × 40 mm^2, attained impedance bandwidth of 2.27 to 5.34 GHz. The key parameters like ECC, DG and isolation are analysed, ensuring wideband coverage and high isolation across n77/n78/n79 band for effective 5G MIMO performance.

Finally, in chapter five, a quad-port staircase U-shaped wideband MIMO antenna is presented for a 5G NR band. The beneficial part of this design is its compact size, which has a dimension of 52 × 31 mm^2. The miniaturization of the configuration is achieved with a staircase U-shaped radiating element, and an I-shaped stub etched with rectangular strips between radiating elements provides enhanced isolation. The measured bandwidth of 4.5 GHz is obtained with an isolation above -15 dB, radiation efficiency above 82%,, and the gain from 2 to 6.5 dBi respectively. Certain parameters, such as ECC, DG, MEG, CCL, and TARC, are also evaluated to ensure that the designed MIMO system adheres to its requirements. Hence, the suggested antenna suits the 5G New Radio applications.

The above discussed results demonstrate that all the antenna designs presented in this thesis functions as optimum solution for sub-6 GHz 5G applications and WLAN bands.

6.2 Future Scope

The antennas designed for 5G applications such as receivers, smartphones, on-body devices, and routers etc., are enabled by the useful design and versatile capabilities of MIMO antenna. The future generation mainly aims to improve the Internet of Everything (IoE) setup, which consists of high throughput and broadband usage for various applications, and MIMO can widen channel capacity by expanding the antenna nodes.

The following suggestions for additional research are discussed here.

1. The simulation and testing of all presented antennas in this thesis was conducted with the use of Ansys HFSS and VNA. Thus, in the near future, antennas designed for 5G applications must be integrated into devices, and their performance must be subsequently tested. The four-element MIMO is recognized for its use in base station

antennas, which require a more complex system that provides higher gain and directional features.

2. This thesis anticipated a compact high-performance 2-element/4-element MIMO for sub-6 GHz 5G applications. As the need for faster and more reliable wireless transmission grows, future study may focus on 8-element, 16-element and massive MIMO arrays. The research focuses on wide-ranging IoT applications which allows simultaneous communication among low-power devices and communication link quality in upcoming investigations to resolve challenges in deploying mMIMO.

3. To further shrink antenna size, the techniques involving meta-surfaces and THz communication can be explored, as they have the potential to significantly achieve miniaturization without compromising 5G MIMO performance.

4. The integration of AI and ML algorithms into antenna systems enables precise tracking, ensuring efficient power allocation and paving the way for more intelligent and adaptive wireless communication networks.

5. Compact reconfigurable broadside-radiating MSAs can enhance gain by offering multi-polarization states across 5G frequency bands. Their high gain and precise beam steering capabilities significantly reduce interference and multipath fading thereby enhancing SNR, diversity, and data rates. Overall, they represent an efficient and adaptable solution for advanced wireless communication.

Appendix-A

Supplementary Information

"New information opens the door to fresh and innovative ideas".

-Zig Ziglar

S.1 Introduction to High isolation 2-element MIMO

Over the past few decades, MIMO system has become increasingly important in the field of digital communication, particularly wireless communication. There has been a major evolution from SISO to MIMO as a result of the hard work of researchers who strive for excellence in the field of MIMO and other wireless technologies. MIMO enhances signal immunity by offering advantages in signal-to-noise ratio and channel capacity. The objective of this 2-element MIMO system is to develop diverse system with several performance parameters, such as mutual coupling between antenna, ECC, isolation, and QoS provided by MIMO. In MIMO array, the numbers of antennas elements deployed for trans-reception has greatly increased from 10 to 100 and extended upto thousand which is quite challengeable. As the data requirement for each user increasing every day, there is scope to develop new cellular era in which features a higher spectral efficiency (bit/sec/Hz/cell), higher cell density, bandwidth (Hz) and sufficient throughput. MIMO has roughly three scenarios i.e. P to P (peripheral to peripheral) MIMO, MU (multi-user)-MIMO and MaMi (massive-MIMO). Also, the MIMO array technology has large available bandwidth and it has advantage of millimetre frequency band and high-capacity gain gives advantage to next-generation mobile networks and cellular services as well as applications.

In this chapter, we are discussing popular wideband MIMO antennas in the era of wireless communication, where the data rate required is on the order of several gigabytes/sec and the problem of multipath fading and capacity can be enhanced. To achieve this goal, MIMO with diverse array combination can do this, as the MIMO technology has several characteristics by which channel capacity can be increased

without any extra bandwidth, along with combat to multipath propagation and a high data rate can be obtained.

S.2 Proposed Model of a single element patch

Case I: In this proposed model, a single element patch proposed antenna is placed on FR4 substrate with a dielectric constant ($\in_r$) of 4.4, a loss tangent (tan δ) of 0.002, and a thickness (t) of 1.6 mm. The optimized structure includes a partial ground with dimensions of 12×2 mm^2 (Lg×Wg), and a substrate of 18×12 mm^2 (L×W) with an improved feed line of 1.5 mm is to attain a characteristic impedance (Z_0) of 50 Ω.

Table S.1 Antenna parameters (in mm).

W	L	L_p	Wp	L_f	W_f	Lt	Lg	W1	L1	Ls
12	18	8.5	8.5	5	1.5	1.5	2	3	3	5.2

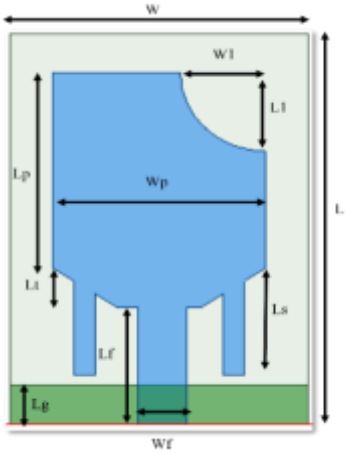


Figure S.1 Geometry of the antenna

Figure S.1 illustrates the geometry of the envisioned single patch antenna consists of a square shaped patch with a slightly etched copper from top right corner (L1 × W1). Here, the symmetric 2-rectangular stub lines are connected on the bottommost end of the patch to improve the bandwidth. The rectangular patch resonates at 5.2 GHz. The simulated reflection coefficient (S11) shows the bandwidth from 4.16 to 6.1 GHz. A minor change in the impedance bandwidth is observed in figure 2 when the width of the feed line is changed from 1 to 1.5 mm.

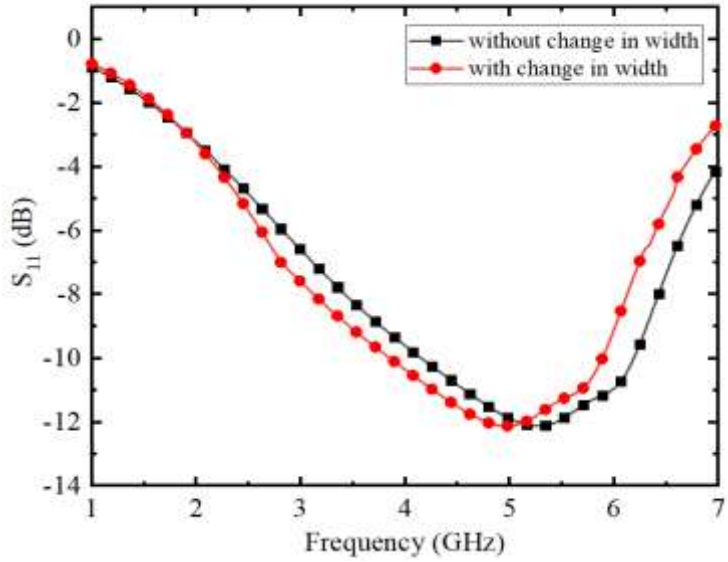


Figure S.2 Reflection coefficient (S_{11}) of Single element antenna

The antenna has simulated gain of 1.9 dB and the efficiency is approximately around 88%. Also, the corresponding vector current distribution of the proposed single antenna is depicted in figure 3, showing the current flows primarily through the feed point, part of the stub, and the lower part of the patch. The bandwidth is considerably narrow in this case probably due to the quality factor.

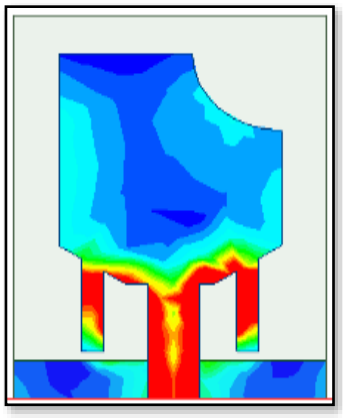


Figure S.3 Vector current density of reference antenna at resonance

Case II: Here, the two-element antenna consists of a square type patch with a slight copper etched from the top right corner, with symmetric 2-rectangular stub lines connected and in the shape of U, etching is done to form a defective ground to obtain a resonant frequency of 5.2 GHz to improve bandwidth for forthcoming 5G band and WLAN applications. In case I, the disadvantage of narrow bandwidth is overcome by using an asymmetric feed line, which improves the bandwidth and gain by 15 % and

0.8 dB, respectively. The proposed antenna is placed on FR4 substrate with a constant (∈r) = 4.4, tan δ= 0.002 and the thickness (t) of 1.6 mm. The optimized structure of dimension 36 × 18 mm_2 (W×L), with an improved feed line of 3 mm to attain a desired characteristic impedance (Z_0) of 50 Ω as shown in Figure S.4.

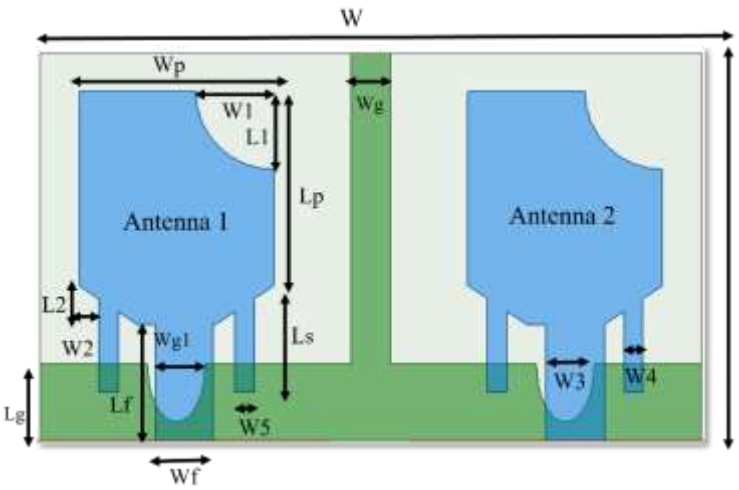


Figure S.4. Geometry of the proposed two-element antenna

Table S.2 Antenna geometry (in mm)

W	L	Lp	Wp	Lf	Wf
36	18	8.5	8.5	5	3.2
W1	L1	W2	W3	W4	
2.8	2.8	1	1.5	1	
Ls	Lg	Wg	Wg1	W5	
5.2	3	2.5	2	1	

The final S-parameters of the above design are shown in Figure S.5. The result shows that the obtained bandwidth is from 3.1 to 5.6 GHz with a minimum isolation -15 dB, and it follows the prerequisite demand of 5G communication for wideband operation. It also covers the 5.2 GHz unlicensed wireless LAN.

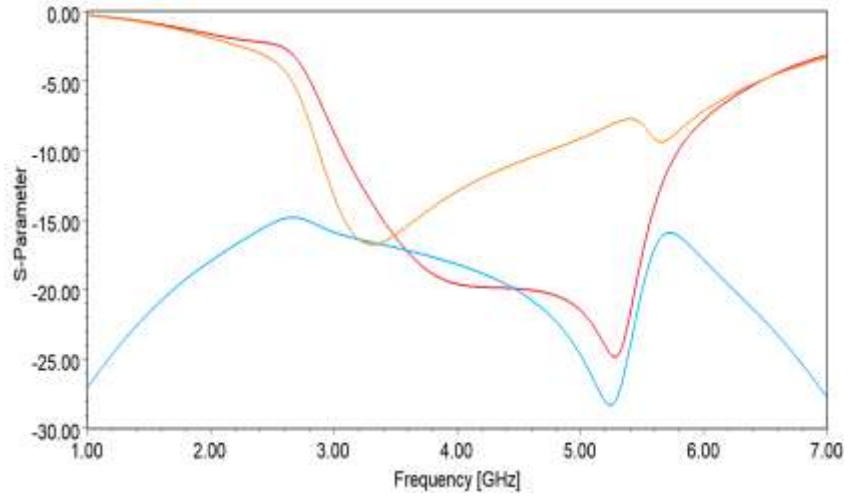


Figure S.5 S-parameter of proposed 2-element MIMO

The simulation study of S-parameters is shown in figure S. 5 for various values of feed line i.e., at 2.8 mm, 3.2 mm and 3.6 mm, respectively. The desired result is obtained at 3.2 mm with sufficient isolation, but isolation can be improved further above -15 dB, if we change feed line width to 3.6 mm, but then other performance parameters are affected. The current passed through the feed point, a portion of the stub, and the lower side of the patch, as shown in the vector current distribution of the suggested single antenna as shown in figure S.6. The bandwidth is broadened in this case with the principle of asymmetrical feed line.

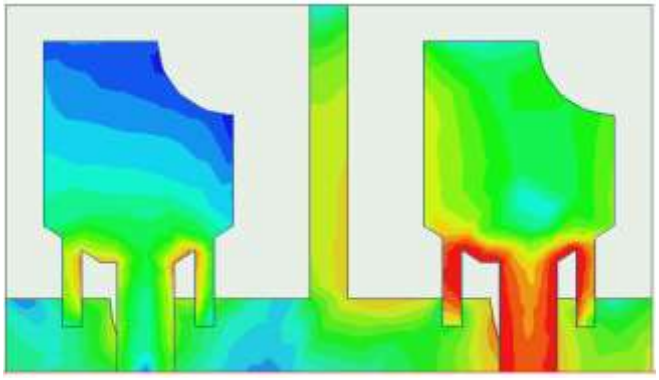


Figure S.6 Vector current density of 2-element antenna

3.3. Parametric Analysis

The figure S.7 shows the 2-D omnidirectional radiation pattern at resonant frequency when one antenna is active and the other is matched terminated. To understand the behaviour of MIMO diversity performance parameter, the ECC Vs frequency was analysed. The ECC should be below 0.5, and the mathematical analysis is specified in

[21]. The TARC and DG versus frequency show that the reflection coefficient is between 1 and 0, the ratio of MEG i.e. (MEG_1/MEG_2) versus frequency has a good effective value, and the CCL versus frequency specifies that the CCL must be below 0.5 bits-per-sec/hertz. It has been observed that all performance parameters are within acceptable range and illustrated in figures S. 8 (A) - (D).

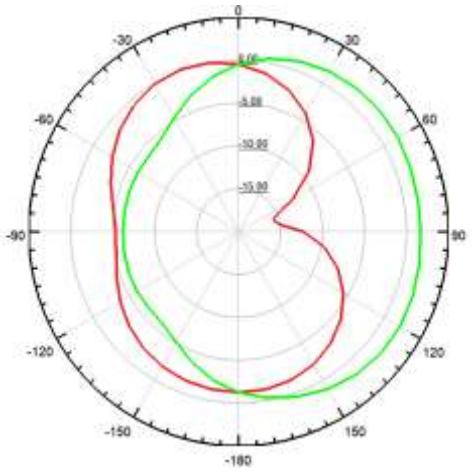
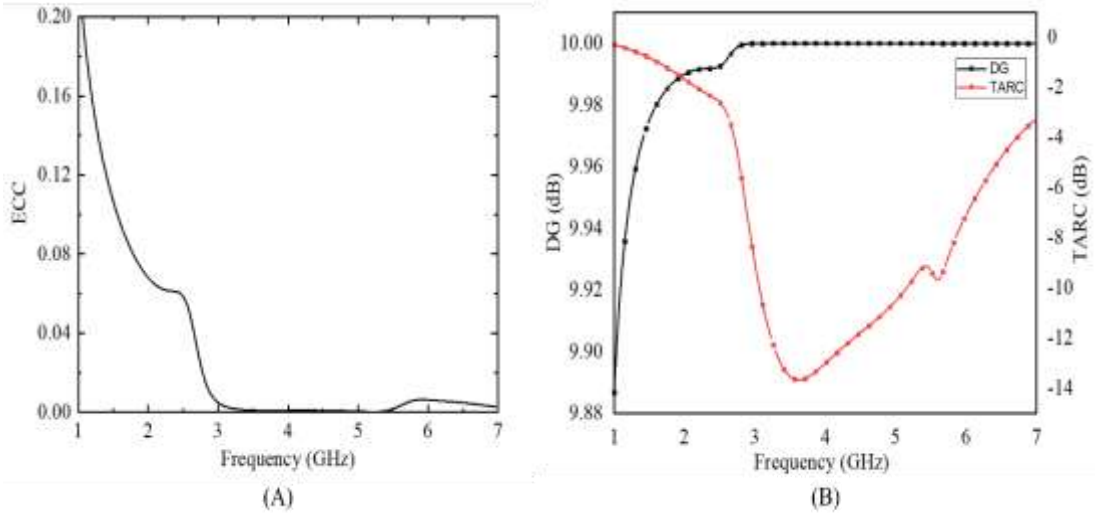


Figure S.7 2-D Radiation pattern of two-element MIMO



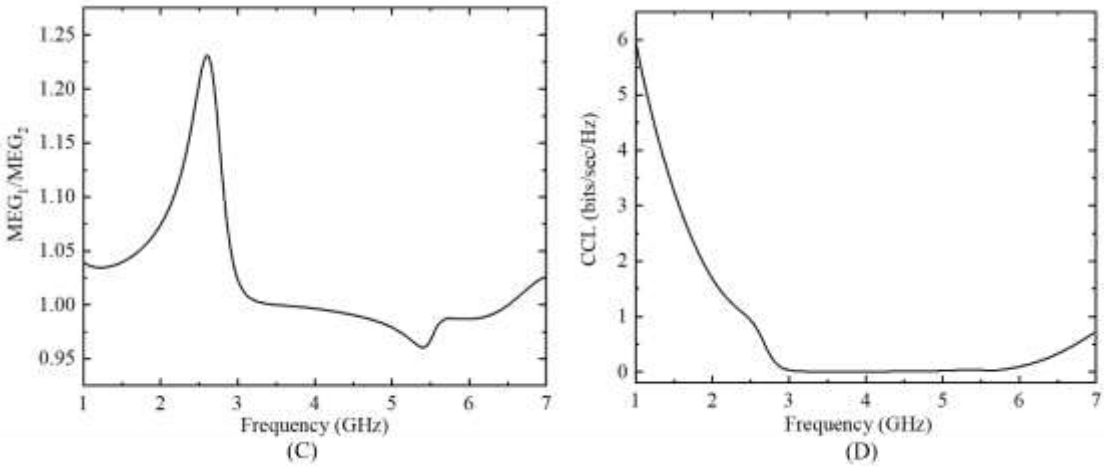


Figure S.8 (A) Correlation coefficient against frequency, (B) TARC and DG against frequency, (C) (MEG1/MEG2) versus frequency, (D) channel capacity loss (CCL) versus frequency

Table S.3. Comparative Investigation of MIMO Antennas

Ref. No.	Area (mm^2)	Substrate	Type of MIMO	Working frequency Range (GHz)	Isolation (dB)	ECC
[20]	145 × 75	FR-4	Adjacent spaced by inserting line decoupling	3.3 – 5	> 10.8	< 0.14
[32]	24 × 25	FR-4	Dual band MIMO using Slot antenna	2.40-2.67/5.46-5.73	≥20	< 0.004
[50]	50 × 80	FR-4	Novel dual band	2.45/5.8	≥20	< 0.01
[51]	20 × 56	FR-4	dual band with decoupling	2.37-2.53/5.10-5.90	≥13	< 0.2
[53]	48.5 × 60.6	F4B	Dual Band closely coupled Patch MIMO	3.7/4.1	NA	< 0.01

[52]	60 × 50	FR-4	Dual band monopole using DGS	2.5/5.5	-20/-40	NA
[63]	38.2 × 95.94	FR-4	2-element patch with/without EBG and inset fed	2.43-2.50	-24.67	0.0087
[65]	240 × 240	FR4	a novel decoupling slot-strip array (DSSA)	1.256- 1.272	> -30	< 0.005
[69]	20×46	FR-4	Dual band MIMO slot	2.40-2.50/4.90-5.75	≥-12	< 0.27
[68]	50 × 100	FR-4	Inverted-F antenna (IFA)	2.7 to 3.6	-25	< 0.3
[104]	60 × 60	FR-4	Calendula patch with rectangular stub	3.26-5.18	> -15	<–0.005
[114]	47.5 × 40	FR-4	Two element arrays with parasitic element	3.11–3.81	42.9	0.001
Proposed	36 ×18	FR-4	Square type patch with asymmetric feed	3.1-5.6	> -15	< 0.0015

In this, various performance parameters like correlation coefficient, isolation of MIMO antennas were studied, along with the diverse types of MIMO available. The analysis in Table I was carried out to compare the performance characteristics of dual band, triband, wide band MIMO. The work presented by various researcher has acceptable isolation and sufficient ECC, but in few research papers, there is a scope of further enhancement. The respectable isolation obtained in most of the papers is around

20 to 25 dB, and the value of ECC is < 0.5. Accordingly, the obtained bandwidth of designed MIMO ranges from 3.1 to 5.6 GHz and the adequate isolation of -28 dB meets demand of 5G communication. The results reveal that throughout the band, ECC is 0.015, DG is around 9.95, TARC is greater than 0.8, and CCL is less than 0.3 bps/Hz. In nutshell, an efficient antenna design approach is deliberated that can be used to achieve exceptional isolation among 2-element compact and small size MIMO for sub-6 GHz 5G applications.

S.5 Four Element MIMO Antenna with PLUS shape radiator arrangement and corporate feed for WLAN and 5G wideband wireless Applications

S.5.1 Introduction

In recent years, there have been significant strides in wireless communication technology. The use of antennas in mobile terminals is imperative as a consequence of the miniaturization process, necessitating their size reduction. Planar antennas, such as microstrip and printed antennas, are favored for their low profile, compact size, and adaptability to conform to mounting hosts. These characteristics make them attractive alternatives for the development of a variety of materials. Consequently, these seem to be highly promising candidates for satisfying this design requirement in the future. As a result, antenna researchers have focused towards developing techniques for compact, broadband, and wideband antenna design. To satisfy their bandwidth requirements, modern mobile cellular communication systems developed a number of unique planar antenna designs. Together, MIMO antennas improve data speeds and solve issues like multipath fading, which are essential for wireless communication. Leveraging MIMO technology through diverse array combinations offers the potential to augment channel capacity without the need of additional bandwidth. This technology effectively addresses multipath propagation, enabling high data rates to be attained. The compact antenna is a primary requirement with closely spaced elements used for wireless communication at a 5.5 GHz WLAN application, which is suitable for MIMO systems. The compact four-element broadband optimized MIMO antenna that prioritizes adequate isolation and wide bandwidth from 2 to 12.27 GHz.

The structure consists of four antenna elements positioned at 90° intervals from each other, mounted on a plus-shaped FR4 substrate. The resulting MIMO antenna system has dimensions of 48(W) × 52(L) × 1.6(h) mm^3. Across all frequency bands,

this MIMO antenna system maintains greater than -20 dB isolation. Moreover, it demonstrates an impressive ECC ≤ 0.3 within the operational band. The proposed MIMO antenna emerges as an optimal solution for compact handheld devices and smartphones, effectively addressing a spectrum of applications, including 5G-IoT, WLAN, and the unlicensed UWB band.

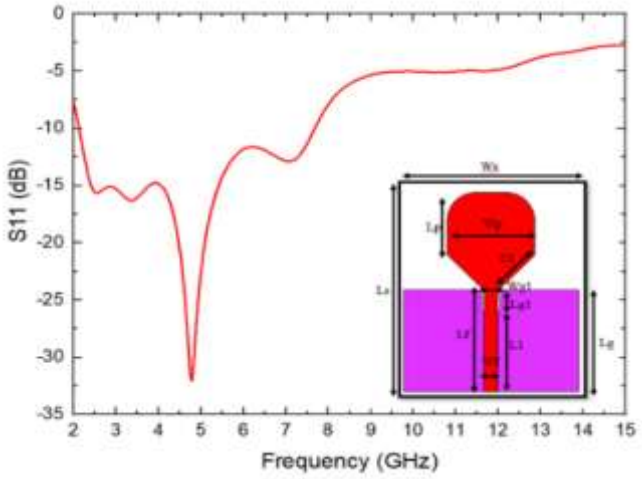


Figure S.9 Simulated S-parameters (S_{11}) against frequency and single element Geometry

In this design as shown in fig. S.9, an antenna utilizing a singular patch element is positioned on an FR-4 material. The substrate possesses ∈r = 4.4, loss tangent = 0.002, and 1.6 mm in thickness. The advanced arrangement incorporates a partial ground plane measuring 12.5 × 24 mm^2 (length × width, denoted as (Lg × Wg), and the substrate dimensions are 26 × 24 mm^2 (length × width, denoted as L × W). An enhanced feed line of 3 mm width is employed to reach a desired char. impedance (Z_0) of 50 Ω.

S.6 Four element wideband MIMO

Antenna arrays permit an antenna system to scan its field of view to improve multiple parameters such as gain and directivity. In microstrip array, elements are organized in the PLUS shape wherein all elements are placed at 90° with each other in the clockwise manner fed by corporate type coaxial feed as shown in fig. S.10. It comprises of four identical radiating elements located on the upper surface of the substrate and a modified square shape common ground is used for isolation improvement. An entire dimension of the designed antenna is only 48 mm x 52 mm = 2496 mm^2. The coupling between ground and rectangular stubs helps to shift the frequency band towards lower side. The

square shape ground plane of dimension ($L_{g3}\times W_{g3}$) 25 mm x 25 mm with corporate feed network and corner etched slot ($L_{g2}\times W_{g2}$) is provided on all four corners of modified ground to expand the mutual coupling. Further, to cover partial ultra-wide band, a square-shape slot ($L_{g1}\times W_{g1}$) is provided on the ground. To cover all 5G-NR bands and wideband corporate coaxial feeding principal is used as shown in figure S.10 (B). The coaxial connector's central conductor extends through the dielectric and is affixed to the radiating patch via soldering. Simultaneously, the outer conductor establishes a connection with the ground plane. This approach offers a notable advantage: it permits flexible positioning of the feed anywhere within the patch area to achieve the desired input impedance match. This feeding technique is both straightforward to manufacture and minimizes unintended radiation. It proves particularly well-suited for broad bandwidth applications when employed with a thick dielectric substrate. The dimensions of the optimized feed line (length and width represented as L_f x W_f) is well-tuned to achieve a characteristic impedance (Z_o) of 50 Ω. Refer table S.4 for the specific optimized measurements.

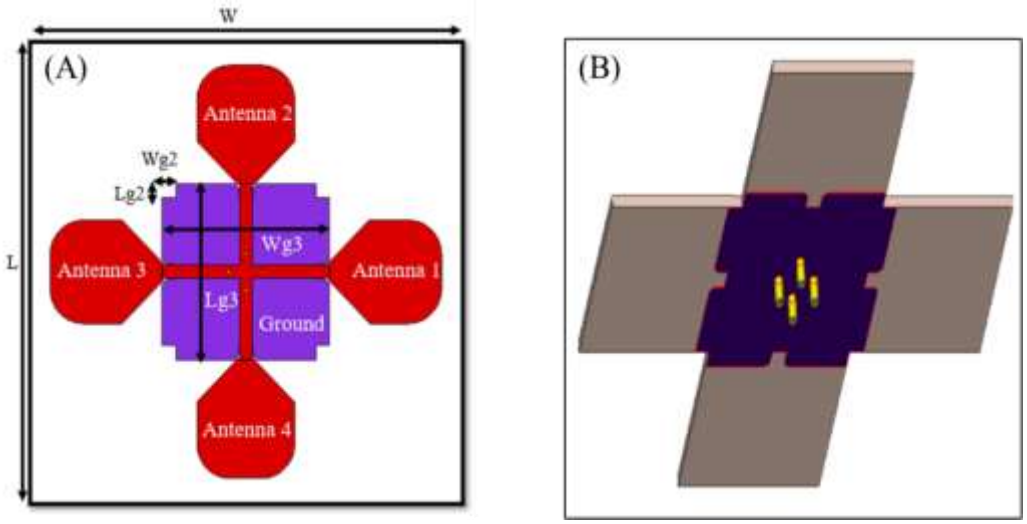


Figure S.10 (A) 4-element patch placement of proposed antenna, (B) Perspective view of proposed antenna

Table S.4 Proposed parameters of the four-element antenna

Ws	Ls	h	L_g	W_p	L_p
24	26	1.6	12.5	10	6.5

W_g	W_f	L_f	C_1	L_{g1}	W_{g1}
24	3	12.5	5.5	3	4
L1	Lg_2		Wg2	Lg_3	Wg_3
9.5	3		3	25	25

S.7 Results and discussion

As shown in figures S.11 (A)-(B), which include a bandwidth of 2 GHz to 12.27 GHz and an isolation level of -20 dB, meet the needs for wideband function in 5G communication.

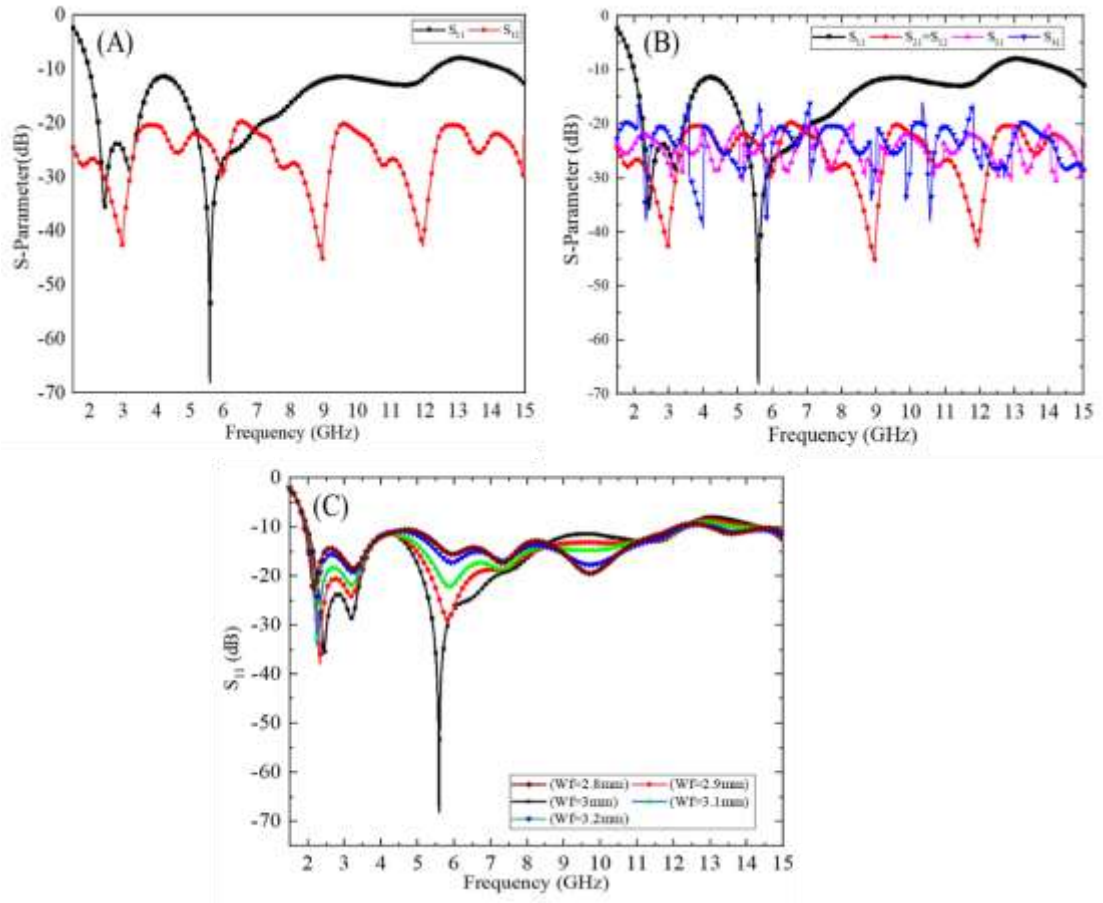


Figure S.11 (A) Simulated S-parameters (S_{11} and S_{12}) versus frequency, (B) Simulated S-parameters ($S_{11}/S_{21}/S_{31}/S_{41}$) versus frequency, (C) Plot of simulated S-parameters versus frequency for different value of Wf

The system supports wireless LANs of 5.5 GHz and ultrawideband frequencies. The figure S.11 (C) illustrates feedline width related to the S_{11} characteristics of the suggested antenna. The change in feedline width, ranging from 2.8 mm to 3.2 mm, remarkably enhances impedance matching between 5 and 6 GHz. Consequently, a feedline width (W_f) of 3 mm is selected as the optimal choice for favourable impedance matching across the entire frequency band.

The variation on the Ground slot length and length of the ground plane (L_{g1} and L_{g3}) is depicted in fig. S.12. From the fig. S.12 (A) displays poor impedance matching at 2 mm, 4 mm and 5 mm. After optimization, a frequency deep is obtained at 5.5 GHz and wide band coverage for L_{g1} = 3 mm. Further, for various ground length value is observed in fig. S.12 (B). For L_{g3}=25 mm, the antenna covers all sub-6 GHz 5G band and ultra-wide-band along with WLAN.

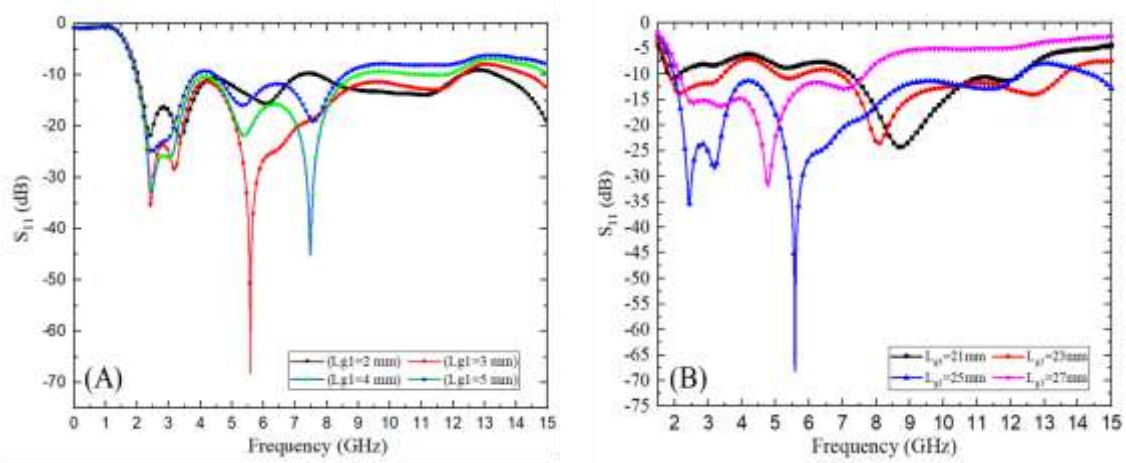


Figure S.12 (A) Plot of simulated S-parameters versus frequency for different values Lg1, (B) Plot of simulated S-parameters versus frequency for different values (Lg3)

The calculation of the ECC, a key indicator of diversity performance, can be accomplished either through a far-field or by using S-parameters. The perfect MIMO array has ECC equal to zero, whereas in real-world scenarios, these values are anticipated to be below 0.50 as observed in fig. S.13 (A).

The DG shows the variations among the time-average SNR signals, indicates the best possible diversity in a communication channel. When compared to a single antenna system, it provides gain relation with other nearby radiating antenna which is represented in fig. S.13 (B).

It is seen from the fig.S.13 (B), that the simulated and the measured value of the DG is almost identical and greater than > 8.2 dB.

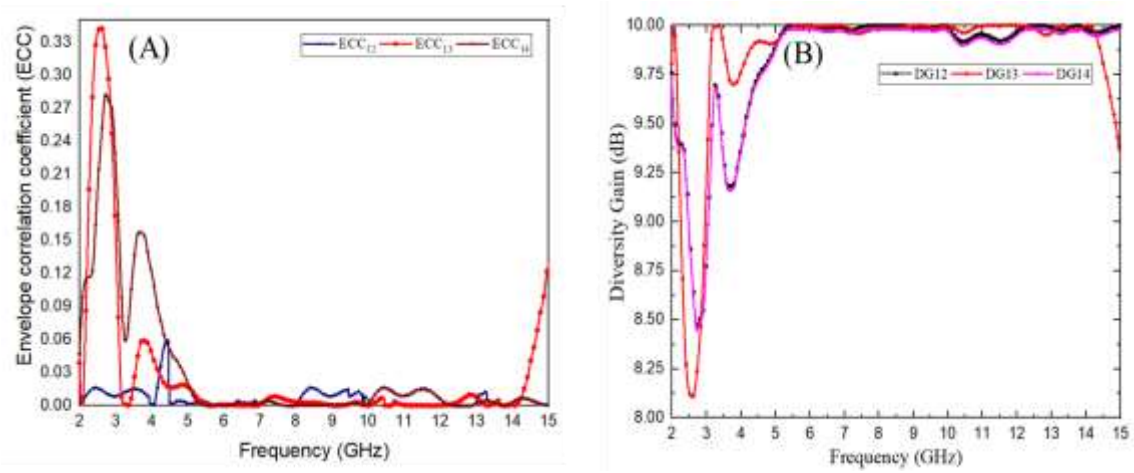


Figure S.13 (A) Simulated ECC of the proposed MIMO, (B) Simulated Diversity gain

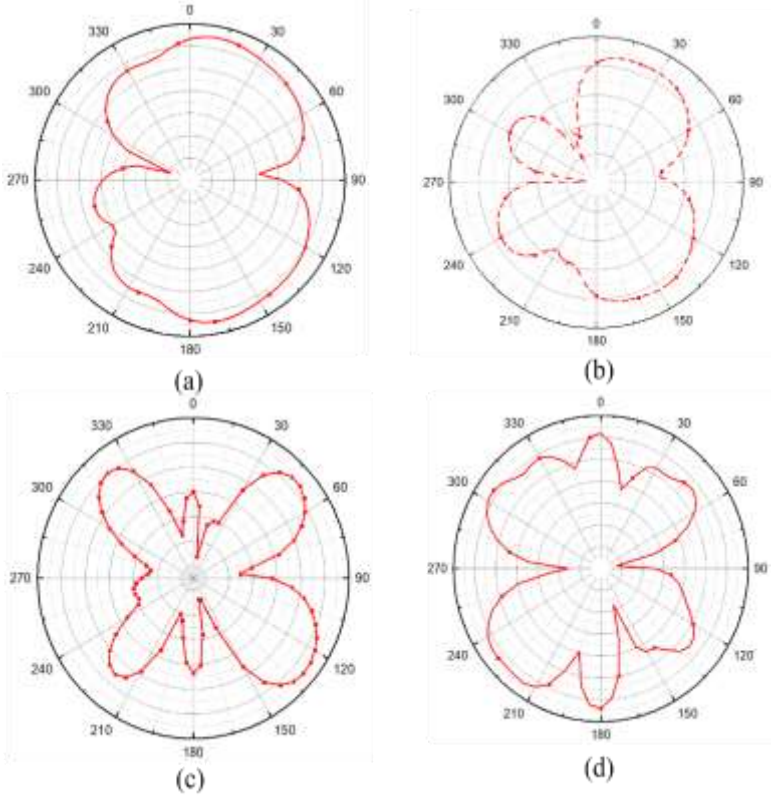


Figure S.14 Two-dimensional radiation pattern of corporate-fed microstrip array antenna: (a) at 4 GHz, (b) at 5.5 GHz, (c) at 8 GHz, and (d) at 9.5 GHz.

The proposed antenna's 2-D radiation pattern at 4 GHz, 5.5 GHz, 8 GHz, and 9.5 GHz is shown in fig. S.14 (a)-(d). This shows that the pattern is dipole-like and omnidirectional.

S.8 Summary

This chapter studies various MIMO antenna performance parameters, including correlation coefficient and isolation. The achieved bandwidth from 2 to 12.27 GHz, along with a minimum isolation of -20 dB, effectively fulfills wireless communication requirements. With a specific focus on 4-element MIMO antennas, the chapter explores the potential for wideband communication applications, and achieves high isolation in sub-6 GHz band used in 5G applications. The findings demonstrate encouraging results, with an ECC of 0.06 and DG of approximately 9.85, both falling well within the acceptable ranges for optimal MIMO performance. In essence, the chapter introduces ongoing research in efficient antenna design approach and contributes to the valuable insights into the performance parameters of MIMO antennas.

References

[1]. Gupta and E. R. K. Jha, ‘‘A survey of 5G network: Architecture and emerging technologies,’’ IEEE Access, vol. 3, pp. 1206–1232, Jul. 2015.

[2]. M. Vaezi et al., "Cellular, Wide-Area, and Non-Terrestrial IoT: A Survey on 5G Advances and the Road Toward 6G," in IEEE Communications Surveys & Tutorials, vol. 24, no. 2, pp.1117-1174, Second quarter 2022, doi:10.1109/COMST.2022.3151028.

[3]. P. Sharma, ‘‘Evolution of mobile wireless communication networks-1Gto 5G as well as future prospective of next generation communication network,’’ Int. J. Comput. Sci. Mobile Comput., vol. 2, no. 8, pp. 47–53,2013.

[4]. J. Parikh and A. Basu, ‘‘LTE advanced: The 4G mobile broadband technology,’’ Int. J. Comput. Appl., vol. 13, no. 5, pp. 17–21, 2011.

[5]. J. A. del Peral-Rosado, R. Raulefs, J. A. López-Salcedo and G. Seco-Granados, "Survey of Cellular Mobile Radio Localization Methods: From 1G to 5G," in IEEE Communications Surveys & Tutorials, vol. 20, no. 2, pp. 1124-1148, Second quarter 2018, doi:10.1109/COMST.2017.2785181.

[6]. L. Chettri and R. Bera, “A Comprehensive Survey on Internet of Things (IoT) Toward 5G Wireless Systems,” IEEE Internet Things J., vol. 7, no. 1, pp. 16–32, 2020, doi: 10.1109/JIOT.2019.2948888.

[7]. 3GPP, TS 22.263, "Service Requirements for Video, Imaging and Audio for Professional Applications (VIAPA)", Dec. 2020.

[8]. R. N. Mitra and D. P. Agrawal, “5G mobile technology: A survey,” ICT Express, vol. 1, no. 3, pp. 132–137, Dec. 2015, doi: 10.1016/j.icte.2016.01.003.

[9]. M. Agiwal, A. Roy, and N. Saxena, “Next generation 5G wireless networks: A comprehensive survey,” IEEE Communications Surveys and Tutorials, vol. 18, no. 3. Institute of Electrical and Electronics Engineers Inc., pp. 1617–1655, Jul. 01, 2016. doi: 10.1109/COMST.2016.2532458.

[10]. S. Nirmal and S. Kumar, "Analysis of Diverse MIMO Antennas for Fifth Generation Application: A Review," 2022 IEEE Wireless Antenna and Microwave Symposium (WAMS), 2022, pp. 1-5, doi: 10.1109/WAMS 54719.2022.9848357.

[11]. R. Chataut and R. Akl, “Massive MIMO systems for 5G and beyond networks—overview, recent trends, challenges, and future research direction,” Sensors (Switzerland), vol. 20, no. 10. MDPI AG, 2020. doi: 10.3390/s20102753.

[12]. Y. Huo, X. Dong, and W. Xu, “5G cellular user equipment: From theory to practical hardware design,” IEEE Access, vol. 5, pp. 13992– 14010, 2017.

[13]. IMT Traffic Estimates for the Years 2020 to 2030, document ITU-R SG05, Jul. 2015.

[14]. Y. Huo, X. Dong, W. Xu, and M. Yuen, “Enabling Multi-Functional 5G and beyond User Equipment: A Survey and Tutorial,” IEEE Access, vol. 7, pp. 116975–117008, 2019, doi:10.1109/ACCESS.2019.2936291.

[15]. 5G NR (New radio) http://3gpp.org

[16]. N. O. Parchin et al., “Eight-Element Dual-Polarized MIMO Slot Antenna System for 5G Smartphone Applications,” IEEE Access, vol. 7, pp. 15612–15622, 2019, doi:10.1109/ACCESS.2019.2893112.

[17]. S. R. Thummaluru, M. Ameen, and R. K. Chaudhary, “Four-port MIMO cognitive radio system for midband 5G applications,” IEEE Trans. Antennas Propag., vol. 67, pp. 5634–5645, 2019, doi: 10.1109/TAP.2019.2918476.

[18]. Rec. ITU-R M.2083-0, Sep. (2015). IMT Vision - Framework and overall objectives of the future development of IMT for 2020 and beyond.

[19]. Yazdan doost and R. Kohno, “Ultra-wideband antenna,” IEEE Communication Magazine, vol. 42, no. 6, pp. 30–38, 2004.

[20]. L. Sun, Y. Li, and Z. Zhang, “Wideband integrated quad-element MIMO antennas based on complementary antenna pairs for 5G smartphones,” IEEE Trans. Antennas Propag., vol. 69, no. 8, pp. 4466–4474, 2021, doi: 10.1109/TAP.2021.3060020.

[21]. Z. N. Chen, M. J. Ammann, X. Qing, X. H. Wu, T. S. P. See and A. Cai, "Planar antennas," in IEEE Microwave Magazine, vol. 7, no. 6, pp. 63-73, Dec. 2006, doi: 10.1109/MW-M.2006.250315.

[22]. L. Zhao, Z. M. Chen, and J. Wang, ‘‘A wideband dual-polarized omnidirectional antenna for 5G/WLAN,’’ IEEE Access, vol. 7, pp. 14266–14272, 2019.

[23]. S. Hussain, S. W. Qu, W. L. Zhou, P. Zhang, and S. Yang, ‘‘Design and fabrication of wideband dual-polarized dipole array for 5G wireless systems,’’ IEEE Access, vol. 8, pp. 65155–65163, 2020.

[24]. Sun, Y. Y., S. W. Cheung, and T. I. Yuk. "Studies of planar antennas with different radiator shapes for ultra-wideband body-centric wireless communications." Progress In Electromagnetics Research Symposium (PIERS). 2011.

[25]. Shannon, Claude Elwood. "A mathematical theory of communication." The Bell system technical journal 27.3 (1948): 379-423.

[26]. Pozar, David M. Microwave engineering. John wiley & sons, 2011

[27]. Winters, Jack. "On the capacity of radio communication systems with diversity in a Rayleigh fading environment." IEEE journal on selected areas in communications 5.5 (1987): 871-878.

[28]. Foschini, Gerard J., and Michael J. Gans. "On limits of wireless communications in a fading environment when using multiple antennas." Wireless personal communications 6.3 (1998): 311-335.

[29]. J.G. Proakis, Digital Communications, 4th Edition. 2001.

[30]. Sanket Nirmal and Richa Chandel, “A Survey of Fifth-Generation Cellular Communications Using MIMO for IoT Applications,” in Microstrip Antenna Design for Wireless Applications, 1st ed., vol. 1st, Praveen Kumar Malik, Sanjeevi kumar Padmanaban, and Jens Bo Holm-Nielsen, Eds., Boca Raton: CRC Press, 2021, pp. 142–152. doi: https://doi.org/10.1201/9781003093558.

[31]. R. K. Mistri et al., “Quad Element MIMO Antenna for C, X, Ku, and Ka-Band Applications,” Sensors (Basel), vol. 23, no. 20, Oct. 2023, doi: 10.3390/s23208563.

[32]. Nandi, S. and A. Mohan, “A compact dual-band MIMO slot antenna for WLAN applications,” IEEE Antennas Wirel. Propag. Lett., Vol. 16, 2457–2460, Jul. 2017, doi: 10.1109/LAWP.2017.2723927.

[33]. Malviya, L., Panigrahi, R. K., & Kartikeyan, M. V. MIMO antennas with diversity and mutual coupling reduction techniques: a review. International Journal of Microwave and Wireless Technologies, 9(8), 1763-1780. 2017.

[34]. D. Q. Liu, M. Zhang, H. J. Luo, H. L. Wen, and J. Wang, ‘‘Dual- band platform-free PIFA for 5G MIMO application of mobile devices,’’ IEEE Trans. Antennas Propag., vol. 66, no. 11, pp. 6328–6333, Nov. 2018.

[35]. H. Shin and J. H. Lee, "Capacity of multiple-antenna fading channels: spatial fading correlation, double scattering, and keyhole," in IEEE Transactions on Information Theory, vol. 49, no. 10, pp. 2636-2647, Oct. 2003, doi: 10.1109/TIT.2003.817439.

[36]. C. A. Balanis, “Antenna Theory: Analysis and Design”, 4th ed. Hoboken, NJ, USA: John Wiley & Sons, 2016.

[37]. S. Kumar, A. S. Dixit, R. R. Malekar, H. D. Raut, and L. K. Shevada, “Fifth generation antennas: A comprehensive review of design and performance enhancement techniques,” IEEE Access, vol. 8, pp. 163568–163593, 2020, doi: 10.1109/ACCESS.2020.3020952.

[38]. L. Xi, “A wideband planar filtering dipole antenna for 5G communication applications,” Microw. Opt. Technol. Lett.,vol. 61, no. 12, pp. 2746-2751, 2019, doi: 10.1002/mop.31966.

[39]. M. S. Sharawi, M. Ikram, and A. Shamim, ‘‘A two concentric slot loop based connected array MIMO antenna system for 4G/5G terminals,’’ IEEE Trans. Antennas Propag., vol. 65, no. 12, pp. 6679–6686, Dec. 2017.

[40]. S. Dixit and S. Kumar, "A Miniaturized Antipodal Vivaldi Antenna for 5G Communication Applications," 2020 7th International Conference on Signal Processing and Integrated Networks (SPIN), Noida, India, 2020, pp. 800-803, doi: 10.1109/SPIN48934.2020.9071075.

[41]. Mohamed Mostafa Morsy, "4-Port Planar MIMO Antenna Using Open-Slot Radiators for 5G New Radio (NR) Frequency Bands n38 (2570 to 2620 MHz) and n41 (2496 MHz -2690 MHz) Applications," *Progress in Electromagnetics Research Letters*, Vol. 104, 87-94, 2022. doi:10.2528/PIERL22021401

[42]. Nadeem, I. and D.-Y. Choi, “Study on mutual coupling reduction technique for MIMO antennas”, IEEE Access, Vol. 7, 563–586, 2019, doi: 10.1109/ACCESS.2018.2885558.

[43]. C.-Y.-D. Sim, V. Dhasarathan, T. K. Tran, J. Kulkarni, B. A. Garner, and Y. Li, “Mutual Coupling Reduction in Dual-Band MIMO Antenna Using Parasitic Dollar-Shaped Structure for Modern Wireless Communication,” IEEE Access, vol. 11, pp. 5617–5628, 2023, doi: 10.1109/ACCESS.2023.3235761.

[44]. N. Hussain, M. J. Jeong, A. Abbas, T. J. Kim, and N. Kim, ‘‘A metasurface-based low-profile wideband circularly polarized patch antenna for 5G millimeter-wave systems,’’ IEEE Access, vol. 8, pp. 22127–22135, 2020.

[45]. A. A. K. Singh et al., “Low-Loss Paper-Substrate Triple-Band-Frequency Reconfigurable Microstrip Antenna for Sub-7 GHz Applications,” Sensors, vol. 23, no. 21, p. 8996, Nov. 2023, doi: 10.3390/s23218996.

[46]. B. A. F. Esmail et al., “Reconfigurable metamaterial structure for 5G beam tilting antenna applications,” Waves in Random and Complex Media, vol. 31, no. 6, pp. 2089–2102, 2021, doi: 10.1080/17455030.2020.1720933.

[47]. H. Ullah and F. A. Tahir, ‘‘Broadband planar antenna array for future 5G communication standards,’’ IET Microw., Antennas Propag., vol. 13, no. 15, pp. 2661–2668, Dec. 2019.

[48]. R. Azim *et al.*, “A multi-slotted antenna for LTE/5G Sub-6 GHz wireless communication applications,” *International Journal of Microwave and Wireless Technologies*, vol. 13, no. 5, pp. 486–496, 2021. doi:10.1017/S1759078720001336

[49]. Z. Li, Y. Sun, M. Yang, Z. Wu, and P. Tang, ‘‘A broadband dual-polarized magneto-electric dipole antenna for 2G/3G/LTE/WiMAX applications,’’ Prog. Electromagn. Res. C, vol. 73, pp. 127–136, Apr. 2017

[50]. X. Ling and R. Li, "A Novel Dual-Band MIMO Antenna Array with Low Mutual Coupling for Portable Wireless Devices," in IEEE Antennas and Wireless Propagation Letters, vol. 10, pp. 1039-1042, 2011, doi: 10.1109/LAWP.2011.2169035.

[51]. Wang, S.-M., Hwang, L.-T., Lee, C.-J., Hsu, C.-Y. and Chang, F.-S. MIMO antenna design with built-in decoupling mechanism for WLAN dual-band applications. Electron. Lett 2015, 51: 966-968. https://doi.org/10.1049/el.2014.4352

[52]. L. Yi, Y. Yu, X. Liu, S. Chen, N. M. Rizka and Z. Gu, "Compact printed dual-band monopole array with high port isolation," 2014 International Symposium on Antennas and Propagation Conference Proceedings, 2014, pp. 463-464, doi: 10.1109/ISANP.2014.7026727.

[53]. Niu, Z., H. Zhang, Q. Chen, and T. Zhong, "Isolation enhancement in closely coupled dual-band MIMO patch antennas," IEEE Antennas Wirel. Propag. Lett., Vol. 18, No. 8, 1686–1690, Aug. 2019, doi: 10.1109/LAWP.2019.2928230.

[54]. Z. Tang, X. Wu, J. Zhan, S. Hu, Z. Xi, and Y. Liu, "Compact UWB MIMO Antenna with High Isolation and Triple Band-Notched Characteristics," IEEE Access, vol. 7, no. c, pp. 19856–19865, 2019, doi: 10.1109/ACCESS.2019.2897170.

[55]. H. Zou, Y. Li, C. Y. D. Sim, and G. Yang, "Design of 8 × 8 dual-band MIMO antenna array for 5G smartphone applications," Int. J. RF Microw. Comput. Eng., vol. 28, no. 9, pp. 1–12, 2018, doi: 10.1002/mmce.21420.

[56]. Zhai, G., Z. N. Chen, and X. Qing, "Mutual coupling reduction of a closely spaced four-element MIMO antenna system using discrete mushrooms," IEEE Trans. Microw. Theory Tech., Vol. 64, No. 10, 3060–3067, 2016.

[57]. Su, S., C. T. Lee, and Y. W. Hsiao, "Compact two-inverted-F-antenna system with highly integrated π-shaped decoupling structure," IEEE Trans. Antennas Propag, Vol. 67, No. 9, 618–6186, Sep. 2019, doi: 10.1109/TAP.2019.2925286.

[58]. Xu, Z., Q. Zhang, and L. Guo, "A compact 5G decoupling MIMO antenna based on split-ring resonators," Int. J. Antennas Propag., 1–10, 2019.

[59]. Zhang, S. and G. F. Pedersen, "Mutual coupling reduction for UWB MIMO antennas with a wideband neutralization line," IEEE Antennas and Wireless Propagation Letters, Vol. 15, 166–169, 2019, https://doi.org/10.1109/LAWP.2015.2435992.

[60]. Yue, T. W., Z. H. Jiang, and D. H. Werner, "A compact metasurface-enabled dual-band dual circularly polarized antenna loaded with complementary split ring resonators," IEEE Trans. Antennas Propag., Vol. 67, No. 2, 794–803, Feb. 2019.

[61]. N. Tiwari and T. Rama Rao, ''Substrate integrated waveguide based high gain planar antipodal linear tapered slot antenna with dielectric loading for 60 GHz communications," Wireless Pers. Commun., vol. 97, no. 1, pp. 1385–1400, Nov. 2017.

[62]. Sharma, A., G. Das, and R. K. Gangwar, “Design and analysis of tri-band dual-port dielectric resonator-based hybrid antenna for WLAN/WiMAX applications,” IET Microwaves, Antennas and Propagation, Vol. 12, No. 6, 986–992, May 2018, doi: 10.1049/iet-map.2017.0822.

[63]. Sharma, K. and G. P. Pandey, “Two port compact MIMO antenna for ISM band applications,” Progress in Electromagnetics Research C, Vol. 100, 173–185, 2020.

[64]. D. Q. Liu, H. J. Luo, M. Zhang, H. L. Wen, B. Wang, and J. Wang, ‘‘An extremely low-profile wideband MIMO antenna for 5G smartphones,’’ IEEE Trans. Antennas Propag., vol. 67, no. 9, pp. 5772–5780, Sep. 2019.

[65]. Gao, D., Z. Cao, X. Quan, M. Sun, S. Fu, and P. Chen, “A low-profile decoupling slot strip array for 2 × 2 microstrip antenna,” IEEE Access, Vol. 8, 113532–113542, 2020, doi: 10.1109/ACCESS.2020.3002862.

[66]. Rajkumar, S., Vivek Sivaraman, N., Murali, S., & Selvan, K. T. Heptaband swastik arm antenna for MIMO applications. IET Microwaves, Antennas & Propagation, 11(9), 1255-1261. 2017.

[67]. P. Shariff B. G. et al., “High-Isolation Wide-Band Four-Element MIMO Antenna Covering Ka-Band for 5G Wireless Applications,” IEEE Access, vol. 11, pp. 123030–123046, 2023, doi: 10.1109/ACCESS.2023.3328777.

[68]. H. T. Chattha, ‘‘4-port 2-element MIMO antenna for 5G portable applications,’’ IEEE Access, vol. 7, pp. 96516–96520, 2019.

[69]. Soltani, S., P. Lotfi, and R. D. Murch, “A dual-band multiport MIMO slot antenna for WLAN applications,” IEEE Antennas Wirel. Propag. Lett., Vol. 16, 529–532, 2017, doi: 10.1109/LAWP.2016.2587732.

[70]. S. C. Chen, C. W. Chiang and C. I. G. Hsu, "Compact Four-Element MIMO Antenna System for 5G Laptops," in IEEE Access, vol. 7, pp. 186056-186064, 2019, doi: 10.1109/ACCESS.2019.2959314.

[71]. M. Khalid et al., “4-port MIMO antenna with defected ground structure for 5G millimeter wave applications,” Electron., vol. 9, no. 1, 2020, doi: 10.3390/electronics9010071.

[72]. R. Ullah, S. Ullah, R. Ullah, F. Faisal, I. B. Mabrouk and M. J. A. Hasan, "A 10-Ports MIMO Antenna System for 5G Smart-Phone Applications," in IEEE Access, vol. 8, pp. 218477-218488, 2020, doi: 10.1109/ACCESS.2020.3042750.

[73]. H. N. Chen, J. -M. Song and J. -D. Park, "A Compact Circularly Polarized MIMO Dielectric Resonator Antenna Over Electromagnetic Band-Gap Surface for 5G Applications," in IEEE Access, vol. 7, pp. 140889-140898, 2019, doi: 10.1109/ACCESS.2019.2943880.

[74]. A. K. Saurabh and M. K. Meshram, "Compact sub-6 GHz 5G multiple-input-multiple-output antenna system with enhanced isolation," Int. J. RF Microw. Comput. Eng., vol. 30, no. 8, pp. 1–11, 2020, doi: 10.1002/mmce.22246.

[75]. W. E. N. Jiang, B. O. Liu, Y. Cui, and W. E. I. Hu, "High-Isolation Eight-Element MIMO Array for 5G Smartphone Applications," IEEE Access, vol. 7, pp. 34104–34112, 2019, doi: 10.1109/ACCESS.2019.2904647.

[76]. A. S. Dixit and S. Kumar, "A Miniaturized Antipodal Vivaldi Antenna for 5G Communication Applications," 2020 7th International Conference on Signal Processing and Integrated Networks (SPIN), Noida, India, 2020, pp. 800-803, doi: 10.1109/SPIN48934.2020.9071075.

[77]. J. Deng, J. Li, L. Zhao, and L. Guo, ''A dual-band inverted-F MIMO antenna with enhanced isolation for WLAN applications,'' IEEE Antennas Wireless Propag. Lett. vol. 16, pp. 2270–2273, 2017.

[78]. D. Q. Liu, M. Zhang, H. J. Luo, H. L. Wen, and J. Wang, ''Dual- band platform-free PIFA for 5G MIMO application of mobile devices,'' IEEE Trans. Antennas Propag., vol. 66, no. 11, pp. 6328–6333, Nov. 2018.

[79]. N. K. Darimi reddy, R. R. Reddy and A. M. Prasad, "A Miniaturized Hexagonal-Triangular Fractal Antenna for Wide-Band Applications [Antenna Applications Corner]," in IEEE Antennas and Propagation Magazine, vol. 60, no. 2, pp. 104-110, April 2018, doi: 10.1109/MAP.2018.2796441.

[80]. N. O. Parchin, Y. I. A. Al-Yasir, H. J. Basherlou, R. A. Abd Alhameed, and J. M. Noras, "Orthogonally dual-polarised MIMO antenna array with pattern diversity for use in 5G smartphones," IET Microwaves, Antennas Propag., vol. 14, no. 6, pp. 457–467, 2020, doi: 10.1049/iet-map.2019.0328.

[81]. M. Abdullah, S. H. Kiani, and A. Iqbal, "Eight Element Multiple Input Multiple-Output (MIMO) Antenna for 5G Mobile Applications," IEEE Access, vol. 7, pp. 134488–134495, 2019, doi: 10.1109/ACCESS.2019.2941908.

[82]. Ghannad, A. A., M. Khalily, P. Xiao, R. Tafazolli, and A. A. Kishk, “Enhanced matching and vialess decoupling of nearby patch antennas for MIMO system,” IEEE Antennas Wirel. Propag. Lett., Vol. 18, No. 6, 1066–1070, Jun. 2019, doi: 10.1109/LAWP.2019.2906308.

[83]. Y. L. Ban, C. Li, C. Y. D. Sim, G. Wu, and K. L. Wong, “4G/5G Multiple Antennas for Future Multi-Mode Smartphone Applications,” IEEE Access, vol. 4, pp. 2981–2988, 2016, doi: 10.1109/ACCESS.2016.2582786.

[84]. V. Kaushal, A. Birwal, and K. Patel, “Diversity characteristics of four-element ring slot-based MIMO antenna for sub-6-GHz applications,” ETRI Journal, 2023, doi: 10.4218/etrij.2022-0113.

[85]. Jayant, S. and G. Srivastava, “Compact 4 × 4 proximity coupled microstrip fed UWB stepped slot MIMO antenna having triple band rejection,” Wireless Pers Commun., Vol. 119, 3719–3734, 2021, https://doi.org/10.1007/s11277-021-08428-w.

[86]. D. K. Raheja, B. K. Kanaujia, and S. Kumar, “Compact four-port MIMO antenna on slotted-edge substrate with dual-band rejection characteristics,” International Journal of RF and Microwave Computer-Aided Engineering, vol. 29, no. 7, Jul. 2019, doi: 10.1002/mmce.21756.

[87]. W. Wu, B. Yuan, and A. Wu, “A quad-element UWB-MIMO antenna with band-notch and reduced mutual coupling based on EBG structures,” Int J Antennas Propag, vol. 2018, 2018, doi: 10.1155/2018/8490740.

[88]. J. A. Tirado-Méndez, H. Jardón-Aguilar, A. Rangel-Merino, L. A. Vasquez-Toledo, and R. Gómez-Villanueva, “Four ports wideband drop-shaped slot antenna for MIMO applications,” J Electromagn Waves Appl, vol. 34, no. 9, pp. 1159–1179, Jun. 2020, doi: 10.1080/09205071.2019.1710578.

[89]. G. Srivastava and A. Mohan, "Compact MIMO Slot Antenna for UWB Applications," in IEEE Antennas and Wireless Propagation Letters, vol. 15, pp. 1057-1060, 2016, doi: 10.1109/LAWP.2015.

[90]. Tiwari, R. N., P. Singh, B. K. Kanaujia, and K. Srivastava, “Neutralization technique based two and four port high isolation MIMO antennas for UWB communication,” AEU-International Journal of Electronics and Communications, Vol. 110, 152828, 2019, doi: 10.1016/j.aeue.2019.152828.

[91]. J. Kulkarni, A. Desai, and C. Y. D. Sim, “Wideband Four-Port MIMO antenna array with high isolation for future wireless systems,” AEU - International Journal of Electronics and Communications, vol. 128, Jan. 2021, doi: 10.1016/j.aeue.2020.153507.

[92]. Pankaj Kumar Keshri, Richa Chandel, Sanjay Kumar Sahu, and Anil Kumar Gautam, "Compact Quad-Port High Performance UWB MIMO/Diversity Antenna with Slotted Ground Structure," *Progress in Electromagnetics Research C*, Vol. 112, 193-205, 2021. doi:10.2528/PIERC21030402 (IEEE format)

[93]. F. Amin, R. Saleem, T. Shabbir, S. ur Rehman, M. Bilal, and M. F. Shafique, “A compact quad-element UWB-MIMO antenna system with parasitic decoupling mechanism,” Applied Sciences (Switzerland), vol. 9, no. 11, Jun. 2019, doi: 10.3390/app9112371.

[94]. A. Megahed, M. Abdelazim, E. H. Abdelhay, and H. Y. M. Soliman, “Sub-6 GHz Highly Isolated Wideband MIMO Antenna Arrays,” IEEE Access, vol. 10, pp. 19875–19889, 2022, doi: 10.1109/ACCESS.2022.3150278.

[95]. A. Desai *et al.*, “Transparent 2-Element 5G MIMO Antenna for Sub-6 GHz Applications,” *Electronics (Switzerland)*, vol. 11, no. 2, Jan. 2022, doi: 10.3390/electronics11020251.

[96]. S. Xi, J. Cai, L. Shen, Q. Li, and G. Liu, “Dual-Band MIMO Antenna with Enhanced Isolation for 5G NR Application,” *Micromachines (Basel)*, vol. 14, no. 1, Jan. 2023, doi: 10.3390/mi14010095.

[97]. H. T. Chattha, M. K. Ishfaq, B. A. Khawaja, A. Sharif, and N. Sheriff, “Compact Multiport MIMO Antenna System for 5G IoT and Cellular Handheld Applications,” *IEEE Antennas Wirel Propag Lett*, vol. 20, no. 11, pp. 2136–2140, Nov. 2021, doi: 10.1109/LAWP.2021.3059419.

[98]. Rekha, S., Jino Ramson, S.R. Parasitically Isolated 4-element MIMO Antenna for 5G/WLAN Applications. Arab J Sci Eng 47, 14711–14720 (2022). https://doi.org/10.1007/s13369-022-06952-w

[99]. M. Ming Gao, H. Liang Niu, J. Chang Nan, W. Hui Liu, and C. Li Liu, “2-Port High Gain Millimeter-Wave MIMO Antenna for 5G Applications,” 2023.

[100]. K.L. Wong, J.Y. Lu, L.Y. Chen, W.Y. Li, Y.L. Ban, “8-antenna and 16-antenna arrays using the quad-antenna linear array as a build- ing block for the 3.5-GHz LTE

MIMO operation in the smart- phone," Microw Opt Techno Lett.; vol. 58, no. 1, pp. 174–181, 2016

[101]. K. -L. Wong, C. -Y. Tsai and J. -Y. Lu, "Two Asymmetrically Mirrored Gap-Coupled Loop Antennas as a Compact Building Block for Eight-Antenna MIMO Array in the Future Smartphone," in IEEE Transactions on Antennas and Propagation, vol. 65, no. 4, pp. 1765-1778, April 2017, doi: 10.1109/TAP.2017.2670534.

[102]. L. Sun, Y. Li, and Z. Zhang, "Wideband Decoupling of Integrated Slot Antenna Pairs for 5G Smartphones," IEEE Trans. Antennas Propag., vol. 69, no. 4, pp. 2386–2391, 2021, doi: 10.1109/TAP.2020.3021785.

[103]. M. Abdullah et al., "Future Smartphone: MIMO Antenna System for 5G Mobile Terminals," IEEE Access, vol. 9, pp. 91593–91603, 2021, doi: 10.1109/ACCESS.2021.3091304.

[104]. T. Addepalli, T. Vidyavathi, K. Neelima, M. Sharma, and D. Kumar, "Asymmetrical fed Calendula flower-shaped four-port 5G-NR band (n77, n78, and n79) MIMO antenna with high diversity performance," Int J Microw Wirel Technol, 2022, doi: 10.1017/S1759078722000800.

[105]. T. Addepalli, "Compact MIMO Diversity Antenna for 5G Sub: 6 GHz (N77/N78 and N79) and WLAN (Wi-Fi 5 and Wi-Fi 6) Band Applications," Wirel Pers Commun, Oct. 2023, doi: 10.1007/s11277-023-10718-4.

[106]. T. Addepalli, M. S. Kumar, C. R. Jetti, N. K. Gollamudi, B. K. Kumar, and J. Kulkarni, "Fractal Loaded, Novel, and Compact Two- and Eight-Element High Diversity MIMO Antenna for 5G Sub-6 GHz (N77/N78 and N79) and WLAN Applications, Verified with TCM Analysis," Electronics (Switzerland), vol. 12, no. 4, Feb. 2023, doi: 10.3390/electronics12040952.

[107]. S. Salihovic and S. T. Imeci, "A stub microstrip patch antenna for sub 6GHz - 5G applications," Heritage and Sustainable Development, vol. 5, no. 1, pp. 99–106, May 2023, doi: 10.37868/hsd.v5i1.104.

[108]. Ruchi, A. Patnaik, and M. V. Kartikeyan, "Compact dual and triple band antennas for 5G-IOT applications," Int J Microw Wirel Technol, vol. 14, no. 1, pp. 115–122, Feb. 2022, doi: 10.1017/S1759078721000301.

[109]. M. Alibakhshikenari et al., “An innovative antenna array with high inter element isolation for sub-6 GHz 5G MIMO communication systems,” Sci Rep, vol. 12, no. 1, Dec. 2022, doi: 10.1038/s41598-022-12119-2.

[110]. R. Dangi, P. Lalwani, G. Choudhary, I. You, and G. Pau, “Study and investigation on 5g technology: A systematic review,” Sensors, vol. 22, no. 1. MDPI, Jan. 01, 2022. doi: 10.3390/s22010026.

[111]. T. Raj, R. Mishra, P. Kumar, and A. Kapoor, “Advances in MIMO Antenna Design for 5G: A Comprehensive Review,” Sensors, vol. 23, no. 14. Multidisciplinary Digital Publishing Institute (MDPI), Jul. 01, 2023. doi: 10.3390/s23146329.

[112]. A. Bhattacharya and B. Roy, “Investigations on an extremely compact MIMO antenna with enhanced isolation and bandwidth,” Microw Opt Technol Lett, vol. 62, no. 2, pp. 845–851, Feb. 2020, doi: 10.1002/mop.32084.

[113]. H. Wang, R. Zhang, Y. Luo, and G. Yang, “Design of MIMO antenna system operating in wideband of 3300 to 6400 MHz for future 5G mobile terminal applications,” International Journal of RF and Microwave Computer-Aided Engineering, vol. 30, no. 12, Dec. 2020, doi: 10.1002/mmce.22426.

[114]. Y. Liu, Z. Yang, P. Chen, J. Xiao, and Q. Ye, “Isolation Enhancement of a Two-Monopole MIMO Antenna Array with Various Parasitic Elements for Sub-6 GHz Applications,” Micromachines (Basel), vol. 13, no. 12, Dec. 2022, doi: 10.3390/mi13122123.

[115]. G. Saxena, P. Jain, and Y. K. Awasthi, “High diversity gain super-wideband single band-notch MIMO antenna for multiple wireless applications,” IET Microwaves, Antennas and Propagation, vol. 14, no. 1, pp. 109–119, Jan. 2020, doi: 10.1049/iet-map.2019.0450.

[116]. S. Nandi and A. Mohan, “CRLH Unit Cell Loaded Triband Compact MIMO Antenna for WLAN/WiMAX Applications,” IEEE Antennas Wirel Propag Lett, vol. 16, pp. 1816–1819, 2017, doi: 10.1109/LAWP.2017.2681178.

[117]. Z. M. Phyo, T. Fujimoto, and C. E. Gaun, “A circularly polarised multiple input multiple output antenna with single-sense for sub-6 GHz 5G applications,” IET Microwaves, Antennas and Propagation, 2023, doi: 10.1049/mia2.12426.

[118]. M. Li, X. Chen, A. Zhang, and A. A. Kishk, “Dual-polarized broadband base station antenna backed with dielectric cavity for 5G communications,” IEEE Antennas Wirel Propag Lett, vol. 18, no. 10, pp. 2051–2055, Oct. 2019, doi: 10.1109/LAWP.2019.2937201.

[119]. A. M. Ibrahim, I. M. Ibrahim, and N. A. Shairi, “Compact MIMO antenna with high isolation for 5G smartphone applications,” Journal of Engineering Science and Technology Review, vol. 12, no. 6, pp. 121–125, 2019, doi: 10.25103/jestr.126.15.

[120]. M. P. Karaboikis, V. C. Papamichael, G. F. Tsachtsiris, C. F. Soras and V. T. Makios, "Integrating Compact Printed Antennas onto Small Diversity/MIMO Terminals," in IEEE Transactions on Antennas and Propagation, vol. 56, no. 7, pp. 2067-2078, July 2008, doi: 10.1109/TAP.2008.924677.

[121]. R. He, B. Ai, G. L. Stüber, G. Wang, and Z. Zhong, ‘‘Geometrical- based modeling for millimeter-wave MIMO mobile-to-mobile channels,’’ IEEE Trans. Veh. Technol., vol. 67, no. 4, pp. 2848–2863, Apr. 2018.

[122]. S. Nirmal, S. Kumar and R. Chandel, "High Isolation 2-Element MIMO for WLAN/Sub-6GHz (n77, n78 and n79) 5G Applications," 2023 1st International Conference on Innovations in High-Speed Communication and Signal Processing (IHCSP), BHOPAL, India, 2023, pp. 81-86, doi: 10.1109/IHCSP56702.2023.10127127.

[123]. S. Nirmal, S. Kumar, and R. Chandel, “High Isolation Compact Two Port 5G MIMO Diversity Antenna with Asymmetrical Feed and Partial Ground Structure,” Progress in Electromagnetics Research C, vol. 136, 2023, doi: 10.2528/PIERC23042202.

[124]. H. Ullah, S. U. Rahman, Q. Cao, I. Khan, and H. Ullah, “Design of SWB MIMO Antenna with Extremely Wideband Isolation,” Electronics (Basel), vol. 9, no. 1, p. 194, Jan. 2020, doi: 10.3390/electronics9010194.

[125]. C. Gao, X.-Q. Li, W.-J. Lu, and K.-L. Wong, ‘‘Conceptual design and implementation of a four-element MIMO antenna system packaged within a metallic handset,’’ Microw. Opt. Technol. Lett., vol. 60, no. 2, pp. 436–444, Feb. 2018.

[126]. Nirmal, S., Kumar, S., Chandel, R., “Four Element MIMO Antenna with PLUS Shape Radiator Arrangement and Corporate Feed for WLAN and 5G Wideband Wireless Applications,” In: Kaiser, M.S., Singh, R., Bandyopadhyay, A., Mahmud, M.,

Ray, K. (eds) Proceedings of the Fifth International Conference on Trends in Computational and Cognitive Engineering. Lecture Notes in Networks and Systems, vol 961, TCCE 2023 Springer, Singapore. https://doi.org/10.1007/978-981-97-1923-5_38

[127]. Rai, J. K., Ranjan, P., Kumar, S., Chowdhury, R., Kumar, S., & Sharma, A. "Machine learning-enabled two-port wideband MIMO hybrid rectangular dielectric resonator antenna for n261 5G NR millimeter wave", International Journal of Communication Systems, e5898, 2024.

[128]. Tiwari, P., Rai, J. K., Gahlaut, V., & Ranjan, P. "Compact quad element dual band high gain MIMO rectangular dielectric resonators antenna for 5G millimeter wave application", AEU-International Journal of Electronics and Communications, vol. 178, 155280, 2024.

[129]. S. R. Pasumarthi, J. B. Kamili, and M. P. Avala, "Design of dual band MIMO antenna with improved isolation," Microw Opt Technol Lett, vol. 61, no. 6, pp. 1579–1583, Jun. 2019, doi: 10.1002/mop.31832.

[130]. R. Mark, H. V. Singh, K. Mandal, and S. Das, "Reduced edge-to-edge spaced MIMO antenna using parallel coupled line resonator for WLAN applications," Microw Opt Technol Lett, vol. 61, no. 10, pp. 2374–2380, Oct. 2019, doi: 10.1002/mop.31911.

[131]. Y. Cheng, H. Liu, B. Q. Sheng, and L. Zhu, "A compact 4-element MIMO antenna for terminal devices," *Microw Opt Technol Lett*, vol. 62, no. 9, pp. 2930–2937, Sep. 2020, doi: 10.1002/mop.32396.

[132]. Z. Ren and A. Zhao, "Dual-Band MIMO Antenna With Compact Self-Decoupled Antenna Pairs for 5G Mobile Applications," IEEE Access, vol. 7, pp. 82288–82296, 2019, doi: 10.1109/ACCESS.2019.2923666.

[133]. J. Khan, S. Ullah, F. A. Tahir, F. Tubbal, and R. Raad, "A Sub-6 GHz MIMO Antenna Array for 5G Wireless Terminals," Electronics (Basel), vol. 10, no. 24, 2021, doi: 10.3390/electronics10243062.

[134]. N. Sghaier and L. Latrach, "Design and analysis of wideband MIMO antenna arrays for 5G smartphone application," Int J Microw Wirel Technol, vol. 14, no. 4, pp. 511–523, May 2022, doi: 10.1017/S1759078721000659.

[135]. Aziz, H.S.; Naji, D.K. “Compact dual-band mimo antenna system for lte smartphone applications”, Prog. Electromagn. Res. C 2020, 102, 13–30.

[136]. M.-Y. Li et al., “Eight-Port Orthogonally Dual-Polarized Antenna Array for 5G Smartphone Applications,” IEEE Trans Antennas Propag, vol. 64, no. 9, pp. 3820–3830, 2016, doi: 10.1109/TAP.2016.2583501.

[137]. M.-Y. Li, Z.Q. Xu, Y.L. Ban, C.Y.D. Sim, and Z.F. Yu, “Eight-port orthogonally dual-polarised MIMO antennas using loop structures for 5G smartphone,” IET Microwaves, Antennas & Propagation, vol. 11, no. 12, pp. 1810–1816, 2017, doi: https://doi.org/10.1049/iet-map.2017.0230.

[138]. C.Y.D. Sim, H.Y. Liu, and C.J. Huang, “Wideband MIMO Antenna Array Design for Future Mobile Devices Operating in the 5G NR Frequency Bands n77/n78/n79 and LTE Band 46,” IEEE Antennas Wirel Propag Lett, vol. 19, no. 1, pp. 74–78, 2020, doi: 10.1109/LAWP.2019.2953334.

[139]. Rai, J. K., Ranjan, P., Chowdhury, R., & Jamaluddin, M. H. “Design and optimization of dual port dielectric resonator-based frequency tunable MIMO antenna with machine learning approach for 5G new radio application”, International Journal of Communication Systems, vol. 37, no. 13, e5856, 2024.

[140]. S. Kumar, R. Kumar, R. Kumar Vishwakarma, and K. Srivastava, “An improved compact MIMO antenna for wireless applications with band-notched characteristics,” AEU - International Journal of Electronics and Communications, vol. 90, pp. 20–29, Jun. 2018, doi: 10.1016/j.aeue.2018.04.008.

[141]. R. Chandel, A. K. Gautam, and K. Rambabu, “Design and Packaging of an Eye-Shaped Multiple-Input-Multiple-Output Antenna with High Isolation for Wireless UWB Applications,” IEEE Trans Compon Packaging Manuf Technol, vol. 8, no. 4, pp. 635–642, Apr. 2018, doi: 10.1109/TCPMT.2018.2806562.

[142]. R. R. Tummala *et al*., "The SOP for miniaturized, mixed-signal computing, communication, and consumer systems of the next decade," in *IEEE Transactions on Advanced Packaging*, vol. 27, no. 2, pp. 250-267, May 2004, doi: 10.1109/TADVP.2004.830353.

[143]. K. Zhu, T. Liao, and Y. Liu, “Intelligent mine vehicle terminal antenna based on LTCC technology,” in Journal of Physics: Conference Series, IOP Publishing Ltd,

May 2021. doi: 10.1088/1742-6596/1920/1/012091.

[144]. B. Hussain *et al*., "Design considerations for LTCC based UWB antennas for space applications," *2014 IEEE International Conference on Wireless for Space and Extreme Environments (WiSEE)*, Noordwijk, Netherlands, 2014, pp. 1-5, doi: 10.1109/WiSEE.2014.6973068.

[145]. M. Al Ahmad and L. J. A. Olule, "Meshed Stacked LTCC Antenna for Space Application," *IEEE Access*, vol. 10, pp. 29473–29481, 2022, doi: 10.1109/ACCESS.2022.3158679.

[146]. G. Brzezina, L. Roy and L. MacEachern, "Planar antennas in LTCC technology with transceiver integration capability for ultra-wideband applications," in *IEEE Transactions on Microwave Theory and Techniques*, vol. 54, no. 6, pp. 2830-2839, June 2006, doi: 10.1109/TMTT.2006.875448.

[147]. M. Abbosh, M. E. Bialkowski, M. V. Jacob and J. Mazierska, "Design of a Planar UWB Antenna with Signal Rejection Capability in a Narrow Sub-band," *2006 IEEE 63rd Vehicular Technology Conference*, Melbourne, VIC, Australia, 2006, pp. 2645-2648, doi: 10.1109/VETECS.2006.1683347.

[148]. K. W. Khoo, Z. N. Chen, A. C. W. Lu, V. Sunappan and L. L. Wai, "Miniaturized Multilayer UWB Antennas on LTCC," in *IEEE Transactions on Antennas and Propagation*, vol. 57, no. 12, pp. 3988-3992, Dec. 2009, doi: 10.1109/TAP.2009.2033441.

[149]. A.M. Abbosh, M.E. Bialkowski, M.V. Jacob and J. Mazierska, "Investigations into an LTCC based ultra-wideband antenna," in APMC, Suzhou, China, 2005.

[150]. X. Qing and Z.N. Chen, "Monopole-like Slot UWB Antenna on LTCC," in ICUWB, Hannover, Germany, 2008.

[151]. B. Yang, A. Vorobyov, A. G. Yarovoy, L. P. Ligthart, S. Rentsch and J. Muller, "A novel shielded UWB antenna in LTCC for radar and communications applications," 2008 IEEE International Conference on Ultra-Wideband, Hannover, Germany, 2008, pp. 117-120, doi: 10.1109/ICUWB.2008.4653365.

[152]. M. Sun and Y. P. Zhang, "Miniaturization of Planar Monopole Antennas for Ultrawide-Band Applications," *2007 International workshop on Antenna Technology: Small and Smart Antennas Metamaterials and Applications*, Cambridge, UK, 2007, pp. 197-200, doi: 10.1109/IWAT.2007.370110.

[153]. Y. Imanaka, "Multilayered Low Temperature Cofired Ceramics (LTCC) Technology", Springer Berlin, ISBN: 0 H. Zhang and A. Shamim, “Wideband and wide beam scanning dual-polarized Phased Array Antenna-in-Package Design for 5G Applications,” *IEEE Open Journal of Antennas and Propagation*, vol. 5, no. 1, pp. 140–152, Feb. 2024, doi: 10.1109/OJAP.2023.3336762.387231307, May2008.

List of Publications

A. International Journal

1. Sanket Nirmal, Sumit Kumar, and Richa Chandel, "High Isolation Compact Two Port 5G MIMO Diversity Antenna with Asymmetrical Feed and Partial Ground Structure", Progress in Electromagnetics Research C, Vol. 136, 23-36, 2023. doi:10.2528/PIERC23042202 (Scopus Indexed)
2. S. Nirmal, S. Kumar, and R. Chandel, "Quad-port Staircase U-shaped Wideband MIMO Antenna for 5G New Radio Applications," Progress in Electromagnetics Research Letters, vol. 125, pp. 43–50, 2025, doi: 10.2528/PIERL24121204. (Science Citation Index Expanded (SCIE)).
3. Sanket Nirmal, Sumit Kumar, and Richa Chandel, "Design of wideband quad-port LTCC 5G-MIMO Antenna for New Radio (NR) and WLAN Applications", *Journal of Integrated Science and Technology, 2025.* (Communicated and Under review) (Scopus Indexed)

B. International Conferences

1. S. Nirmal, S. Kumar and R. Chandel, "Analysis of Diverse MIMO Antennas for Fifth Generation Application: A Review," 2022 IEEE Wireless Antenna and Microwave Symposium (WAMS), Rourkela, India, 2022, pp. 1-5, doi: 10.1109/WAMS54719.2022.9848357. (Scopus Indexed)
2. S. Nirmal, S. Kumar and R. Chandel, "High Isolation 2-Element MIMO for WLAN/Sub-6GHz (n77, n78 and n79) 5G Applications," 2023 1st International Conference on Innovations in High-Speed Communication and Signal Processing (IHCSP), BHOPAL, India, 2023, pp. 81-86, doi: 10.1109/IHCSP56702.2023. 10127127. (Scopus Indexed)
3. S. Nirmal, S. Kumar and R. Chandel, "Quad-Radiator MIMO with asymmetric feed line for (n77/n78/n79/WLAN) 5G-Wireless Applications," 2023 IEEE 7th Conference on Information and Communication Technology (CICT), Jabalpur, India, 2023, pp. 1-6, doi: 10.1109/CICT59886.2023.10455275. (Scopus Indexed)
4. Nirmal, S., Kumar, S., Chandel, R., "Four Element MIMO Antenna with PLUS Shape Radiator Arrangement and Corporate Feed for WLAN and 5G Wideband Wireless Applications," In: Kaiser, M.S., Singh, R., Bandyopadhyay, A.,

Mahmud, M., Ray, K. (eds) Proceedings of the Fifth International Conference on Trends in Computational and Cognitive Engineering. Lecture Notes in Networks and Systems, vol 961, TCCE 2023 Springer, Singapore. https://doi.org/10.1007/978-981-97-1923-5_38 (Scopus Indexed)

C. Book Chapter

1. Sanket Nirmal and Richa Chandel, "A Survey of Fifth-Generation Cellular Communications Using MIMO for IoT Applications," in Microstrip Antenna Design for Wireless Applications, 1st ed., vol. 1st, Praveen Kumar Malik, Sanjeevi kumar Padmanaban, and Jens Bo Holm-Nielsen, Eds., Boca Raton: CRC Press, 2021, pp. 142–152. doi: https://doi.org/10.1201/9781003093558.

D. Copyright

1. ©Lovely Professional University, Sanket Nirmal, Sumit Kumar, and Richa Chandel, "Framework of MIMO array for n77/n78/n79 (5G) and WLAN band", Registration Number: L-154235/2024, Granted on: 24/09/2024.